Touched With Fire: How MYC Drives Life and Oncogenesis

By

Gabriel M. Cohn

A Dissertation

Presented to the Cancer Biology Program and Oregon Health & Science University School of Medicine in partial fulfillment of the requirements for the degree of Doctor of Philosophy

09/19/2025

School of Medicine

Oregon Health & Science University

CERTIFICATE OF APPROVAL

This is to certify that the PhD dissertation of

Gabriel M. Cohn

has been approved by

Mentor/Advisor: Rosalie Sears, PhD

_____

Committee Chair: Matthew Thayer, PhD

_____

Member: Mushui Dai, MD, PhD

_____

Member: Andrew Adey, PhD

_____

Member: Jonathan Brody, PhD

_____

Member: Anupriya Agarwal, PhD

_____

TABLE OF CONTENTS

LIST OF FIGURES

LIST OF ABBREVIATIONS

APH	Aphidicolin
ATM	Ataxia-Telangiectasia Mutated
ATR	Ataxia-Telangiectasia and Rad3 related
Bleo	Bleomycin
CDK9	Cyclin Dependent Kinase 9
Co-IP	Co-immunoprecipitation
CyclicIF	Cyclic Immunofluorescence
DDR	DNA Damage Response
DI-PLA	DNA Damage In Situ Ligation followed by Proximity Ligation Assay
DMEM	Dulbecco's Modified Eagle's Medium
DMSO	Dimethyl Sulfoxide
Dox	Doxycycline
DSB	Double Strand Break
ERK	Extracellular Receptor Kinase
FBS	Fetal Bovine Serum
GSK3β	Glycogen Synthase Kinase 3β
HAT	Histone Acetyltransferase
HDAC	Histone Deacetylase
HLH	Helix Loop Helix
HR	Homologous Recombination
KO	Knockout
MB0	MYC Box 0
MB1	MYC Box 1
MB2	MYC Box 2

MEFs	Mouse Embryonic Fibroblasts
NHEJ	Non-Homologous End Joining
NPC	Nuclear Pore Complex
NUP153	Nucleoporin 153
NUP98	Nucleoporin 98
P-TEFb	positive transcription elongation factor
PCR	Polymerase Chain Reaction
PDAC	Pancreatic Ductal Adenocarcinoma
PDCL	Patient-Derived Cell Lines
PIN1	peptidyl-prolyl cis/trans isomerase, NIMA-interacting 1
PLA	Proximity Ligation Assay
PP2A	Protein Phosphatase 2A
pS62-MYC	phosphorylated serine 62 MYC
pT58-MYC	phosphorylated Threonine 58 MYC
PTM	Post-Translational Modification
qChIP	quantitative Chromatin immunoprecipitation
rDNA	Ribosomal DNA
RIME	Rapid Immunoprecipitation Mass Spectrometry of Endogenous Proteins
RNAPII	RNA Polymerase II
shRNA	Short hairpin RNA
TNBC	Triple-Negative Breast Cancer
TPR	Translocated Protein Region
TRRAP	Transformation/transcription domain-associated protein
WB	Western Blot
WT	Wild-Type

ACKNOWLEDGEMENTS

I would like to express my deepest gratitude to everyone who has supported me throughout this journey.

First and foremost, I want to thank my PI, Dr. Rosalie Sears, for her extraordinary mentorship on this journey. Your guidance has shaped me into the scientist I am today by supporting my intellectual freedom and encouraging me to follow my curiosity. You gave me the space to make mistakes and to learn how to think and troubleshoot for myself. You have always been a strong advocate for me, offering guidance with kindness, respect, and genuine belief in my potential. You have my deepest respect and gratitude for your mentorship and wisdom.

I am also profoundly grateful for my Dissertation Advisory Committee (DAC), Dr. Mattew Thayer (Chair), Dr. Andrew Adey, Dr. Mushui Dai, Dr. Jonathan Brody, and Dr. Anupriya Agarwal (external reader). Meeting with you every six months was always a highlight, and I left every meeting feeling supported, encouraged, and more confident in my work. Your thoughtful questions, valuable insights, and steady support challenged me to grow and helped shape both this dissertation and my development as a scientist. I am grateful not only for your guidance in shaping this work, but also for the example you set as scientists and mentors. I have learned so much from you all, and your influence has been paramount in my development as a researcher.

Thank you to all the members of the Brenden-Colson and Sears labs, past and present who have been there to support me along the way, whether through scientistic advice, troubleshooting experiments, or sharing a much-needed laugh. To my fellow graduate students, Dr. Isabel English, Kevin Hawthorne, Jackie Phipps – Thank you for the constant support and camaraderie. To many of the lab members who have helped me along the way, especially Dr. Jenny Eng and Carl Pelz, thank you for your expertise and time.

Colin Daniel, you were my rock in every sense. Experimentally, intellectually, and emotionally you helped me stay grounded. Our decompression lunches kept me sane, and your steady guidance and honest perspective meant the world to me. I am grateful for your expertise and even more grateful for your friendship.

Dr. Daniel Liefwalker, thank you for being my day one guide and helping me find my footing in the lab. You taught me to think provocatively and continue to mentor me in and outside the lab. Thank you for all the great memories from running the windy river relay to our Viking dinner in Stockholm.

Dr. Ellen Langer, you swooped in like a superhero whenever I needed helping help, especially on my first publication and my qualifying exam; your generosity of time and wisdom meant more than I can say.

Karyn Taylor, none of this would have been possible without you. Your problem-solving skills and ability to untangle every administrative headache has been so incredibly helpful. Sincerely thank you for everything.

Ariffin Ali, my mentee with the CURE program for two summers. Mentoring you has been one of the most rewarding experiences of my graduate career. Watching you grow intellectually and gain confidence as a young scientist has been an honor, and I am grateful to have been part of your journey.

Lola Bichler, thank you keeping me on track throughout graduate school. Your kind (and sometimes much needed) second or third reminder emails were always appreciated. I deeply grateful for your patience, support, and steady presence behind the scenes.

To all my non-academic friends and roommates who have made Oregon feel like home, I love you all and I am so grateful for the community we built together. To Mt. Hood, thank you for the powder-filled morning that fueled my soul before long nights in the lab. To Nova, my sweet dog, unwavering companion, and quiet confidant. Your joy, loyalty, and unconditional love has brought light to every day. You've been with me through it all, and I cannot wait for many trips to the 1000-acre dog park once this dissertation is complete!

And finally, to my family. No words on this page could ever reach the depth of love, appreciation, and unwavering gratitude I feel for you all. Your support has been my foundation, your encouragement my compass, and your friendship a constant source of strength. To my older brother Samuel who passed away in 2006, thank you for teaching that life is a precious gift meant to be cherished. I feel your bright smile with me every day, reminding me to welcome each moment with joy and to hold tightly to what matters most. I hope I've made you proud, big brother.

To my eldest brother Maxwell and sister-in-law, Becky. Thank you for bringing so much color and excitement into my life. You've taught me to expect the unexpected and continue to inspire me to embrace my creativity and build meaningful communities. My name might not be MYC, but I know without a doubt that I need my MAX to truly thrive in this lifetime.

To my parents - Mom and Dad, you are my truest north stars, always guiding me with love, wisdom, and unwavering support. If grow up to be even half the people you are, I would consider my life a resounding success. Mom, you taught me how to break down complex problems into tangible, achievable steps, a skill that has been essential not only in graduate school but in life. Your love radiates across the 3,000 miles that separates us, and I feel it every day. To my Dad (Dr. Zatar), you gave me the incredible gift of discovering science not in a class room, but through playful experiments often involving high voltage and large backyard explosions. I have never met a kinder, gently, and more lovable mad scientist than you. You've always been my greatest hero. Thank you, Mom and Dad, I love you both deeply.

And lastly, thank you to all of the incredible faculty, students, and staff at OHSU who have given me such a meaningful and enriching education. I am deeply grateful for everything

I have learned and for the many friendships that have made this experience so memorable.

There are good ships and wood ships, ships that sail the sea, but the best ships are friendships, and may they always be.

– Irish Proverb

ABSTRACT

MYC is an enigmatic master regulator implicated in nearly every facet of cellular biology. Throughout my PhD research and deep engagement with the literature, my singular goal has been to uncover MYC's fundamental roles in normal cell function and to understand how these roles become corrupted during oncogenesis. In Chapter 1, I begin with a historical examination of the discovery of MYC in avian tumor viruses and trace its trajectory to its fundamental role in human cellular growth, survival, and tissue regeneration. I discuss the dual nature of MYC in its roles in driving proliferation through transcriptional amplification, as well as the compensatory mechanisms it employs to mitigate the genomic instability that accompanies rapid cell division. This dissertation explores two distinct functions of MYC: Chapter 2 examines how MYC drives rapid cell division in response to growth signals required for tissue regeneration, while Chapter 3 explores novel mechanisms by which MYC promotes DNA repair to support cell survival. Within these chapters, I examine how MYC functions as a molecular "accelerator," linking extrinsic signals to transcriptional amplification, and how its post-translational regulation, particularly serine 62 phosphorylation and PIN1-mediated isomerization, enables context-specific control of MYC stability and activity. In Chapter 2, using proximity-based proteomics and biochemical assays, I define a nuclear pore-associated MYC interactome that may facilitate gene gating and rapid transcriptional response to mitogenic signals. Chapter 2 highlights how PIN1-mediated isomerization of phosphorylated serine 62 on MYC is required for its engagement with target gene and co-activator at the nuclear pore. In Chapter 3, I investigate MYC's regulation and function at sites of DNA damage, demonstrating that phosphorylation at serine 62 enables robust association with DNA double strand breaks and promotes the recruitment of repair factors. In Chapter 4, I

discuss how these findings expand our understanding of MYC's role in oncogenesis and reveal therapeutic opportunities to target aggressive MYC-driven tumors. These tumors are often genetically unstable and heavily rely on fragile compensatory repair mechanisms that can be selectively disrupted. I highlight how indirect destabilization of MYC, such as by reducing serine 62 phosphorylation, may impair both its ability to amplify transcription of growth signals at the nuclear pore and its role in facilitating DNA repair. Ultimately, this dissertation details a multiscale understanding of MYC's biology, revealing its central role as a torchbearer guiding the path from cellular survival to oncogenic transformation.

Chapter 1: Introduction

1.1 Hidden in the Henhouse: How Chicken Viruses Cracked Open the Origins of MYC and Modern Oncogenes.

"In an extraordinary act of unintentional benevolence, retroviruses have brought to view cellular genes whose activities may be vital to many forms of carcinogenesis."

-J. Michael Bishop[1]

Cancer is an old disease, with written descriptions appearing in ancient Egypt as early as 3000 BC[2]. For millennia, philosophers as well as medical and religious practitioners sought to explain the transformation of normal tissue into malignancy through various theories and experiments. Technological and scientific breakthroughs over the past century have catapulted our understanding of the molecular drivers of oncogenesis and have led to the development of lifesaving treatments. These efforts identified more than 70 human proto-oncogenes that drive oncogenesis across different cancer types[3], with MYC emerging as one of the most frequently dysregulated proteins in human cancers[4-6]. The discovery of MYC followed breakthroughs that linked retroviral infection to tumorigenesis[7]. With "germ theory" dominating medicine at the turn of the 20th century, largely driven by the work of Robert Koch and Louis Pasteur, scientists began searching for microbial-driven origins of cancer. The first connection emerged in the early 1900s, when two Danish scientists, Vilhelm Eilermann and Oluf Bang, demonstrated that leukemia could be transmitted between chickens using cell free extracts[8]. The scientific community gave little credence to this finding, as leukemias were not yet considered true malignancies and chickens were regarded as uninteresting experimental models. A few years later and across the Atlantic, a farmer from Long Island arrives at the Rockefeller Institute with a prized Plymouth Rock chicken bearing a tumor

on its right breast, seeking a remedy or explanation[1]. The farmer was referred to Francis Peyton Rous, who ultimately sacrificed the chicken and performed a landmark experiment, echoing the work of Ellermann and Bang, by isolating cell free filtrates from the tumor and injecting them into healthy chickens, which subsequently developed similar sarcomas[9, 10]. Rous noted that repeat bacteriological tests yielded negative results, and with the recent discovery of viruses in the late 1890s, he predicted that the invisible "poison" within cell free agent was a virus (Latin word for poison) was responsible for causing the chicken cancers[11]. Rous temporarily abandoned his search for cancer-causing viruses after a fruitless effort to identify a mammalian virus capable of producing tumors similar to those he had observed in chickens. It wasn't until 1933 that Rous's colleague and friend, Dr. Richard Shope, consulted him about a virus that caused large warts on the skin of wild cottontail rabbits found in the southwestern United States. This discovery, along with other findings of cancer promoting virus, including his namesake, Rous Sarcoma Virus (RSV), was gradually vindicated over the following five decades and ultimately earned Rous the Nobel Prize in Medicine or Physiology in 1966. In his Nobel Lecture, Rous reflected on this discovery: "Few situations are more exasperating to the inquirer than to watch a tiny nodule form on a rabbit's skin at a spot from which the chemical agent inducing it has long since been gone, and to follow the nodule as it grows, and only too often becomes a destructive epidermal cancer. What can be the why for these happenings?"[11].

This poignant question resonated through the scientific community, inspiring two independent hypotheses for how viruses might induce cancer. One hypothesis was that viruses carried a molecular Trojan horse that corrupts normal cell biology to drive cancer

formation. The other model supported the “Oncogene Hypothesis” proposed in 1969 by Drs. Robert Huebner and George Todaro, which posits that all normal cells harbor intrinsic genetic elements that, when dysregulated by viral infection, can lead to tumorigenesis[12]. In a rare convergence of scientific inquiry, both models ultimately reflected complementary mechanisms of viral-induced cancer. The Trojan horse hypothesis benefited from the power of simplification: While the human genome has approximately 20,000 genes, most viruses encode fewer than a dozen, narrowing the search for the viral driver of oncogenesis. In 1970, Dr. Steven Martin used temperature-sensitive mutants of RSV to discover the gene v-*src* which was essential for both the initiation and maintenance of cancer, but dispensable for viral replication[13, 14]. RSV contains only four genes, three involved in viral replication and a fourth, *v-src*, responsible for its oncogenic potential. The presence of v-*src* in RSV puzzled Dr. J. Michael Bishop and his recent postdoctoral fellow, Dr. Harold Varmus, leading them to hypothesize that v-*src* may have originated from an ancient virus that mistakenly incorporated a normal cellular gene. To investigate this, Varmus and Dr. Dominique Stehelin developed a molecular probe to detect a cellular gene with DNA homology to the recently discovered *v-src*. In October of 1974, Stehelin identified the cellular *src* gene (*c-src*) in chickens, and subsequentially detection it across all bird species examined, thereby identifying the first cellular oncogene[15]. Two years later, *c-src* was identified in a wide range of vertebrates such as humans, cows, mice, and fish, all previously uninfected by virus[16]. This finding vindicated the Trojan horse hypothesis, revealing that RSV carried a viral version of *c-src* that hijacked normal cellular machinery to drive unchecked growth and tumor formation.

The discovery of *c-src* raised the question whether it was a unique anomaly among retroviruses or an archetype for a broader class of cellular oncogenes. The answer lay in studies of four avian retroviruses MC29, MH-2, CMII, and OK10, which were shown to transform monocytes/macrophages in vitro and consistently induce myelocytomas, endotheliomas, and kidney tumors in fowl[17, 18]. Within these four viruses, researchers identified a shared genetic element that lacked homology with *c-src*, was dispensable for viral replication, yet essential for the virus's transformative activity[19-24]. This viral oncogene was initially referred to as mcv or mac, but the field ultimately adopted the name *v-myc* due to its role in promoting **my**elo**c**ytomatosis. In 1979, Dr. Diana Sheiness in Bishop's lab identified the highly conserved cellular counterpart, *c-myc*, in close competition with Dr. Dominique Stehelin, Bishop's former post-doctoral fellow, who had then established his own lab in France[19, 25]. The viral *v-myc* gene often encodes for a chimeric GAG-MYC protein, which is a fusion protein that contains segments from both MYC and the structural retroviral protein, GAG[21, 26-28]. Similar to RSV's SRC protein, the GAG-MYC represents another viral-derived mimic of a cellular gene that acts as a molecular Trojan horse which drives uncontrolled growth following viral infection. In 1981, Drs. William Hayward, Benjamin Neel, and colleagues published a landmark discovery showing that avian leukosis virus (ALV) induces lymphoid leukosis through retroviral insertion near the *c-myc* gene, leading to its overexpression[29, 30]. Follow-up validation of retroviral insertions proximal to the *c-myc* gene in chicken bursal lymphomas galvanized the "Oncogene Hypothesis," demonstrating that dysregulation of intrinsic proto-oncogenes can drive cancer development[31, 32].

The relevance of *c-myc* dysregulation in human cancer was underscored by consistent chromosomal abnormalities in biopsies from Burkitt's lymphoma patients[33, 34]. In these cases, the *c-myc* gene translocated from chromosome 8 translocated to chromosome 14, which contains the immunoglobulin enhancer element, resulting in constitutive *c-myc* expression and the development of lymphoma[35-37]. Further hybridization screens using v-myc probes identified additional genes with sequence homology to cellular c-myc gene, suggesting a broader *myc* gene family[38-40]. These studies led to the identification of *n-myc* and *l-myc* genes, named for their gene amplification in human neuroblastoma and small cell lung cancer tumors, respectively. The pivotal discovery from the Varmus-Bishop lab that n-myc is dramatically amplified in neuroblastoma and serves as a prognostic marker for poor survival and aggressive disease established oncogene dysregulation as a fundamental driver of oncogenesis and sparked a widespread search for *myc* gene abnormalities across cancer types[38, 41, 42]. Consistently, all three members of the *myc* gene family were amplified in every cancer ranging from hematopoietic malignancies to solid tumors[4, 6]. A comprehensive pan-cancer analysis of the *myc* family oncogenes and its proximal network genes, using data from 33 tumor types and over 9,000 samples in the Cancer Genome Atlas, revealed that 28% of all samples had amplification of at least one *myc* family paralog[5]. Gene amplification is one of several mechanisms that dysregulate MYC activity, alongside upstream and downstream synergistic mutations that stabilize MYC within the cell, resulting in MYC contributing to approximately 70% of all human malignancies[4, 43-45]. In agreement, synergistic mutations that enhance MYC's stability and buffer oncogenic stress frequently co-occur in MYC amplified tumors[46-48].

Following the discovery of MYC and its dysregulation in human malignancies, more than 52,000 PubMed-searchable publications have explored MYC (as of May 2025), implicating it in nearly every aspect of biological function and every hallmark of cancer[6, 45, 49]. Understanding MYC's function in the context of cancer has obscured MYC's physiological function within the cell and normal tissue biology. To possibly oversimplify, MYC acts as a proliferative signal that drives cell multiplication during development and supports tissue maintenance and repair adulthood. A study in the late 1980s foreshadowed this understanding of MYC's core function, demonstrating that *v-myc* retroviral inflection of the bursa Fabricius in chickens led to rapid cellular proliferation and a markedly enhanced ability to repopulate follicles following chemical ablation, compared to non-infected controls[50]. Although emergent functions of MYC may arise when it becomes dysregulated, the following section will explore MYC activity within the context of normal tissue physiology to better illuminate its enigmatic role throughout oncogenesis.

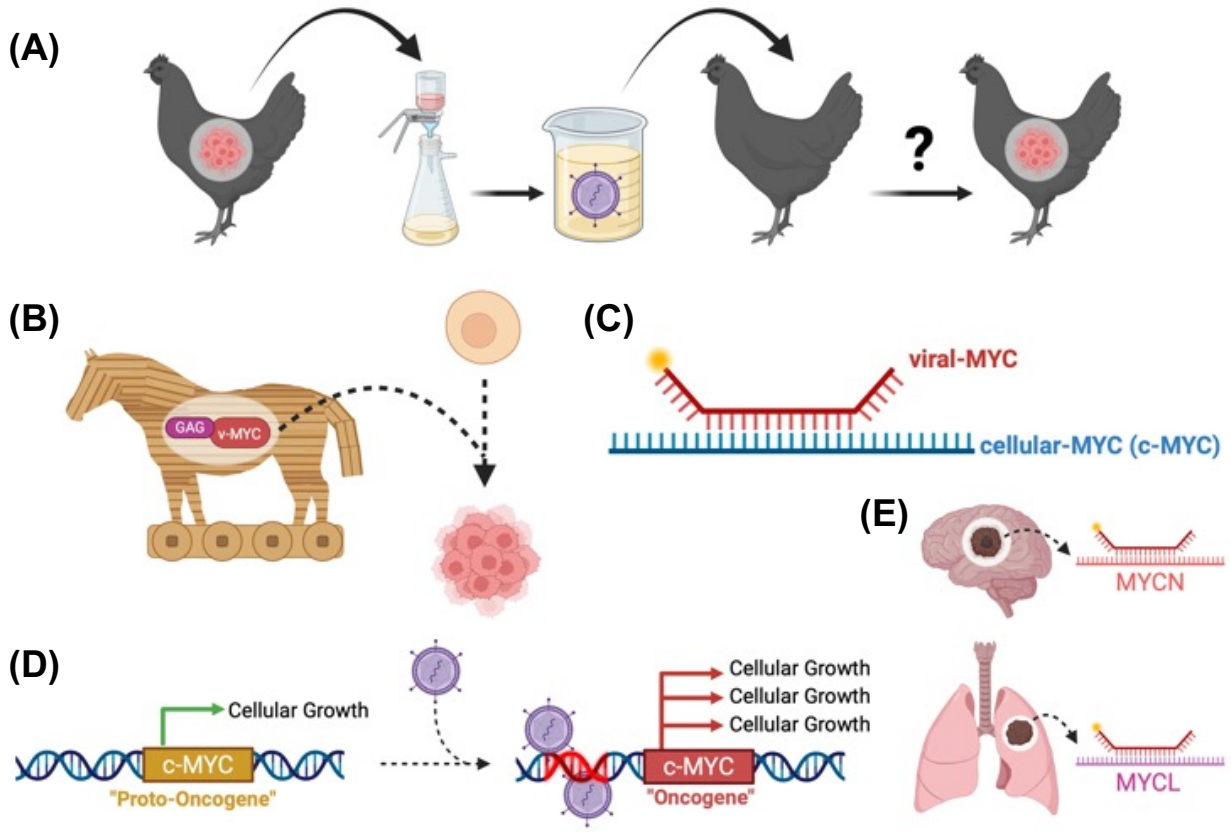

Figure 1.1.1 The History of MYC.

(**A**) Research into four avian retroviruses MC29, MH-2, CMII, and OK10 consistently revealed their ability to induce myelocytomas and other tumors in chickens. Notably, these retroviruses lacked homology with the recently discovered *c-src* gene, suggesting the presence of additional oncogenes. (**B)** Subsequent analysis showed that these viruses act as molecular Trojan horses by delivering a GAG-v-MYC fusion protein that drives tumorigenesis. (**C**) Using a radioactively labeled hybridization screen, researchers identified cellular MYC (c-MYC) in the genomes of all multicellular organisms screened. (**D**) Retroviral insertion near the c-MYC locus disrupted its regulation, promoting tumorigenesis and providing strong support for the “Oncogene Hypothesis.” (**E**) Further hybridization screens in human tumors led to the discovery of c-MYC homologs, MYCN and MYCL, which drive neuroblastoma and lung cancer, respectively. Figure created with BioRender.com.

1.2 MYC in Tissue Development and Homeostasis

MYC in Embryonic Development

MYC's role in tissue development and homeostasis is paramount for understanding both its normal biological function and its potent capacity to drive oncogenesis. During mouse gestation, knockout of MYC results in embryonic lethality between days E9.5 and E10.5, and heterozygous females exhibit significantly reduced fertility[51]. Examination of the embryos revealed numerous developmental abnormalities including defects in the heart, neural tube, and pericardium. Another study demonstrated that many of these developmental defects could be rescued when MYC was conditionally deleted in the epiblast while functional MYC remained in the trophectoderm and primitive endoderm[52]. However, these embryos survived only until embryonic day E12 due to fetal liver hypoplasia and major dysfunction within the hematopoietic stem cell compartment, leading to severe anemia. This finding suggests that the observed organ abnormalities result primarily from placental insufficiency due to the loss of MYC. Mechanistically, MYC is responsible for activating the transcription of immediate embryonic gene activation (iGA) programs that drive proper cytokinesis, which is essential for normal tissue development and morphology[53]. Inhibition of MYC resulted in an approximate 95 percent reduction in iEGA expression and lead to acute developmental arrest. In terms of morphogenesis, reduced MYC expression in the developing face has been identified as a contributing factor to the congenital malformation cleft lip with or without cleft palate (CL/P), a condition that affects approximately one in every 500 to 1000 human births[54-56]. This reduction in MYC was mapped to a long-range enhancer, a 640-kb noncoding sequence located at 8q24, that drives its robust transcription. Alterations to this *cis*-activating enhancer led to decreased MYC expression

and disruption of MYC-associated gene programs and drove CL/P. In summary, these observations underscore the critical role of MYC in driving early embryonic developmental events to maintain proper tissue architecture.

MYC in Mammalian Tissue Regeneration

Following embryonic development, as the need for massive cellular growth diminishes, MYC's role shifts towards regulating mammalian tissue regeneration, a function thoroughly reviewed by Illi et al[57]. This shift in function explains why MYC is tightly regulated, possessing a short half-life of approximates 10-20 minutes, and is virtually undetectable in quiescent cells in G0 phase[58]. Depending on the tissue's responsiveness to external signals, it can be classified as either stimuli-permissive or non-permissive, and this distinction underlies MYC's function in mammalian tissues after development. In stimuli permissive tissues such as the intestinal tract, WNT signaling activates MYC expression to drive proliferation of progenitor cells within the intestinal crypts[59]. However, MYC is dispensable for overall function of intestinal epithelium, and its expression levels remain low under normal physiological conditions. The intestinal tract is frequently exposed to DNA damaging toxins and possess an innate capacity for regeneration following injury. This regeneration response requires WNT-driven activation of MYC, which in turn promotes the expression of the integrin effector protein Focal Adhesion Kinase (FAK) to facilitate intestinal repair[60]. Similarly, the liver relies on dynamic MYC regulation during both development and regeneration. During embryonic development, inactivation of MYC results in reduced hepatocyte size, altered cell ploidy, and disorganized liver morphology. These phenotypes arise from a loss of MYC driven transcription required for proper embryonic mRNA translation and mitochondrial function,

leading to liver features characteristic of non-fatty alcoholic liver disease (NFALD). However, in postnatal hepatocytes, MYC is largely absent under normal conditions and is only induced following injury, such as partial hepatectomy. In this context, crosstalk between MYC and MLX regulates the transition from G0/G1 to S-phase, which is necessary for effective liver regeneration[61, 62]. Interestingly in the pancreas, MYC is required for the proper embryonic development of the acinar compartment, but not the islet compartment[63, 64]; however, it plays an important role in the stimuli permissive nature of pancreatic islet cells in response to glucose. High glucose increases MYC expression in pancreatic β-cells, which is required for β-cell expansion in young mice but not adult mice[65, 66]. In young mice, failure to proliferate following metabolic stress of a high-fat diet leads to β-cells dysfunction, death, and the onset of type 2 diabetes. Stabilization of MYC through serine 62 phosphorylation (discussed in later sections) has been shown to be essential for proper β-cell expansion in response to metabolic stress[67].

Non-permissive tissues are refractory to external growth-inducing stimuli and do not modulate MYC expression, except in the context of tissue regeneration following injury. Even in non-permissive tissues with detectable levels of MYC, such as the heart, MYC binds to gene promoters but fails to induce transcription and cellular proliferation. In the heart, MYC-driven proliferation was only reactivated when key transcriptional co-activators, such as the positive transcription elongation factor (P-TEFb), were also upregulated which is necessary for tissue regeneration[68]. This suggests that in these tissues, MYC-driven regeneration is additionally regulated by the availability of its co-activators. Another example of non-permissive cells are neurons, where MYC has been

shown to promote retinal ganglion cell survival and axon regeneration following injury to the optic nerve[69]. Mechanistically, MYC drives activation of the telomerase reverse transcriptase (TERT) as well as p53, and the MYC-TERT-p53 signaling pathway drives axon regeneration in vitro and in vivo following injury[70].

In conclusion, during embryogenesis, MYC is required to drive cellular proliferation to establishment proper tissue architecture and morphology. After birth, MYC is tightly regulated and remains inactive or at low levels unless cellular proliferation is required, such as during tissue regeneration following stress or injury. This is reflected in the fact that MYC's primary co-regulators, such as MAX, are highly stable proteins, positioning MYC stabilization as a decisive molecular switch for cell division[71, 72]. Following tissue repair, extrinsic signals subside and MYC levels return to physiological baseline, effectively releasing the accelerator pedal on cellular proliferation. The tightly controlled regulatory mechanisms of MYC allows tissues to regenerate when needed while preventing uncontrolled growth. However, if MYC becomes dysregulated, cellular proliferation remains constitutively active, and when the oncogenic "breaks" fail, MYC-driven growth ultimately leads to tumorigenesis. In the following sections, I will explore MYC's cellular functions and how they are altered during oncogenesis to support tumor progression.

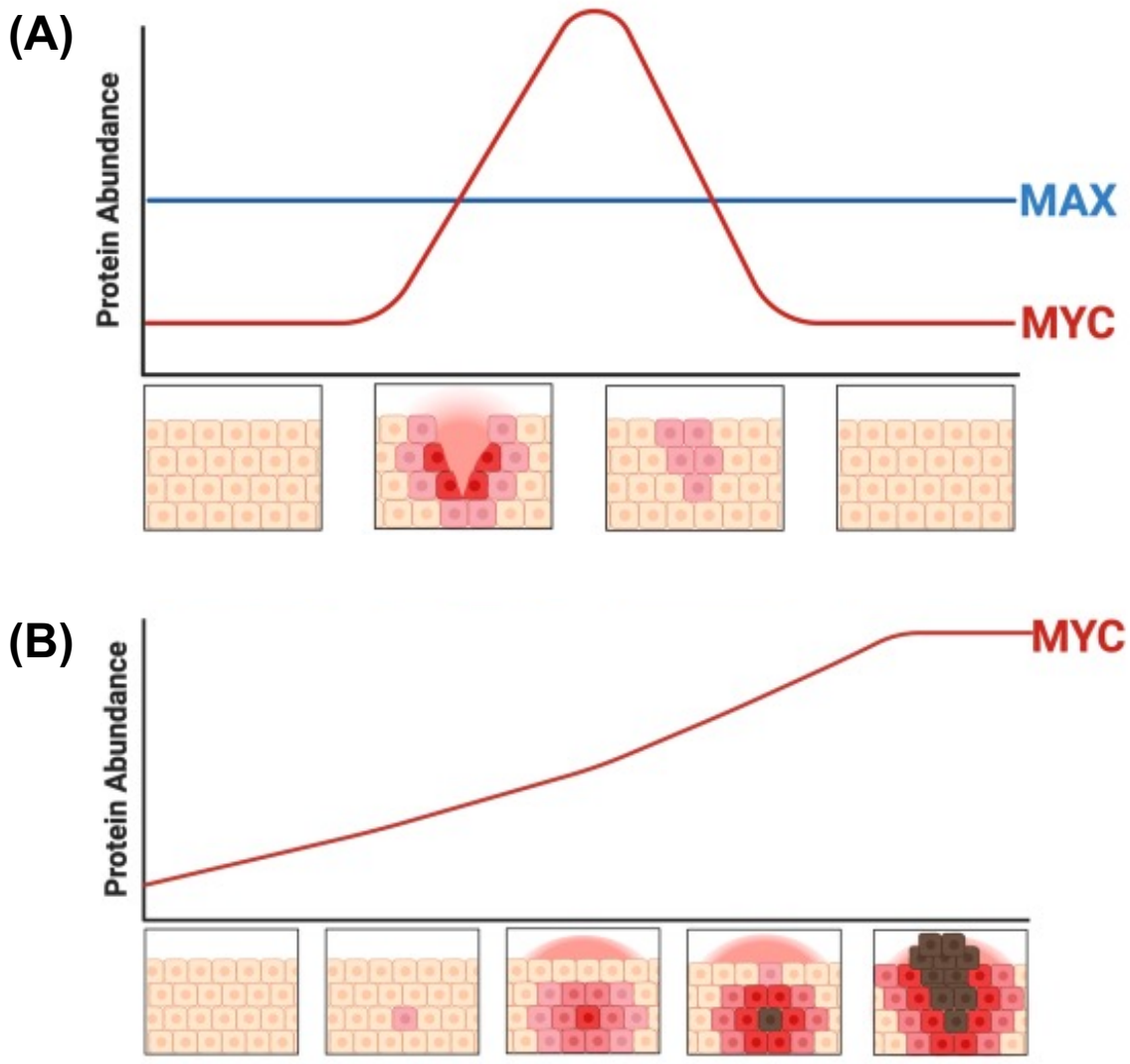

Figure 1.2.1 MYC Protein Stability Regulates Tissue Regeneration.

(**A**) In mammalian tissues, MYC protein is virtually undetectable until stabilized following a growth promoting signal, such as those triggered by wound healing after an injury (deep red cells). In contrast, MYC's co-activator MAX is constitutively expressed and is highly stable. The tight regulation of MYC stabilization enables cell growth and proliferation in response to external signals. Once the wound is healed and proliferative cues subside, MYC protein levels are rapidly diminished. (**B**) In the absence of injury, pre-cancerous mutations that stabilize MYC (pink cell) can induce a regeneration-like state, activating cellular growth and proliferation without the need for extrinsic signals. In the presence of additional genetic mutations, such as the loss of tumor suppressor genes, these pre-cancerous cells can progress into malignant tumors with constitutively stabilized MYC (black cells). Figure created with BioRender.com.

1.3 MYC Cellular Function

MYC as a Transcription Factor

Given that MYC lacks any known enzymatic domain but possesses a DNA-binding domain, its structure indicates that it functions as a transcription factor. Initial unbiased genome-wide investigations confirmed that MYC binds robustly to genes, with a preference for promoter regions. In Burkitt's lymphoma, it was estimated that MYC/MAX complexes occupy approximately 15% of all gene promoters[73]. Among these, MYC exhibits a higher affinity for promoters containing the consensus CACGTG DNA sequence, known as an E-box[74]. A large-scale screen of MYC-binding sites confirmed this affinity for E-box containing promoters but also revealed that MYC occupancy is largely governed by its tightly regulated protein abundance. Moreover, non-physiological levels of MYC can invade gene promoters indiscriminately, a phenomenon known as "MYC-saturation" [75]. Both MYC and MYCN have been implicated in regulating gene expression through binding to E-boxes within enhancer elements, showing identical abundance-dependent affinity dynamics to their association with promoter sequences. This enhancer association was shown to be tissue-specific, suggesting that MYC's target gene signature is less fixed than that of other transcription factors and can shift depending on cell type identity[76]. The vast number and diversity of MYC gene targets raises important questions about its function and underlying mechanisms in gene expression.

To address these questions, researchers examined MYC's protein interactome and revealed that its primary role in gene expression lies in its ability to rapidly recruit and release factors, enabling efficient transcriptional regulation[77-79]. To better understand MYC's immediate functional regulation, a pan-cancer study defined the Proximal MYC

Network (PMN), a superfamily of bHLHZ-containing proteins including MAX, MGA, MAD1, MAD3, MAD4, MXI1, MLXIP, MNX, MLX, and MLXIPL[5]. This study showed that MYC interacts with various PMN members to either induce or repress gene expression, helping to explain why widespread mRNA amplification often does not correlate with MYC promoter-binding[80]. A comprehensive understanding of the crosstalk between MYC and the PMN is still evolving; however, it is clear that MYC's ability to drive transcription is shaped by changes in its interactions with various transcriptional machinery (Figure 1.3.1). Initial studies revealed that MYC binds most strongly to E-box-containing promoters within pre-acetylated chromatin and further enhanced histone acetylation at these sites[75]. The transcriptional-activating function of MYC is universal and dependent on its interaction with the Transactivation/Transformation Association Protein (TRRAP)[81, 82], which functions as a scaffold for SWI/SNF chromatin remodelers[83] and histone acetyltransferases (HATs), GCN5 and Tip60[84]. The MYC-TRRAP-directed recruitment of HATs enables chromatin acetylation which is more permissive for RNA polymerase II (RNAPII) recruitment and subsequent transcription[85, 86]. On the other hand, different association of MYC and components of the PMN family can repress gene expression. For example, MYC's association with MIZ1 promotes the recruitment of co-repressors like histone deacetylases (HDACs) while disrupting MYC's recruitment of co-activator such as like CBP/p300[87-90]. The outcome of MYC-driven gene activation versus repression appears to depend on the stochiometric ratios between MYC and members of the PMN family; for example, a MYC/MIZ1 ratio greater than one promotes transcriptional activation, while a lower ratio favors repression [91]. Furthermore, higher levels of MAD and MNT family protein will displace MYC and heterodimerize with MAX at

gene promoters and facilitate the recruitment of HDAC1 and HDAC3 to promote gene silencing[92-94]. Altogether, MYC is a versatile and potent transcriptional modifier whose dynamic interactions with co-activator and co-repressors modulate gene expression across a significant proportion of the genome.

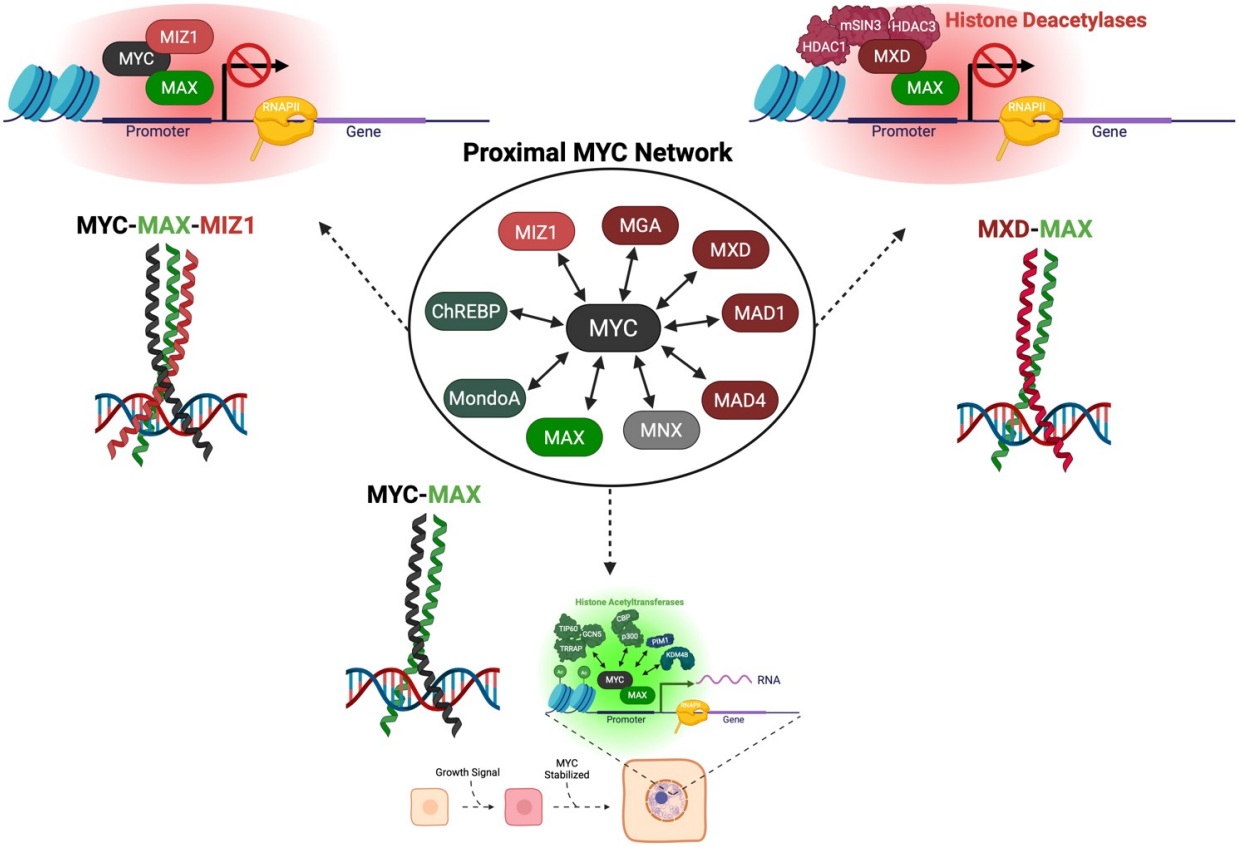

Figure 1.3.1 Proximal MYC Network (PMN) regulates the transcriptional outcome of MYC promoter binding. In response to growth signals, MYC is stabilized and recruited to target gene promoters. The specific composition of the proximal MYC network (PMN) determines whether MYC functions as a transcriptional activator (green) or repressor (red). Interactions with distinct PMN components modulate gene expression by facilitating the recruitment of chromatin-modifying complexes that either promote or suppress transcription at MYC-bound loci.

PIN1 Provides Dynamic Control of MYC in Response to Extrinsic Signals

The following section is a perspective article published in Frontiers in Cell and Developmental Biology in April of 2020. This perspective builds on the previous section by exploring how MYC's transcriptional activity and stability are regulated through protein-protein interactions with co-activators and co-repressors. Here, we focus specifically on the peptidyl-prolyl cis/trans isomerase NIMA-interacting 1 (PIN1), and how it temporally and spatially regulates MYC's function. We also introduce and discuss the implications of MYC's phosphorylation, a regulatory mechanism that forms the foundation for the research presented in this dissertation.

PIN1 Provides Dynamic Control of MYC in Response to Extrinsic Signals

Gabriel M. Cohn[1], Daniel F. Liefwalker[1], Ellen M. Langer[1,2,*], Rosalie C. Sears[1,2,3,*]

[1]Department of Molecular and Medical Genetics, School of Medicine, Oregon Health & Science University, Portland, Oregon 97239, USA;

[2]Knight Cancer Institute, Oregon Health & Science University, Portland, Oregon 97239, USA;

[3]Brenden-Colson Center for Pancreatic Care, Oregon Health & Science University, Portland, Oregon 97239, USA.

*Corresponding Authors:

Ellen M. Langer

langere@ohsu.edu

Rosalie C. Sears

searsr@ohsu.edu

Published in Frontiers in Cell and Developmental Biology in April 2020

Abstract

PIN1 is a phosphorylation-directed member of the peptidyl-prolyl *cis*/*trans* isomerase family that facilitates conformational changes in phosphorylated targets such as c-MYC (MYC). Following signaling events that mediate phosphorylation of MYC at Serine 62, PIN1 establishes structurally distinct pools of MYC through its *trans-cis* and *cis-trans* isomerization activity at Proline 63. Through these isomerization steps, PIN1 functionally regulates MYC's stability, the molecular timing of its DNA binding and transcriptional activity, and its subnuclear localization. Recently, our group showed that Serine 62 phosphorylated MYC can associate with the inner basket of the nuclear pore (NP) in a PIN1-dependent manner. The poised euchromatin at the NP basket enables rapid cellular response to environmental signals and cell stress, and PIN1-mediated trafficking of MYC calibrates this response. In this perspective, we describe the molecular aspects of PIN1 target recognition and PIN1's function in the context of its temporal and spatial regulation of MYC.

Introduction

Proline isomerization of cellular proteins provides post-translational control of target protein structure, and therefore function, within the cell. Proline residues within peptides can exist in two distinct energetically-stable states, *cis* or *trans*. While proline residues exhibit an intrinsic ability to isomerize, this process occurs on a very slow biomolecular timescale as a result of the high-energy barrier associated with this conformational change. This high-energy barrier isolates the *cis* and *trans* protein states, and rapidly switching between these two conformational states requires a catalyst. The

evolutionarily conserved peptidyl-prolyl *cis*/*trans* isomerases (PPIases) catalyze this conformational change and are required to drive isomerization in a timeframe relevant to dynamic signaling cascades within the cell [95, 96]. By functioning as molecular switches to toggle targets between their *cis* and *trans* conformations, these enzymes can affect target protein stability, localization, activity, and protein-protein interactions [95, 97, 98].

The Peptidyl-prolyl *cis*/*trans* isomerase, NIMA-interacting 1 (PIN1) is the only known PPIase that specifically recognizes phosphorylated serine or threonine residues that immediately precede a proline (pSer/pThr-Pro). This pSer/pThr-Pro motif accounts for over 25% of all phosphorylation sites identified in a global phosphorylation study [99]. The proline-directed kinases that target these sites are central to extracellular stimuli responses [100] and cell cycle progression [101, 102]. The selectivity of PIN1 for phosphorylated proteins provides it with the potential to modify and functionally regulate a variety of targets involved in these phospho-signaling cascades. Indeed, PIN1 has been shown to target important cell cycle phospho-proteins such as Cyclin D1 [103] as well as proteins in the NF-κB, WNT, and AKT pathways, where extrinsic signals result in phosphorylation-regulated cascades that ultimately alter gene transcription to affect cell phenotype [104-106]. Despite PIN1's involvement in critical signaling pathways, PIN1 null mice are viable. The major phenotype of mice lacking PIN1 is a defect in cellular proliferation that contributes to stunted body size and infertility [103, 107]. Consistent with this, mouse embryonic fibroblasts (MEFs) from PIN1 knockout mice, that exhibit similar proliferation relative to wildtype (WT) MEFs during asynchronous growth in culture, display significantly delayed proliferation relative to WT MEFs when stimulated with mitogens after being starved to G_0 arrest [107, 108]. This result supports an important

role for PIN1 in dynamic signaling pathways to elicit an efficient response to extracellular stimuli.

Loss of PIN1 also renders cells resistant to transformation and, strikingly, PIN1 knockout mice have delayed tumor formation when crossed with tumor-driving mutants of HER2 or RAS [109, 110]. Phospho-signaling is increased in cancer, often in a cell-intrinsic manner by oncogenic mutations in signaling pathways (e.g. RAS or HER2), but also through cell-extrinsic signals from the tumor microenvironment (e.g. TGFβ or FGF). These conditions lead to an abundance of proline-directed kinases driving oncogenic signaling cascades that control tumorigenic phenotypes [111]. PIN1 regulates a large number of these cancer-related targets from extracellular receptors such as NOTCH1 [112] or HER2 [113], to intracellular effector proteins like RAF1 [114] or FAK [115], and ultimately to transcription factors such as c-MYC [116], β-catenin [105], or NF-κB [104]. The overexpression of PIN1 is common in many types of cancer and is correlated with poor outcomes [101, 117]. For example, in pancreas cancer, elevated levels of PIN1 were shown to cooperate with MYC and NRF2 to maintain redox balance, allowing for tumor cell proliferation and survival [118] . In a mouse model of B-cell lymphoma, loss of PIN1 suppresses MYC-driven proliferation and lymphomagenesis [119]. In breast cancer, the overexpression of PIN1 can regulate Notch signaling and increase cancer stem cell-like phenotypes, including tumorigenicity and drug resistance [120, 121]. PIN1 also enhances the tumorigenic characteristics of mutant p53 in breast cancer by co-activating aggressive oncogenic transcriptional programs. When PIN1 expression is decreased, the malignant activity of mutant p53 is remarkably reduced [122]. A more comprehensive list of oncogenes and tumor suppressors that PIN1 can target is reviewed elsewhere [117].

Here, we discuss the role of PIN1 as a critical controller of dynamic phosphorylation signaling cascades in response to extrinsic signals that governs gene transcription to alter phenotypic responses in normal and diseased states. PIN1 affects a variety of target transcription factors in such cascades, but we focus on work describing PIN1's temporal and spatial control of the bHLH-LZ transcription factor c-MYC (hereafter MYC), which PIN1 functionally regulates in both physiologic and pathologic responses. We will describe how PIN1-dependent isomerization temporally and spatially influences the phosphorylation cascade that affects MYC stability and activity in the nucleus. Together, these roles frame PIN1 as a promising therapeutic target for controlling oncogenic MYC.

PIN1 regulates MYC stability and activity

The proto-oncogene *MYC* encodes a critical transcription factor that influences transcription across the genome to control a multitude of cellular processes including proliferation, survival, metabolism, and morphology [45, 75]. In physiologic conditions, MYC protein levels are mitogen responsive and are influenced by two sequential and interdependent, proline-directed phosphorylation events on Ser62 (pS62) and Thr58 (pT58) in the conserved MYC Box 1 (MB1) region of MYC's transactivation domain. Phosphorylation at each site influences PIN1's interaction with the MB1 region of MYC and isomerization at Pro63 [116, 123]. Briefly, MYC is stabilized and activated downstream of growth stimuli through RAS-induced kinases and/or cyclin-dependent kinases (CDKs), which phosphorylate MYC at Ser62 when Pro63 is in *trans* [124, 125]. Phosphorylation of Ser62 primes MYC for subsequent phosphorylation at Thr58 by the processive GSK3 kinase [126]. Phosphorylation at Thr58 then facilitates the proline-

directed, *trans*-specific phosphatase, PP2A-B56α, to remove the activating S62 phosphate [127, 128]. pT58-MYC is then targeted for ubiquitination by the E3 ubiquitin ligase Fbw7, resulting in MYC's degradation [129, 130].

As depicted in Figure 1.4.1, PIN1 plays a critical role regulating MYC stability and activity, as the kinases and phosphatase that target Ser62 and Thr58 are *trans*-specific enzymes. Thus, PIN1 can interrupt the progression of pS62-MYC through its degradation cascade by stabilizing Pro63 in the *cis*-conformation. This sterically protects the Ser62 phosphate from PP2A-mediated dephosphorylation, allowing for prolonged pS62-MYC interaction with DNA and increasing target gene transcription [116]. However, PIN1 can also direct MYC towards degradation following GSK3 phosphorylation of Thr58, associated with subsequent Ser62 dephosphorylation by the *trans*-specific phosphatase, PP2A-B56α [131]. Like Ser62, Thr58 is followed by a proline, however, Proline 59 falls within a poly-proline domain, likely structured as a rigid *trans* isomer helix [132]. Thus, while Thr58 phosphorylation introduces an additional binding site for PIN1, PIN1-mediated isomerization of MB1 is likely to center on the sterically more flexible Proline 63. From this, we speculate that the re-engagement of PIN1 with pT58 drives a *cis*-*trans* isomerization of Pro63, allowing for the function of PP2A at pSer62. However, additional research is required to understand precisely how Thr58 phosphorylation promotes the dephosphorylation of pSer62, and how this additional phosphorylation affects PIN1's activity on MYC.

Structural studies into PIN1's substrate interactions indicate that a flexible interdomain, which connects PIN1's WW phospho-substrate binding domain to its PPIase catalytic domain, can exist in different rigidity states that influence PIN1 target binding

and isomerase activity [133]. Furthermore, a study involving molecular dynamic simulations of PIN1 binding suggests that the two subdomains are allosterically regulated in a two-step mechanism. Upon initial substrate binding, PIN1 is primed in an enzymatically quiescent state until the substrate becomes phosphorylated and engages PIN1's WW domain, triggering PIN1-dependent isomerization [134]. In support of both primed and activated states for PIN1, a study specifically investigating PIN1's physical interactions with MYC demonstrated that PIN1 binds to unphosphorylated MYC at a conserved motif, designated MYC Box 0 (MB0), N-terminal to MB1 [123]. This pre-anchoring of PIN1 to the MB0 region resembles the first quiescent state of PIN1's substrate engagement, which precedes Ser62 phosphorylation. Phosphorylation of Ser62 triggers PIN1's WW domain binding and subsequent isomerization of Pro63. However, phosphorylation of Ser62 also increases the dissociation-rate of PIN1 from MB1, suggesting release following enzymatic conversion of Pro63 to *cis*. This dynamic interaction may provide a rational role for the additional phosphorylation at Thr58 to re-engage PIN1 with MB1 to mediate a second isomerization event from *cis* to *trans* at the more flexible Pro63. The dual function of PIN1 in promoting both MYC's activity and degradation through two isomerization events is supported by experiments assessing the effects of point mutations in the MB0 domain that disrupt PIN1 pre-anchoring or of PIN1 knockdown. Both conditions result a reduction in MYC DNA binding, and a corresponding decrease in target gene activation, cellular proliferation and cellular transformation, even though there is an increase in pS62-MYC and MYC stability [116, 123].

In addition to directly controlling the conformation of MYC to affect its activity vs. ubiquitination, other proteins regulate and are regulated by PIN1 that contribute to the

MYC degradation pathway. For example, PIN1 can downregulate the E3 ubiquitin ligase FBW7 [135], which could disrupt MYC degradation. SENP1 is an enzyme that deSUMOylates MYC, which reduces MYC's FBW7-directed ubiquitination and degradation; SENP1 also deSUMOylates PIN1 [136], which increases PIN1's activity [137]. PIN1 is also subject to phosphorylation that can decrease its catalytic activity [138]. These additional players and levels of post-translational control likely contribute to the differential regulation of PIN1 on MYC in physiologic and pathologic conditions, however, the molecular details require additional research.

PIN1 regulates temporal and spatial dynamics of MYC

Understanding the dynamics of MYC regulation is critical in order to elucidate the pleiotropic effects of MYC in the genome and its control of diverse cellular phenotypes. PIN1 plays a key role in this regulation by imparting both temporal and spatial regulation of MYC activity in the nucleus. Temporal studies of MYC DNA binding revealed that MYC oscillates on and off DNA at E-box containing promoters in response to cell growth signaling [116]. This dynamic binding of MYC to DNA is dependent on Ser62 and Thr58 phosphorylation and PIN1-mediated Pro63 isomerization. Timed MYC DNA binding assays indicate that phosphorylation of Ser62 accelerates MYC E-box promoter binding in a PIN1-dependent manner while Thr58 phosphorylation accelerates the release of MYC from DNA. This mechanism creates an oscillatory binding of MYC to target gene promoters with a periodicity of approximately 20 minutes, and loss of PIN1 suppresses this cyclic DNA binding. The temporal control of MYC by PIN1 also regulates its association with its co-activators, which similarly oscillate on and off DNA, in a PIN1-dependent manner, with the same kinetics as MYC (e.g. p300, GCN5, CDK9, and SNF5).

MYC's dynamic binding to coactivators and DNA affects subsequent gene expression by triggering RNA polymerase release and elongation [139]. Inhibition or reduction in PIN1 levels results in decreased MYC oscillation on DNA and decreased MYC-dependent gene expression, even with an observed increased in MYC protein levels [116].

In addition to temporally regulating MYC activity, PIN1 regulates the subnuclear localization of MYC under normal mitogen stimulation conditions, during wound healing, and in cancer cell lines [108]. Initial observations of MYC at the nuclear periphery were recently extended to show that transcriptionally active pS62-MYC associated with Lamin A/C [140-142]. This observation is surprising since the majority of chromatin in lamin-associated domains (LADs) at the nuclear periphery is transcriptionally silent heterochromatin. At the nuclear pore, however, there are regions of open chromatin that are poised for transcription [143-145]. Using proximity ligation assay (PLA) with confocal microscopy and super-resolution stochastic optical reconstruction microscopy (STORM), we showed that pS62-MYC associated with the interior basket proteins of the nuclear pore complex (NPC) [108]. Although the mechanism of pS62-MYC trafficking to the nuclear pore remains unclear, PIN1-mediated isomerization is necessary for stabilizing pS62-MYC at the NPC. In addition, the recruitment of MYC-associated coactivators and epigenetic modifiers, such as GCN5, to the NPC is also PIN1-dependent. This PIN1-dependent spatial reorganization of MYC appears to impact epigenetic regulation in response to extrinsic signals. Upon serum stimulation in starved MEFs, the PIN1-dependent trafficking of pS62-MYC and its associated epigenetic modifiers to the nuclear pore results in increased histone acetylation and transcription of NPC-resident genes. Whether this also involves oscillatory DNA binding by MYC at these NPC-resident genes

will require future research. Global chromatin accessibility assays indicate that early response chromatin site opening is PIN1-dependent and overlaps with MYC gene program activation, suggesting that these early events involve NPC-associated euchromatin. In the absence of PIN1, the cellular response to mitogen stimulation is delayed, which results in reduced cellular proliferation as well as decreased MYC-associated chromatin remodeling, supporting a critical role for PIN1-MYC regulation of NPC associated euchromatin for efficient response to cellular stimulation.

The PIN1-driven spatial reorganization of MYC to specific chromatin domains at the nuclear pore suggests that post-translational control of transcription factors in response to environmental signals may dictate their involvement in regulating specific topologically associated domains or TADs. Interestingly, the number and composition of nuclear pores is increased and altered in cancer cells [146, 147]. In addition, the nuclear pore region is speculated to be a site of epigenetic memory for genes associated with rapid response to environmental signals [148]. PIN1 drives a relocation of MYC to chromatin regions at the nuclear pore, and if these regions comprise a subset of rapid response genes, this could provide a mechanism for MYC's differential activity on subsets of cell-context specific genes [108, 149].

These findings suggest that in response to extrinsic signals, PIN1 facilitates the generation of a distinct pool of post-translationally modified MYC that associates with chromatin near the inner basket of the nuclear pore. This pool may be distinct from the population of MYC within the nuclear interior that binds promoter regions in open chromatin. There is much discussion in the field for whether oncogenic MYC acts as a global transcriptional amplifier or if there is a more specific MYC-driven gene program

that drives malignancies [150-154]. Our data suggest that the PIN1-dependent subnuclear reorganization of MYC into distinct pools might allow a population of MYC to drive a specific subset of genes, while the PIN1-independent population may accomplish its global transcriptional amplification function. Future investigation into the dynamic distribution of MYC's transcriptional activity is necessary for bolstering this hypothesis.

Conclusion

Here we present a perspective of the role of PIN1 in regulating dynamic response phenotypes, focusing on its isomerization of MYC in multiple cellular contexts. PIN1's interaction with and isomerization of MYC supports the physiologic and oncogenic activity of MYC [108, 116, 123, 131, 155]. Mechanistically, this involves regulation of MYC stability, its DNA binding and transcriptional activity, and its subnuclear localization to the nuclear pore. In normal cells, PIN1's regulation of MYC contributes to increased proliferation, migration, and wound healing [108]. In cancer, PIN1's regulation of MYC has been shown to affect oncogenic transformation, proliferation, redox maintenance, and cell survival [108, 116, 118, 119, 123]. PIN1 fine-tunes the rapid spatial and temporal control of MYC by integrating isomerization of Pro63 with the sequential phosphorylation events at Ser62 and Thr58 (Figure 1). Whether the dynamic nature of PIN1-dependent regulation of MYC extends to PIN1-dependent regulation of other transcription factors will be of great interest.

Multiple efforts to therapeutically reduce or control MYC's oncogenic activity have been unsuccessful for several reasons, including an inability to specifically control MYC expression and the lack of an enzymatic region to target with small molecules [45]. The

direct targeting of PIN1 to modulate MYC activity provides a promising therapeutic opportunity with numerous drugs under investigation [96]. For example, the inhibition of PIN1 with PiB reduced the rate of MYC binding to target DNA promoters in MCF10A cells, leading to decreased expression of oncogenic gene signatures and decreased tumor growth [116]. In addition, Juglone [156] and ATRA [157] have been shown to potently reduce PIN1's oncogenic activity in breast cancer models; however, the efficacy of these drugs on reducing MYC's oncogenic activity remains to be studied. Furthermore, a recent covalent PIN1 inhibitor, KPT-6566, has shown potency for reducing PIN1-dependent cancer phenotypes [158]. Since PIN1 null mice are viable, taking advantage of the upstream functional control of phosphorylated MYC via PIN1 enzymatic blockade could reduce systemic toxicity associated with total loss of MYC, while specifically targeting

signaling-activated oncogenic MYC. This specificity provides a compelling rationale for PIN1-dependent therapeutic strategies to treat MYC-dependent cancers.

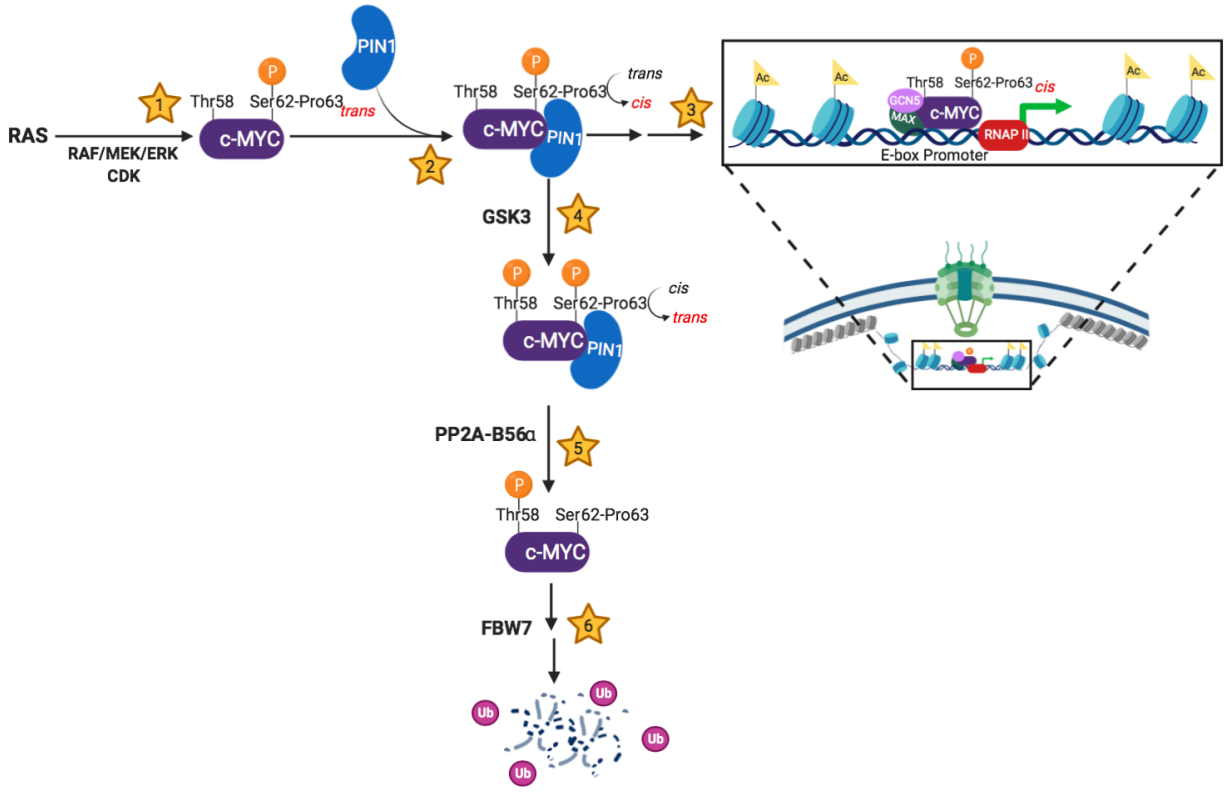

Figure 1.3.2 Schema showing PIN1's involvement in the molecular events regulating MYC's stability and activity.

(**1**) c-MYC becomes transcriptionally active following Ser62 phosphorylation by *trans*-specific RAS-induced kinases and/or cyclin-dependent kinases (CDKs). (**2**) PIN1 stabilizes pSer62-Pro63-MYC in the *cis* conformation, sterically preventing phosphatase activity. (**3**) The transcriptionally active, pSer62-*cis*-Pro63-MYC has increased DNA binding to E-box promoters and increased co-activator association (MAX, GCN5, etc.), which results in increased chromatin accessibility. Additionally, PIN1-directed isomerization of pSer62-MYC has been shown to locate MYC to the basket of the nuclear pore. (**4**) c-MYC is directed towards degradation via Thr58 phosphorylation by the GSK3 kinase. This phosphorylation event promotes phosphatase activity at pSer62, which requires a *cis* to *trans* isomerization of pSer62-Pro63-MYC. (**5**) The *trans*-specific phosphatase, PP2A-B56α, removes the activating phosphate on Ser62-MYC. (**6**) pThr58-MYC signals the E3-ubiquitin ligase, FBW7, to poly-ubiquitinate c-MYC, leading to proteasome degradation. Created with Biorender.com.

MYC as a Global Amplifier of Transcription

MYC's nearly ubiquitous association with all actively transcribed and open promoters[159] suggests that it functions as a global amplifier of transcription. However, distinguishing between MYC's sequence-specific target gene activation and general amplification functions remains a subject of ongoing debate within the field. One widely supported hypothesis posits a dosage-dependent switch in which low protein levels of MYC selectively regulate a conserved set of target genes, whereas saturating levels of protein MYC lose DNA sequence specificity and amplify gene expression at all activated genes. Initial evidence showed that high levels of MYC drove a 2-3-fold increase in total RNA production, suggesting that MYC does not function as a simple on/off switch of transcription but rather as a nonlinear amplifier of gene expression acting universally on all active genes. [150, 153]. Given that transcription is a multistep and energetically demanding biological process, MYC is thought to amplify basal transcription of active genes by facilitating the rapid recruitment of co-activators, thereby alleviating key rate-limiting steps in gene expression[77, 160, 161]. Transcriptional kinetic studies demonstrated that MYC extends the residency of core transcriptional machinery at gene promoters, universally extending the duration of transcriptional ON-time, while the frequency of these events remained unchanged[162]. Furthermore, MYC overexpression leads to the formation of punctate MYC-foci at super-enhancers and increases the frequency of contacts between TADs, promoting robust promoter-enhancer interactions and enhancing transcriptional output[163].

For MYC-driven transcriptional amplification to occur, MYC recruits key co-activators to lower the activation energy required at each step of the transcription

process[164]. For example, to reinforce transcriptional initiation, MYC preferentially recruits the TATA-binding protein (TBP) to promoters already occupied by basal transcriptional machinery, enhancing the formation of the TFIID initiation complex further[165]. To promote the transition from transcription to elongation, MYC recruits factors that facilitate RNAPII Serine-5 phosphorylating of its C-terminal domain[166, 167]. MYC directly binds to and recruits SPT5, a subunit of the DSIF elongation complex, to RNAPII, thereby triggering the initiation of transcriptional elongation[168]. The positive transcription elongation factor b (P-TEFb) is a key multiprotein complex essential for transcriptional elongation and is tightly regulated through SUMOylation of its catalytic subunit, CDK9 for proper Serine-2 phosphorylation of paused RNAPII. CDK9 SUMOylation inhibits global transcriptional activity by preventing the interaction between CDK9 and Cyclin T1, which is necessary for P-TEFb activation. MYC robustly promotes RNAPII pause release by enhancing Serine-2 phosphorylation through suppression of CDK9 SUMOylation, thereby ensuring efficient formation and activation of the P-TEFb complex[169, 170]. Altogether, MYC is capable of amplifying transcriptional activity by recruiting key co-activators to each step of transcription. Although this evidence is compelling, the field remains unconvinced that transcriptional amplification is MYC's sole function, as MYC's occupancy at promoters and enhancers appears to be independent

of RNA amplification. This suggests that, beyond its canonical role, MYC also carries out distinct, non-canonical functions, which will be explored in the following sections.

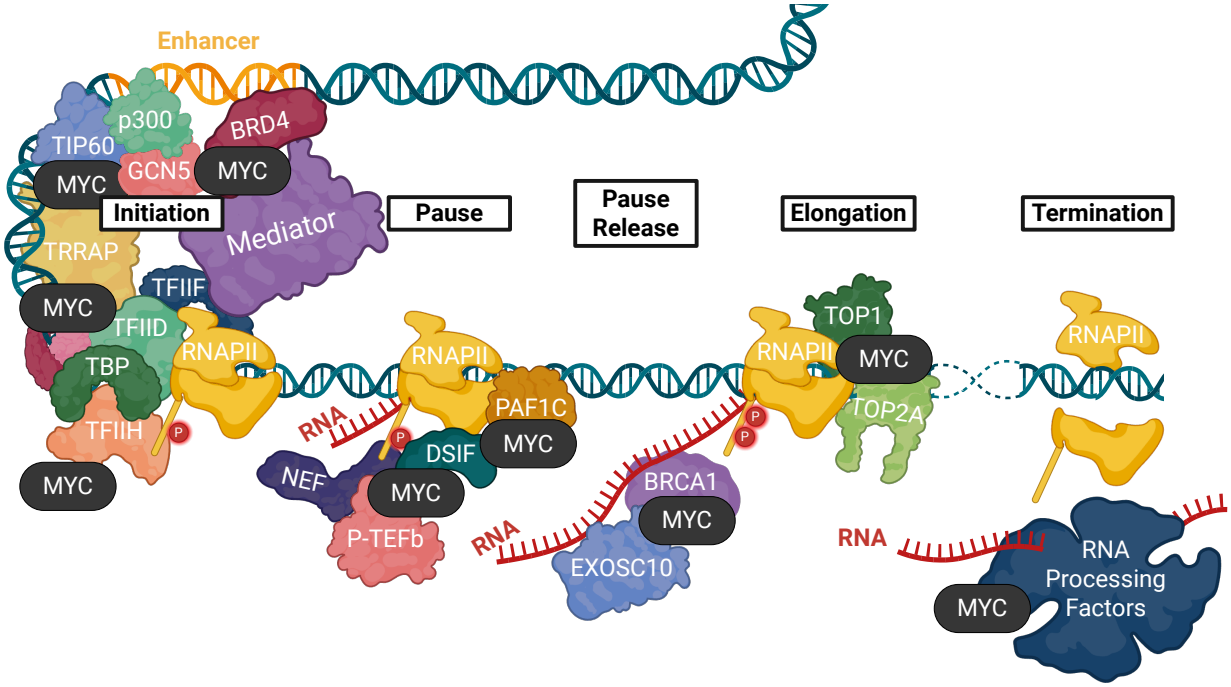

Figure 1.3.3. MYC Amplifies Transcription Through Facilitating the Recruitment of Co-Activators.

Schematic illustrating the major stages of mammalian transcription and the protein complexes MYC is known to recruit at each step. In addition to recruiting co-activators, MYC prolongs their dwell time, enhancing RNA polymerase activity and amplifying gene expression. The MYC-driven recruitment is modulated by its stability and regulated by the proximal MYC network factors, such as MAX, which enhances recruitment or MIZ-1, which attenuates it (not shown). Figure generated using BioRender.com.

1.4 MYC and Genomic Instability

Preface

"The capacity to blunder slightly is the real marvel of DNA. Without this special attribute, we would still be anaerobic bacteria and there would be no music."

-Dr. Lewis Thomas[171] (American physician and poet)

Arguably, the greatest survival hurdle during oncogenesis is overcoming the burden of genomic damage that accompanies cellular transformation. Over billions of years, evolution has refined mechanisms that support cellular growth and proliferation while preserving genomic integrity. The resulting DNA damage repair (DDR) mechanisms have evolved to maintain a delicate balance to ensure multicellular survival by detecting and repairing DNA damage, while remaining tightly linked to apoptosis to prevent the accumulation of deleterious mutations which promote tumorigenesis. Since MYC is essential for tumorigenesis and contributes to drug resistance against DNA-damaging chemotherapeutics, its role in genomic instability has been extensively studied. MYC's role in genomic instability appears to be context-dependent, with enigmatic results that vary depending on experimental design which are compounded by the presence of additional co-mutations. Thus, a paradoxical relationship emerges between MYC and genomic instability, as studies have shown that elevated MYC levels promote DNA damage while also augmenting DNA repair. In the following section, I will summarize the major findings and argue that MYC contributes to oncogenesis in distinct co-mutational backgrounds where elevated MYC activity enhances DDR and promote tumor survival.

MYC Drives Cell Cycle Progression

Under non-oncogenic, physiological conditions, MYC levels are effectively undetectable in G0 and quiescent cell states but rise sharply following mitogen stimulation, where MYC regulates the transition into G1[172-174]. MYC promotes the expression of numerous genes that drive cell cycle progression while repressing cell cycle antagonists[175]. In line with this, MYC knockout in rat fibroblasts results in significantly prolonged G1 and G2 phases, along with a marked delay in S-phase entry[176]. MYC is such a potent driver of cell cycle progression that its ectopic expression can lock a cell in constitutive proliferation, bypassing the need for mitogen stimulation[177]. The cell cycle is tightly regulated to ensure accurate cell division without genomic alterations, and accelerating this process inevitably increases replication stress and genomic damage[178]. During oncogenesis, MYC functions like a stuck accelerator pedal for cellular proliferation, driving tumorigenesis at the expense of increasing genomic instability. Overexpression of MYC disrupts key cell cycle checkpoints, including impairing G1/S arrest in response ionizing radiation[179]. In normal human mammary epithelial cells, MYC-driven inappropriate entry into S phase following irradiation led to the emergence of a sub-G1 population characterized by severe aneuploidy. Furthermore, MYC prevented DNA damage-induced G2/M cell cycle arrest following ionizing radiation by upregulating cyclin B1[180]. In these normal cells, the MYC-driven checkpoint attenuation ultimately sensitized the cells to apoptosis, highlighting that elevated MYC is toxic to normal cells. To survive high levels of MYC, tumor cells need to accumulate synergistic mutations that accommodate the accelerated proliferation. This is evidence by the fact that inhibition of the tumor suppressor protein p53, or its downstream target

$p21^{CIP/WAF}$, significantly alters MYC-driven proliferation[174], a topic that will be discussed further in a later section.

MYC Promotes DDR Signaling

One of the earliest responses to DNA double-strand breaks is the activation of Ataxia telangiectasia mutated (ATM) kinase, which initiates the DDR signaling cascade with the phosphorylation-direct foci formation of histone H2AX (γH2AX) and other proteins such as Nijmegen Break Syndrome (NBS1). In rat cells, following ionizing radiation or exposure to the bacterial cytolethal distending toxin, the formation of γH2AX and NBS1 foci was found to required MYC[181]. In HeLa cells, the kinetics and efficacy of DNA double-strand break repair were found to be significantly impaired in the absence of MYC[182]. This study also demonstrated that phosphorylated serine-62 MYC impacted ATM kinase activity and formed overlapping foci with γH2AX and phosphorylated DNA-PKcs (This co-localization is explored further in Chapter 3). Taken together, these findings suggest that MYC can enhance DDR signal cascades following DNA damage exposure.

MYC Transcriptional Regulation of DDR

Among its many target genes, MYC binds to and regulates the expression of several key DNA repair proteins and is thought to maintain their abundance to support rapid proliferation[73, 183]. DNA replication increases the risk of DNA damage accumulation, and MYC as well as MYCN have been shown to directly upregulate all three components of the MRN complex (MRE11-RAD50-NBS1) which is essential for sensing and repairing DNA damage[184, 185]. The MRN complex directly activates and recruits ATM to sites of DNA damage, initiating phosphorylation and activation of key DDR proteins such as histone H2AX, CHK2, and p53[186, 187]. MYC's transcriptional

upregulation of the MRN complex suggests there is possibility of a feedback loop in which ATM activation enhances DDR protein expression through MYC-driven transcription. At the transcriptional level, MYC has been shown to upregulate components of both HR and NHEJ pathways for DSB repair pathways[188]. However, since MYC's stability is increased during the cell cycle, and HR is primarily active during S and G2 phases, greater attention has been given to MYC's role in on HR-directed repair. For example, MYC induction was shown to increase both *Hus1* and *Rad1* which protein products association with RAD9 to form the 9-1-1 complex which drives HR-direct DNA repair[189]. Furthermore, MYC upregulates HR-repair protein RAD51, a mechanism that led to a synthetic lethality clinical trial combining inhibition of PARP1 and MYC activity in triple-negative breast cancer[183, 190]. This highlights a dependency on MYC-induced HR protein expression and efficient of DNA repair. To reduce stalled replication forks and subsequent DNA damage, MYC upregulates nucleotide biosynthesis, ensuring sufficient supply for rapid genomic duplication[191]. MYC's transcriptional role in DDR is not limited to gene activation; following UV-induced damage, MYC was shown to inhibit p53-mediated cell cycle arrest by binding to MIZ1[87]. Mechanistically, MIZ1 is negatively regulated by TopBP1 and UV irradiation releases MIZ1 allowing it to bind to MYC. The binding of MIZ1 to MYC negatively regulates *p21Cip1* (CDKN1A) gene expression which subsequently reduces p53-induce cell cycle arrest. Although MYC can regulate numerous DDR proteins, MYC-dependent transcription alone was not sufficient to sensitize cells to ionizing radiation or mitomycin C[183], suggesting that MYC's contribution to genomic stability may involve additional functions beyond transcriptional regulation.

MYC Augments DNA Repair

MYC drives numerous cellular functions, most notably cellular proliferation, primarily through transcriptional amplification. These two processes substantially increase the risk of DNA damage through replication stress and transcription induced torsional stress, both of which are exasperated during oncogenesis[192, 193]. In line with the MYC driven recruitment of transcriptional regulators described in previous sections, MYC also promotes the accumulation of key DNA maintenance machinery to support transcriptional amplification while minimizing DNA damage. At active promoters, MYC couples transcriptional elongation with DSB repair through the transfer of PAF1c onto RNAPII to ensure genomic integrity[194]. Transcription significantly increases the risk of recently transcribed RNA hybridizing with DNA to form R-loops, a physical obstacle that can cause DNA damage when they collide with various helicases involved in both transcription and DNA replication. MYCN was shown to recruit BRCA1, along with the endonuclease EXOSC10, to paused RNAPII, where it helps to stabilize an mRNA decapping complex and prevent the formation of R-loops[195, 196]. MYCN's recruitment of BRCA1 and EXCOSC10 was also directed to stalled replication forks, where it played a protective role in preventing transcriptional-replication conflicts. These conflicts become significantly more frequent during oncogenesis due to amplified transcription and disruption of replication timing[197, 198]. MYC's involvement in DNA repair has been shown to be responsive to a variety of cellular stressors, including disruptions in DNA replication, mRNA splicing, transcriptional elongation, and proteasomal degradation processes. Following these cellular perturbations, part of the stress response involves pausing or terminating critical processes such as transcription and replication to prevent DNA damage accumulation. MYC was shown to play an integral role in this signaling

response by dissociating from active promoters and forming large multimeric sphere-like structures, helping to prevent transcription-replication conflicts and promote transcriptional termination[199]. These multimeric structures enable robust MYC directed recruitment of ATR, FANCD2, and BRCA1 to stalled replication forks, preventing their degradation and reducing DNA damage at those sites.

Much like its role in driving transcriptional amplification, MYC helps prevent DNA damage through its interactome, safeguarding genomic fidelity at sites most vulnerable to genomic instability. In fact, these MYC-driven functions appear to be independent of each other in certain contexts. A clear example is MYC's well characterized interaction with the HAT complex NuA4/TIP60, which primarily promotes chromatin relaxation enabling robust MYC-driven transcription[200]. However, haploinsufficiency of TIP60 in a MYC-driven lymphoma model did not affect MYC-driven transcription but resulted in a significant increase in DNA damage, suggesting that through its interactome, MYC promotes genomic maintained to ensure robust gene expression[201]. In line with this, the transcriptional process generates significant torsional stress, creating both positive and negative supercoiling of the DNA, which would inevitably hinder gene expression and promote DNA damage if not properly resolved[192, 202]. To support MYC's transcriptional amplification, MYC assembles a "topiosome" complex at actively transcribed genes with both topoisomerases 1 and 2, stimulating their activities to relieve the transcription induced torsional stress[203]. Since topoisomerases cleave DNA to relieve torsional stress, the MYC-topiosome has been proposed to become acutely DNA damaging when MYC is hyperactive. This led to the discovery of a shift in topoisomerase association from the MYC-topiosome to a p53-topisome, which promotes MYC's

proteasomal degradation and activates p53 target genes when the DNA damage burden becomes too great[204]. This cross talk between MYC and p53 in the context of DNA damage is paramount for understanding how MYC contributes to genomic integrity in a normal cell compared to a cancer cell that lacks functional p53 pathway activity. This crosstalk will be explored further in the following section.

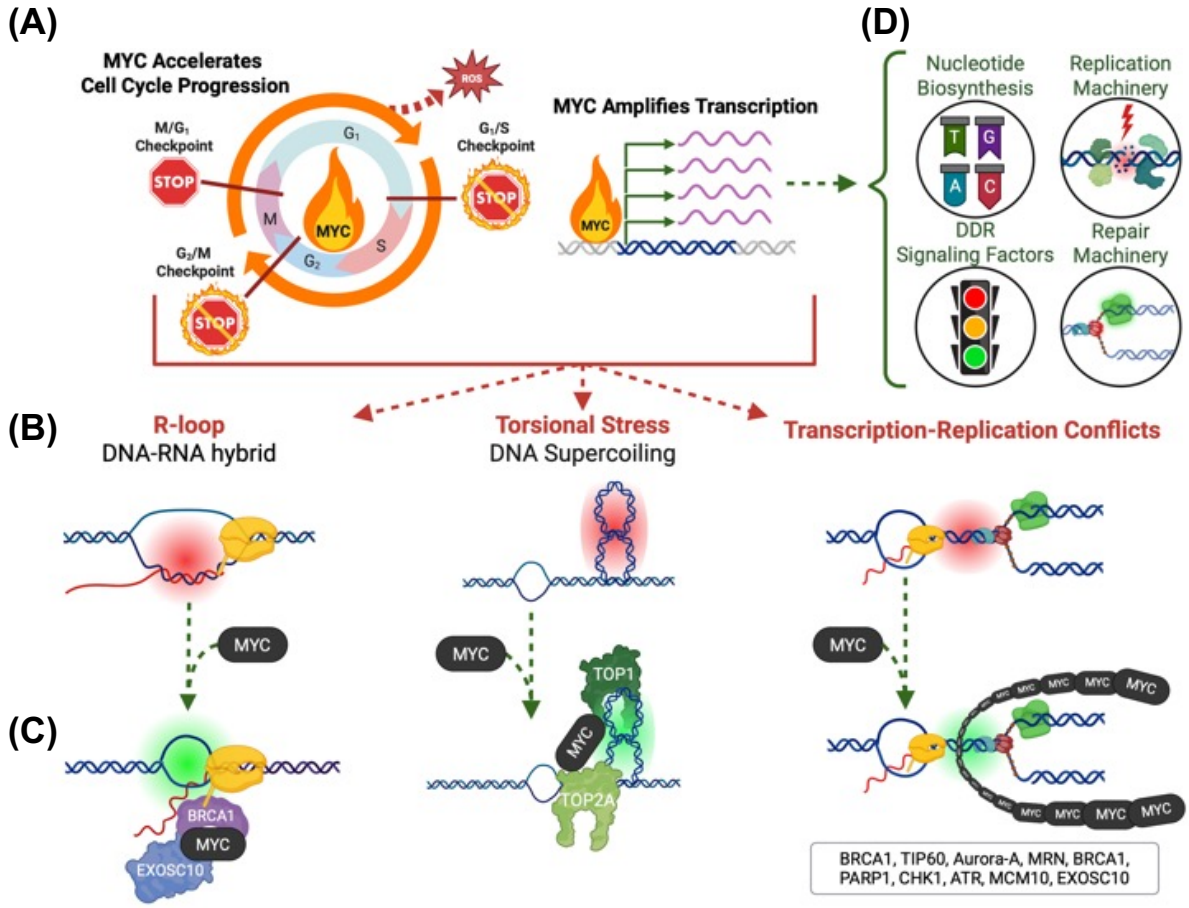

Figure 1.4.1 Summary of MYC's Involvement in Genomic Stability.

(A) MYC promotes cell cycle progression, and when deregulated will disrupt both G1/S and G2/M checkpoints. MYC modulates metabolic processes to support cell growth and division, a function that concurrently leads to the production of reactive oxygen species (ROS). In addition, MYC can broadly amplify gene expression across the genome. (B) Together, these MYC-driven processes elevate genomic stress by promoting R-loop formation, DNA torsional strain, and altered replication timing, ultimately increasing

transcription-replication conflicts. (C) In response to elevated genomic stress, MYC engages genoprotective mechanisms to maintain genome integrity. It recruits factors such as BRCA1 and EXOSC10 to stalled RNAPII to prevent R-loop formation and assembles a topiosome complex with TOP1 and TOP2A to alleviate torsional strain. Under conditions that heighten transcription-replication conflicts, MYC also recruits additional stabilizing proteins and forms multimers to shield replication forks from RNAPII. (D) In addition, MYC transcriptionally upregulates factors that mitigate genomic stress during cell cycle, including enzymes for nucleotide biosynthesis, components of the replication machinery, DNA damage response (DDR) proteins, and DNA repair proteins. Figure generated using BioRender.com

MYC and p53: The Accelerator Versus the Brake Pedal of Oncogenesis

Before delving into the molecular crosstalk between MYC and p53, I will first briefly explore the evolutionary implications of this relationship. MYC is essential for driving the transformation from a single fertilized egg to an organism composed of trillions of cells. Consequently, blocking MYC expression in mice results in embryonic lethality before day 10.5 of gestation[51]. The emergence of multicellularity necessitates extensive cellular proliferation, inherently increasing the risk of acquiring genetic mutations. This would suggest that larger animals, having more cells, should experience a higher incidence of cancer compared to smaller ones. This postulate was investigated in the 1970s by English epidemiologist and statistician Sir Richard Peto, who discovered that at the species level, cancer incidence does not correlate with the number of cells in an organism[205, 206]. This observation, known as Peto's paradox, suggests that increased cellular proliferation is accompanied by the evolution of strict and efficient mechanisms to correct errors and suppress oncogenic growth. This paradox reinforced the scientific pursuit to understand what oncogenic-suppressive mechanisms larger animals possess. In 2015, researchers involved with the San Diego Zoo discovered that elephants carry 19 additional copies of the tumor suppressor gene, *TP53*, compared to humans[207, 208]. This increase in p53 provides enhanced genomic surveillance and ensures reliable elimination of cells

harboring oncogenic mutations through cell-cycle arrest and/or apoptosis. Although no single mechanism fully explains Peto's paradox, the crosstalk between p53 and MYC is highly conserved and tightly regulated to support decades of tumor free survival in humans and other larger organisms. Loss of p53 signaling loss is widely considered a necessary step for the progression of MYC-driven oncogenes.

Transcriptionally, WT p53 strongly represses *myc* gene expression, whereas mutant p53 expressing cells lose the repression of MYC, contributing to dysregulated MYC activity [209, 210]. The accumulation of p53 and MYC within the cell is cell state dependent and mutually exclusive. In response to DNA damage, there is an oscillatory increase in p53 which drives a corresponding counter-oscillatory decrease in MYC[211]. Additionally, RNA sequencing of newly transcribed RNA revealed a global decrease in gene expression, with the most highly transcribed genes showing the greatest reduction, while p53 target genes remained unaffected. Counteracting this p53 driven reduction by ectopic expression of MYC decreased cell-cycle arrest and increased apoptosis following DNA damage[212]. There are a few proposed mechanisms by which MYC and p53 counteract cell cycle progression. For example, following DNA damage, p53 induces the expression of the growth asset and DNA-inducible 45 alpha protein (GADD45A), which suppresses cellular proliferation in response to genotoxic stress. Ectopic expression of MYC has been shown to override this growth arrest by suppressing *gadd45* gene expression, thereby promoting continued cell cycle progression[213]. One of p53's most well-established target gene is *CDKN1A*, which encodes the protein p21, a potent inhibitor of cyclin-dependent kinases (CDKs). By inhibiting CDKs, p21 promotes cell cycle arrest, particularly at the G1/S transition, allowing time for DNA damage repair before the

cell resumes division[214]. Elevated levels of MYC form a repressive complex with MIZ1 at the *CDKN1A* promoter, inhibiting its p53-induced expression in response to DNA damage[90, 215, 216]. The MYC-driven decrease in p21 occurred independently of an increase in CDKs or other cyclins, highlighting how elevated MYC can disrupt p53-signaling pathways[217]. Furthermore, following DNA damage, the p53-p21 axis induces either cell cycle arrest or apoptosis and MYC's suppression of p21 drives the p53 response to favor apoptosis[218]. This underscores how the abundance of MYC protein influences apoptosis in the context of functional p53, a critical barrier that must be overcome during oncogenic progression. Taken together, p53 counteracts and abolishes much of MYC-driven activity in the presence of cellular stress such as genomic instability (Figure 1.4.2)

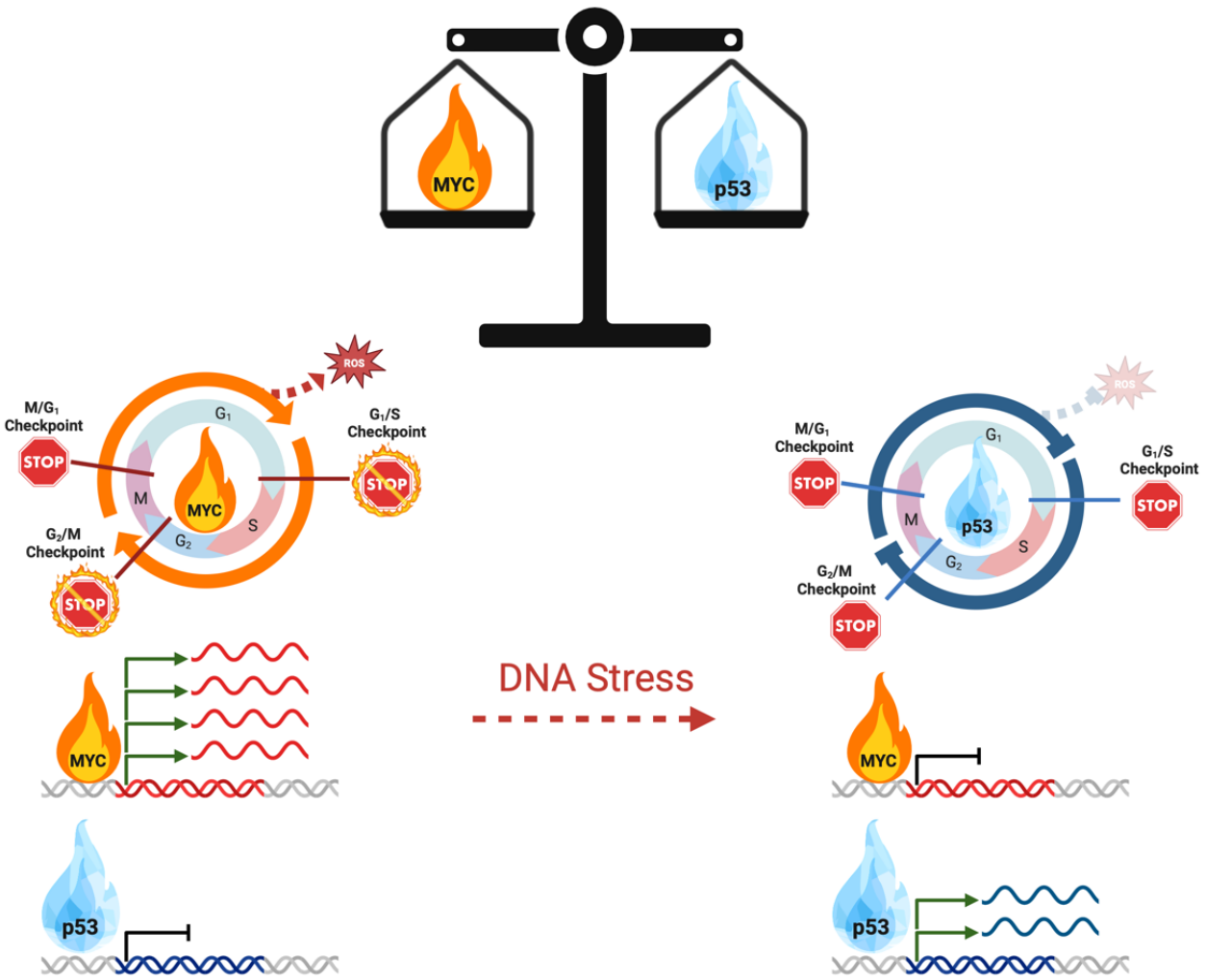

Figure 1.4.2 MYC and p53 form a dynamic, antagonistic regulatory axis that integrates cellular stress signals to determine cell fate. Under normal conditions, MYC promotes cell cycle progression and transcription of pro-proliferative genes, while p53 restrains these processes to maintain genomic integrity. In response to DNA damage, this balance shifts as p53 activation suppresses MYC expression and activity, tipping the transcriptional landscape toward growth arrest or apoptosis depending on cellular context and MYC abundance.

MYC Drives Apoptosis in the Context of Functional p53 Signaling

In non-transformed cells, p53 facilitates the rapid decrease in MYC levels in response to DNA damage, halting MYC-driven processes that promote genomic instability, such as gene amplification and rapid cellular proliferation (discussed further in the next section). In cellular contexts with functional p53 signaling, alterations that stabilize MYC levels shift the p53-driven response to DNA damage towards accelerated cellular apoptosis[219]. This influence appears to be cell cycle dependent, as MYC-induced expression of Cyclin A and subsequent activation of CDK2 were required for the early initiation of apoptosis in G2 phase, but had no effect during G1 phase[220]. Mechanistically, in response to MYC deregulation in both cells and mouse models, the accumulation of DNA damage activates ATM signaling cascade, which in turn triggers p53-driven cellular apoptosis[221]. In Rat1 fibroblasts, both topoisomerase 1 and 2 poisons, camptothecin (CPT) and etoposide (ETO), induce apoptosis through p53 and activation of protein kinase C delta (PKCδ). This apoptotic response was abrogated in MYC null cells and resulted in reduced p53-induced activation of PDCδ, highlighting that MYC abundance influences p53 mediated apoptosis[222, 223]. MYC was also shown to inhibit the expression of antiapoptotic proteins BCL-XL and BCL-2[224]. MYC-driven apoptosis following either CPT or ETO can be blocked by the ectopic expression of HSP70, which disrupts MYC-induced caspase activation[225]. In MYC-deficient intestinal enterocytes, p53 activation was abrogated following both ionizing irradiation and cisplatin treatment[226]. In these MYC knockout cell lines, this p53 inactivation was linked to the upregulation of the E3 ubiquitin ligase MDM2, which promoter p53 degradation. Furthermore, low level overexpression of MYC had no effect on basal apoptosis but

triggered robust apoptosis following DNA damage, further highlighting the intimate crosstalk between MYC and p53 in regulating the apoptotic response. In summary, p53 functions as a tumor suppressor by eliminating MYC dysregulated cells.

Coordinated MYC Suppression in Response to Genotoxic Stress

The crosstalk between MYC and p53 creates a dynamic push and pull between promoting proliferation and enforcing cell cycle arrest or apoptosis in response to DNA damage. An imbalance of excessive MYC or loss of p53 leads to increased genomic instability, as initially observed with transient MYC expression overriding cell-cycle checkpoints and promoting tumorigenesis[227, 228]. MYC overexpression has also been shown to increase reactive oxygen species and impair DSB repair, resulting in substantial accumulation of chromosomal damage in untransformed cells[229-231]. Therefore, in response to DNA damage, cells activate several mechanisms to rapidly downregulate MYC, a process that has been extensively reviewed[232]. As DNA damage accumulated following 24 hours of treatment with topoisomerase inhibitors in MCF-7 cells, MYC mRNA and protein levels decreased by more than 90 percent[233-236]. Several mechanisms have been proposed to explain MYC's reduction in response to DNA damage. Following etoposide or UV treatment, p53 upregulates the microRNAs miR-34c and miR-130a, which bind to the 3'-untranslated region of MYC mRNA to suppress its translation[237, 238]. In cells lacking p53, miR-34c was induced through an alternate pathway involving p38 MAPK and its downstream affecter MK2. DNA damage induces MYC protein degradation through the ubiquitin-proteosome system[239]. Following UV irradiation, the ubiquitin-specific protease USP28 dissociates from the F-box protein FBW7, permitting MYC ubiquitination and subsequent degradation[240]. FBW7 triggers MYC degradation

following phosphorylation at threonine 58[130, 241]; however, UV-induced MYC degradation still occurred in cells expressing T58A- and S62A-MYC mutants. This suggests that FBW7 may bind to an alternate site on MYC or that an indirect intermediate protein is involved in this degradation mechanism[242]. In summary, MYC overabundance is acutely toxic to the genome through multiple mechanisms, and its degradation, largely driven through p53-signaling, is necessary for maintaining genomic integrity. During oncogenesis, the loss of p53 and other tumor suppressor functions occurs alongside MYC overactivity. This creates immense selective pressure for cancer cells to adapt to MYC's dominant mutator phenotype, which accelerates the intrinsic mutation rate to acquire additional oncogenic "hits"[243]. In this context, through years of cellular selection, mutations arise in MYC-driven tumors that become oncogene-addicted, meaning their survival and function are coopted to mitigate the stress associated with dysregulated MYC. The concept of MYC-addicted tumors and their targetable vulnerabilities will be explored in the next section.

Strategic Vulnerabilities: Targeting MYC-Addicted Tumors with Lessons from World War II

MYC's potent biological role can be distilled to its function as a driver of cellular growth and survival. During oncogenesis, additional mutational "hits" such as the loss of p53 disable normal cellular checkpoints, leaving MYC activity unchecked. This creates strong selective pressure for cells that harbor mutations that mitigate MYC-induced stress, establishing MYC's ability to drive cellular transformation as a "mutator phenotype"[243, 244]. Since MYC activity is disproportionally increased in the majority of human tumors[245, 246], targeting MYC has been the focus of a multidecade pursuit[247]. Directly targeting MYC has shown some promise in the clinic but remains

challenging due to several factors, including MYC's essential role in normal cell biology[247]. As a result, research into targeting MYC-driven vulnerabilities to specifically cripple tumors with MYC high activity remain a promising therapeutic strategy. In theory, applying the logic of survivorship bias to oncogenesis suggests that cells lacking specific adaptations to MYC-induced vulnerabilities are selected against and eliminated. Consequently, the MYC-high tumors we observe represent only those that have survived the vulnerability of oncogenesis. This logic of survivorship bias finds a compelling historic parallel in the work of the Jewish Hungarian mathematician, Abraham Wald, who studied bomber aircrafts during World War II. While working with the Statistical Research Group at Columbia University to apply statistical methods to reduce bomber loss from enemy fire, Wald observed that bullet holes on returning aircrafts were unevenly distributed. The highest concentration of damage was found in the fuselage, leading the military to initially assume that this area required additional protection. Wald corrected this survivorship bias by proposing that the true vulnerabilities lay in areas without bullet holes, such as the engines, since damage to these regions would likely down the plane, leaving no data from aircrafts that sustained such critical hits[248, 249]. This concept of survivorship bias can be applied to therapeutic targeting strategies for MYC-driven tumors. Just as the absence of bullet holes in certain areas on bombers indicate fatal vulnerabilities, the survival mechanisms observed in MYC-high tumors reflect acquired adaptations that may be exploited for therapeutic gain. Thus, by identifying these vulnerabilities in MYC-driven tumors, we can develop therapeutic strategies that induce synthetic lethality and selectively trigger tumor cell death.

In MYC-driven tumors, the constant pressure to proliferate creates a critical vulnerability by increasing replication stress, which the cell compensates for through a variety of targetable mechanisms. For example, the key component of the cohesin complex, RAD21, was found to be dispensable in MYC-driven transcription but essential to mitigating MYC-induce replication stress[250]. Inactivation or loss of RAD21 triggered a strong replication stress response, altered replication fork dynamics, and led to cell-cycle arrest in MYC-driven tumor cells. The MYC-induced acceleration of S-phase also relies on the Werner DNA helicase protein (WRN) to prevent replication stress catastrophe[251]. The WRN helicase is involved in repairing defective replication structures, and its depletion leads to cellular senescence and death in the context of MYC overexpression. In neuroblastoma, where MYCN is amplified in approximately 25 percent of the human tumors, inhibition of MRE11 using its pharmacological inhibitor Mirin results in significant accumulation of replication stress and subsequent DNA damage[252]. MRE11 is a key component of the MRN complex (MRE11-RAD50-NBS1), which is essential for sensing and repairing DSBs. MYCN also transcriptionally upregulates all three components of the MRN complex[73, 184, 185]. In breast cancer stem-like cells, the minichromosome maintenance protein 10 (MCM10) was shown to compensate for MYC-induced DNA replication stress, providing a strong preclinical rationale for targeting this dependency in MYC-driven tumors[253]. Beyond directly targeting replication stress machinery, inhibiting factors involved in DDR signaling can also induce synthetic lethality in MYC-driven tumors. For example, targeting the multifunctional protein TRIM33 led to the accumulation of replication-induced DNA damage, which delayed oncogenesis in cells overexpressing MYC[254]. Synthetic lethality was also identified between MYC and

the DNA dependent protein kinase catalytic subunit (PRKDC), where ablation of PRKDC selectively killed of MYC-high tumor cells in a pooled short hairpin RNA screen[255].

Vulnerabilities in MYC-driven tumors can also be exploited through combination therapies, such as the dual inhibition of Aurora-A and ATR kinases, which has shown efficacy in high risk MYCN-amplified neuroblastoma[256]. Mechanistically, during S-phase, MYCN is stabilized by Aurora-A kinase, and together they suppress R-loop formation. Inhibition of Aurora-A disrupts this interaction, leading to increased transcription-replication conflicts and activation of ATR, which in turn initiates DDR signaling. Dual inhibition of both Aurora-A and ATR impairs the cell's ability to resolve the MYCN-induced DNA damage, resulting in the selective death of MYCN-driven neuroblastoma cells. In MYC overexpressing ovarian cancer, the combination of Olaparib, a PARP1/2 inhibitor, and Palbociclib, a CDK4/6 inhibitor, demonstrated synergistic effects both in vitro and in vivo[257]. Olaparib induces widespread DNA damage; however, cells that upregulate DDR pathway activity can survive, leading to the development of Olaparib-resistant tumors. CDK4/6 is transcriptionally regulated by MYC, and Palbociclib induces homologous recombination (HR) deficiency by reducing MYC-driven activation of HR pathway genes. The combination of Palbociclib and Olaparib disrupts the MYC-induced upregulation of HR pathway genes, resulting in increased cell death and tumor regression. This mechanism is echoed in triple-negative breast cancer (TNBC), where MYC activity is associated with Olaparib sensitivity[258]. Knockdown of the PRMT1 arginine methyltransferase reduced MYC stability and led to decreased expression of HR-related genes in TNBC.

In summary, MYC-driven tumors present a complex interplay between unchecked proliferation and adaptive response that mitigate lethal DNA damage. Although these tumors evolve to survive the onslaught of MYC-induced replication stress, they do so by selecting for cells that harbor fragile compensatory mechanisms. By uncovering these vulnerabilities, from compromised replication machinery to dysregulated DDR signaling, we can identify novel targets for synthetic lethality. This knowledge lays the groundwork for therapeutic strategies aimed at selectively eradicating MYC-high tumors while sparing normal cells.

1.5 Conclusions

A multiscale examination of MYC's biological function reveals how tissue-level processes such as regeneration and tumor growth arise from molecular mechanisms that govern MYC's stability and activity. In adult tissues, MYC supports cellular proliferation but remains tightly regulated, becoming active only in response to growth signals such as during tissue regeneration[57, 63]. Oncogenic transformation involves genetic alterations that compromise the regulatory control of MYC, leading to persistent proliferative signaling. This drives the development of tumors with elevated replication stress and genomic instability, which nevertheless persist by acquiring adaptive survival mechanisms that can resist DNA damaging therapies. The work presented in this dissertation interrogates the regulatory molecular mechanisms that govern MYC's ability to drive rapid cellular proliferation and promote cell survival in the face of genomic damage. MYC's function within the cell is governed by post-translational modifications and dynamic alterations in its interactome, which together influence its stability, activity, and spatial distribution within the nucleus. Therefore, I hypothesize that changes in MYC's phosphorylation status and associated interactome regulate its activity in response to distinct cellular stimuli. Chapter 2 will characterize the dependence of MYC's nuclear pore-associated interactome and function on PIN1 following mitogen stimulation. Chapter 3 will investigate how MYC's phosphorylation status influences its association with DNA double-strand breaks and examine the dynamic remodeling of its interactome under replication stress. In Chapter 4, I will discuss the broader implications of my dissertation findings on the field of MYC biology, highlighting its roles in both normal physiological function and during oncogenesis.

Chapter 2: Characterization of the PIN1-Dependent MYC Interactome at the Nuclear Pore.

Gabriel M. Cohn[1], Yulong Su[2], Colin J. Daniel[1], Hisham Mohammed[1,4], Daniel F. Liefwalker[3], Rosalie C. Sears[1,5,6]

[1]Department of Molecular and Medical Genetics, School of Medicine, Oregon Health and Science University, Portland, OR, USA

[2]Fred Hutch Cancer Center, University of Washington, Seattle, WA, USA

[3]Department of Biochemistry and Biophysics, Oregon State University, Corvallis, OR, USA

[4]Center for Early Detection Advanced Research, Oregon Health and Science University, Portland, OR, USA

[5]Brenden-Colson Center for Pancreatic Care, Oregon Health and Science University, Portland, OR, USA

[6]Knight Cancer Institute, Oregon Health and Science University, Portland, OR, USA

Corresponding Author:

Rosalie C. Sears

Oregon Health & Science University

searsr@ohsu.edu

2.1 Abstract

MYC is a potent master transcriptional regulator that regulates many cellular processes such as cell growth, proliferation, and its aberrant activity is involved in driving almost all hallmarks of cancer. MYC is essential for wound healing following tissue injury, as it drives cellular proliferation and differentiation required for effective tissue repair. Despite its well-establishes roles, the molecular mechanisms by which MYC translates extrinsic growth signals to promote cellular proliferation and tissue regeneration remain incompletely understood. Signal transduction activates genes that are trafficked to the nuclear pore for efficient gene expression through a process known as gene gating, and MYC has been implicated in facilitating this serum-induced activity at the nuclear pore. Here, we demonstrate that the peptidyl-prolyl *cis*/*trans* isomerase PIN1 is essential for regulating MYC's DNA binding and its association with the nuclear pore complex (NPC) in mouse embryonic fibroblasts (MEFs) and pancreatic ductal adenocarcinoma (PDAC) cells. Using a combination of quantitative chromatin immunoprecipitation (qChIP), proximity ligation assays (PLA), and rapid immunoprecipitation mass spectrometry of endogenous proteins (RIME), we show that loss of PIN1 markedly reduces MYC binding to target genes and disrupts a shared serum-responsive interactome between MYC and the NPC. Furthermore, we develop a MYC- and NUP153-BioID2 system to enable future characterization of subtle changes in MYC's interactome at the nuclear pore. Our findings suggest that MYC may participate in gene gating at the NPC and that targeting PIN1 could serve as a potential therapeutic strategy to reduce MYC-driven transcription at the NPC, thereby impairing MYC function in MYC-driven tumors.

2.2 Introduction

MYC is one of the most investigated master transcription factors which regulates the expression of at least 15% of the entire genome[44] with distinct regulatory roles in major cellular processes such as apoptosis, cell cycle progression, proliferation, and differentiation and many others[6, 75]. MYC protein is tightly regulated through the deposition and removal of specific post-translational modifications (PTMs) which orchestrate its transcriptional activity & stability, and more recently, its localization within the nucleus. MYC protein levels stabilize downstream of mitogen stimuli through RAS-induced and/or cyclin-dependent kinases phosphorylation of serine 62 (pS62-MYC)[131, 259]. The phosphorylation-directed peptidyl-prolyl *cis*/*trans* isomerase, NIMA-interacting 1 (PIN1), further stabilizes pS62-MYC by isomerizing proline 63 into the *cis*-conformation, which sterically protects pS62-MYC from dephosphorylation by the *trans*-specific PP2A phosphatase[123, 127]. PIN1-direct stabilization of pS62-MYC promotes MYC's engagement with target genes and its interaction with coactivators such as p300, GCN5, SNF5, and CDK9, facilitating robust MYC-driven transcription[116].

In addition to temporally regulating MYC activity, PIN1 also controls the subnuclear localization of MYC in response to various extrinsic signals, such as serum-stimulation and wound healing. Following stimulation, PIN1 drives the interaction of pS62-MYC with euchromatin associated with the nuclear pore complex (NPC) where it is thought to regulate a subset of inducible gene programs [108]. Additionally, global chromatin accessibility investigation indicated that the serum-induced early response of chromatin opening is PIN1-dependent and coincides with MYC target gene activation. When PIN1 is lost, the cellular response is delayed, resulting in reduced proliferation, suggesting that

PIN1-directed trafficking of MYC to the NPC regulates a subset of serum-responsive gene programs. MYC's association with the NPC suggests that it may play a role in gene gating, a mechanism where actively transcribed genes are tethered to the NPC, coupling transcription, nuclear export, and translation to ensure robust gene expression in response to stimuli[260, 261].

Further investigation is required to understand the underlying mechanisms of MYC's interaction with the NPC and how these interactions contribute to MYC-driven cellular processes. To explore this mechanism, we apply a MYC proteomic and genetic approach to define MYC's interactome at the nuclear pore following serum stimulation. We demonstrate that PIN1 is essential for regulating MYC's DNA binding and its association with the NPC in response to serum stimulation in PDAC cells. We show that PIN1 modulates MYC's interactome by promoting interactions with coactivators and transcriptional machinery, thereby facilitating gene gating and robust gene expression of growth-promoting pathways. Targeting PIN1 disrupts MYC target gene engagement and the serum-responsive interactome at the NPC, underscoring its potential as a therapeutic target in MYC-driven cancers.

2.3 Results

PIN1 regulates MYC's binding to target genes and its association with the nuclear pore complex in human PDAC cells.

To investigate how PIN1 affects MYC's target gene engagement, we conducted MYC chromatin immunoprecipitation followed by quantitative PCR (qChIP) in HPAFII cells with PIN1 knockdown. In addition to knockdown, we used two PIN1 inhibitors, PiB and Sulfapin. Consistent with our lab's prior studies showing that PIN1 enhances MYC's DNA binding, preliminary studies in PDAC lines show that shPIN1 reduced MYC binding to the target genes E2F2 and NCL1 compared to scramble control (Figure 2.3.1A,B). PiB treatment also reduced MYC's target gene engagement, lowering binding to both E2F2 and NCL1 compared to the vehicle control. Sulfapin reduced MYC binding to E2F2 but did not affect binding to NCL1 in these preliminary experiments. Our lab previously demonstrated that PIN1 is required for the trafficking of phosphorylated serine-62 MYC (pS62-MYC) to the nuclear pore complex (NPC) in response the serum stimulation in mouse embryonic fibroblasts. To validate these findings in conventional human PDAC cells, we performed proximity ligation assays (PLA) in MIA PaCa-2 cells and observed a strong association of MYC and pS62-MYC with PIN1 as well as with NUP153, a component of the NPC (Figure 2.3.1C,D,E). In agreement, we see that the interaction between MYC and NUP153 is robustly responsive to serum stimulation (Figure 2.3.1F), suggesting that MYC may play a serum-responsive role at the NPC in human PDAC cells. To begin to explore the relevance of MYC's association with the NPC in patient PDAC cell lines, we performed PLA in early passage patient-derived cancer cell line (ST-00013312). We observed a robust interaction between MYC and NPC basket

components (NUP153 and TPR), but limited interaction with NUP98, a component of the NPC inner rings (Figure 2.3.1G,H). Interestingly, MYC's association with NUP153 in ST-00013312 cells is responsive to chemotherapy, as demonstrated by a dose-dependent increase following Olaparib treatment (Figure 2.3.1I). In response to stimuli, transcriptionally activated genes translocate to the nuclear pore, coupling transcription, nuclear export, and translation for rapid gene expression, a process known as gene gating [260-262]. To determine whether MYC and NPC share binding to target genes, we performed qChIP using transcriptionally activated pS62-MYC and Mab414, a pan NPC antibody that detects phenylalanine-glycine repeat motif found in many nucleoporins. We observed robust binding of pS62-MYC and Mab414 to known MYC target genes, NCL1 and SYT1 in MIA PaCa-2 cells (Figure 2.3.1J, K). Furthermore, gemcitabine treatment in MIA PaCa-2 cells resulted in robust interaction of total MYC (N262 antibody), pS62-MYC, and Mab414 with the SYT1 gene (Figure 2.3.1L). However, this induction was greatly reduced upon PIN1 knockdown compared to the scramble shRNA control. Together, these findings suggest that PIN1 regulates MYC's engagement with target genes and its association with the NPC, particularly in response to serum stimulation and chemotherapy. Our results further support the hypothesis that MYC plays a role in gene gating at the nuclear pore, with PIN1 being critical for this process in human PDAC cells.

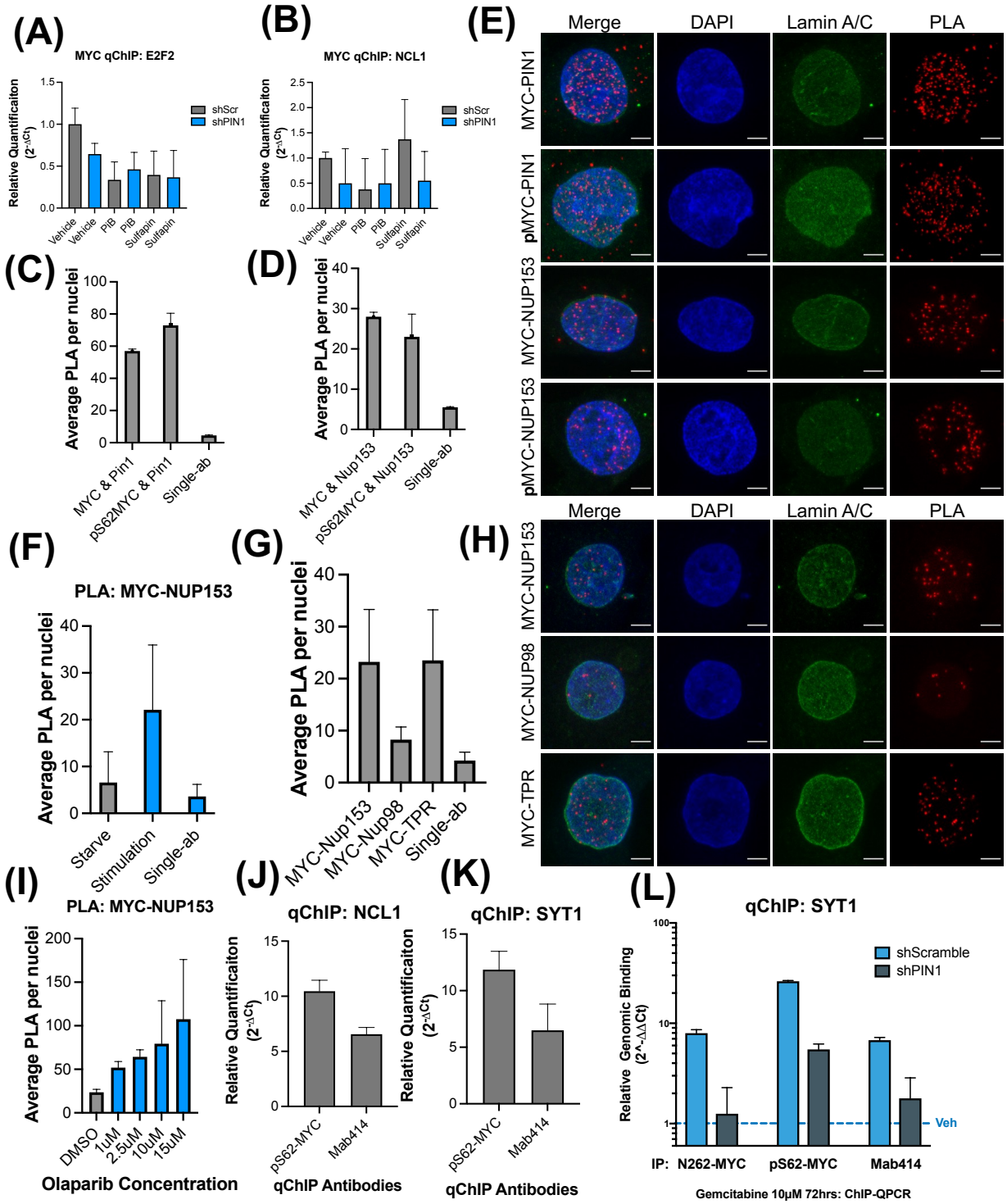

Figure 2.3.1. PIN1 regulates MYC's binding to target genes and its association with the nuclear pore complex in human PDAC cells.

(A, B) qChIP of MYC binding to E2F2 and NCL1 in HPAFII cells with either shPIN1 or shScramble (shScr) control. Treatments included 24-hour incubation of either DMSO (vehicle), Sulfopin (2.5μM), or PiB (1.5μM). (C, D) Quantification of average PLA per nuclei between either MYC or pS62MYC (pMYC) with PIN1 or NUP153 in MIA PaCa-2 cells and representative images in (E) with Lamin A/C co-stain. (F) Quantification of average PLA per nuclei between MYC-NUP153 following 0.2%FBS serum starvation or 4-hour 20% FBS serum stimulation in MIA PaCa-2 cells. (G) Quantification of average PLA per nuclei between MYC-NUP153, -NUP98, or -TPR in ST-00013312 patient derived PDAC cell line with representative images in (H). (I) Quantification of average PLA per nuclei between MYC-NUP153 following 48-hours of Olaparib treatment in ST-00013312 cell line. (J,K) qChIP of either pS62-MYC or Mab414 binding to NCL1 or SYT1 in MIA Paca-2 cells. (L) qChIP binding of MYC, pS62-MYC, or Mab414 to SYT1 following 72-hour 10μM gemcitabine treatment in shScramble or shPIN1 MIA PaCA-2 cells. All experiments are n=1 and error bars are SD.

PIN1-dependent MYC interactome in response to serum stimulation.

To investigate MYC's role in gene gating, we first examined how PIN1 influences MYC's interactome and target gene engagement using rapid immunoprecipitation mass spectrometry of endogenous proteins (RIME)[263]. We performed RIME in mouse embryonic fibroblasts (MEFs) using either IgG antibody control or MYC (N262) antibodies for pulldown, comparing genetic PIN1 knockout ($PIN1^{-/-}$) or sibling MEF wild-type (WT) cell lines under serum-starved or 4-hour, 20% serum-stimulated conditions. Unfortunately, the DNA precipitated from this experiment was insufficient for DNA sequencing; however, co-immunoprecipitation (Co-IP) followed by mass spectrometry successfully detected a total of 1,481 target proteins. After normalization and background subtraction of the IgG control, we performed fold change analysis on the MYC-interacting targets to compare enrichment in response to serum-stimulation in WT or $PIN1^{-/-}$ MEFs. MYC-interacting targets were then manually clustered into nine groups based on the magnitude of serum-induced fold changes between WT or $PIN1^{-/-}$ conditions (Figure 2.3.2A). We identified a serum-responsive, PIN1-dependent cluster of 181 MYC-interacting targets, where the fold change was high in WT but greatly diminished in $PIN1^{-}$

$^{/-}$ condition (Figure 2.3.2A: 0,High). This suggests that PIN1 loss prevents MYC's serum-induced interaction with these targets. We then investigated MYC's interactome network within this cluster using the StringApp in Cytoscape[264-266] and confirmed that PIN1 was a key component in the cluster (Figure 2.3.2B). To gain insight into the function of the PIN1-dependent serum-induced MYC interactors, we performed Gene Ontology (GO) biological process and Reactome pathway enrichment analysis. The top hits align with MYC's canonical functions in response to serum-stimulation, including gene expression, RNA metabolism and ribosome biogenesis (Figure 2.3.2C,D). These results highlight a critical role of PIN1 in facilitating MYC's interactome in response to serum stimulation.

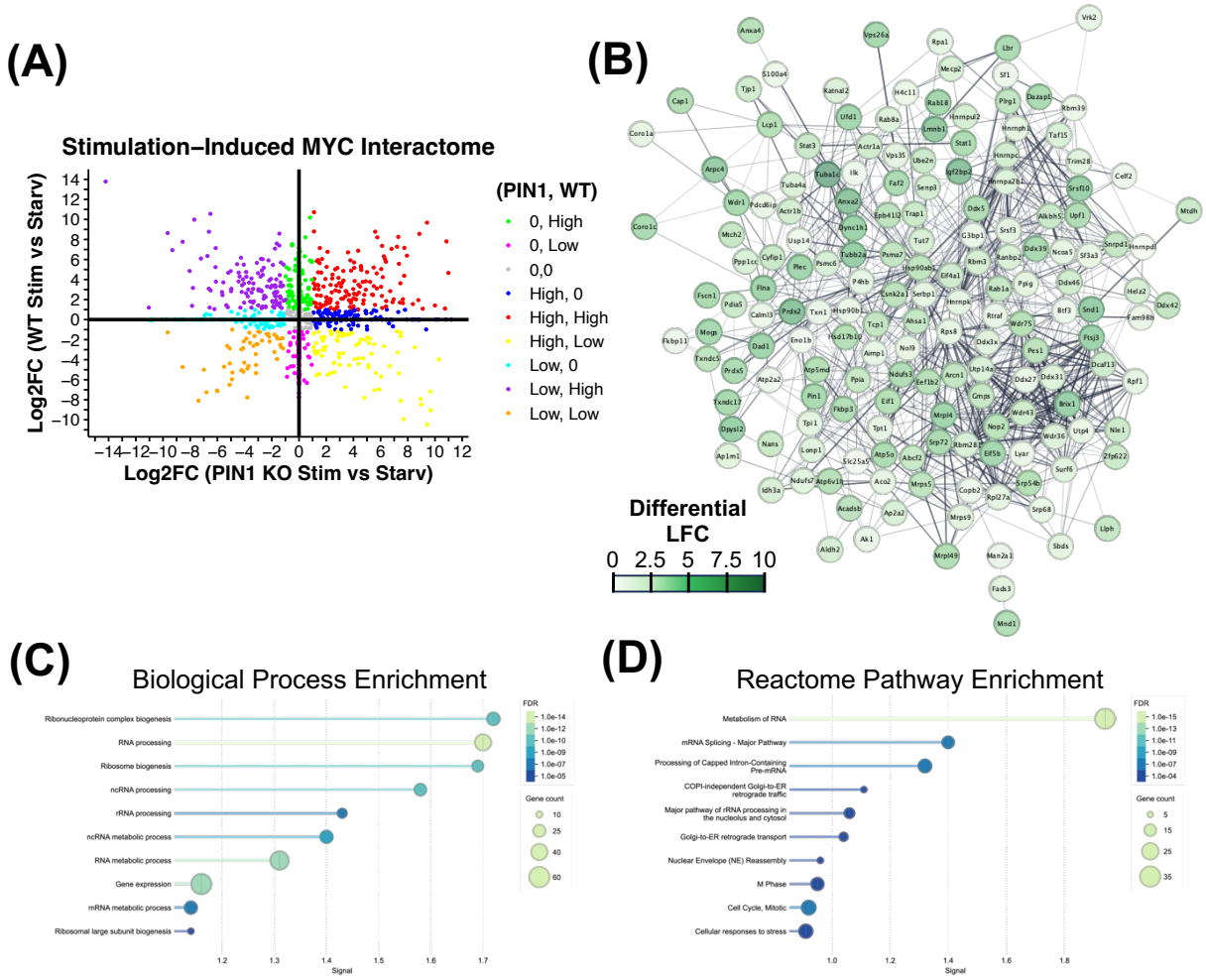

Figure 2.3.2. PIN1-dependent MYC interactome in response to serum stimulation.

(A) Clustered classification following Log2FC of MYC interacting targets following serum stimulation in either WT or PIN1KO MEFs. Targets that had a FC between -1 and +1 were classified as “0”, otherwise a less than -1FC was classified as “Low” and a +1FC was classified as “High”. (B) Cytoscape STRING analysis of MYC interacting targets that were in the PIN1=”0” and WT=“High” (lime green) cluster in (A). Darkness of green shading denotes differential in LFC with a larger value representing a greater serum-induced difference between WT and PIN1KO MEFs. (C) Top ten Gene Ontology Biological Process enrichment scores for targets identified in (B). (D) Top ten Reactome Pathway enrichment scores for targets identified in (B).

PIN1 is crucial for the overlap of MYC-NPC interactomes that drive MYC-mediated transcriptional responses to stimuli.

Since MYC's association with the nuclear pore following serum-stimulation is reliant on PIN1 [108], we included two NPC antibodies in the RIME experiment: TPR (nuclear pore basket) and Mab414, a general NPC antibody that recognizes phenylalanine-glycine repeats found in several nucleoporins. Similar to MYC's interactome, we identified 186 TPR-interacting targets that lost stimulation-induced enrichment in the PIN1$^{-/-}$ cell lines (PIN1$^{-/-}$FC ~0, WT TPR FC = High) (Figure 2.3.3A). Using the Mab414 antibody, we identified fewer targets in this cluster, with 107 PIN1-dependent interactions in response to serum stimulation (Figure 2.3.3B). To examine the PIN1-dependent overlap of protein targets enriched in both MYC and TPR, we first compared fold changes in WT MEFs following serum-stimulation between MYC and TPR interactors (Figure 2.3.3C). The serum-responsive cluster (High, High) contained 107 shared targets (Figure 2.3.3D), which was reduced to only 25 shared targets in the PIN1$^{-/-}$ cells (Figure 2.3.3E,F). Notably, only two shared MYC-TPR enriched targets (SNIP1 and XRN2) were found when comparing WT and PIN1$^{-/-}$ conditions, indicating that loss of PIN1 significantly alters the MYC-TPR interactome in response to serum-stimulation (Figure 2.3.3G). Furthermore, GO enrichment of the WT PIN1-dependent cluster showed robust enrichment in canonical MYC-related functions such as ribosome biogenesis and gene expression in the overlapping MYC-TPR interactome (Figure 2.3.3H) while PIN1$^{-/-}$ lost known MYC-related functions for GO analysis. Together, these results demonstrate that PIN1 is essential for the serum-induced interactome overlap between MYC and TPR.

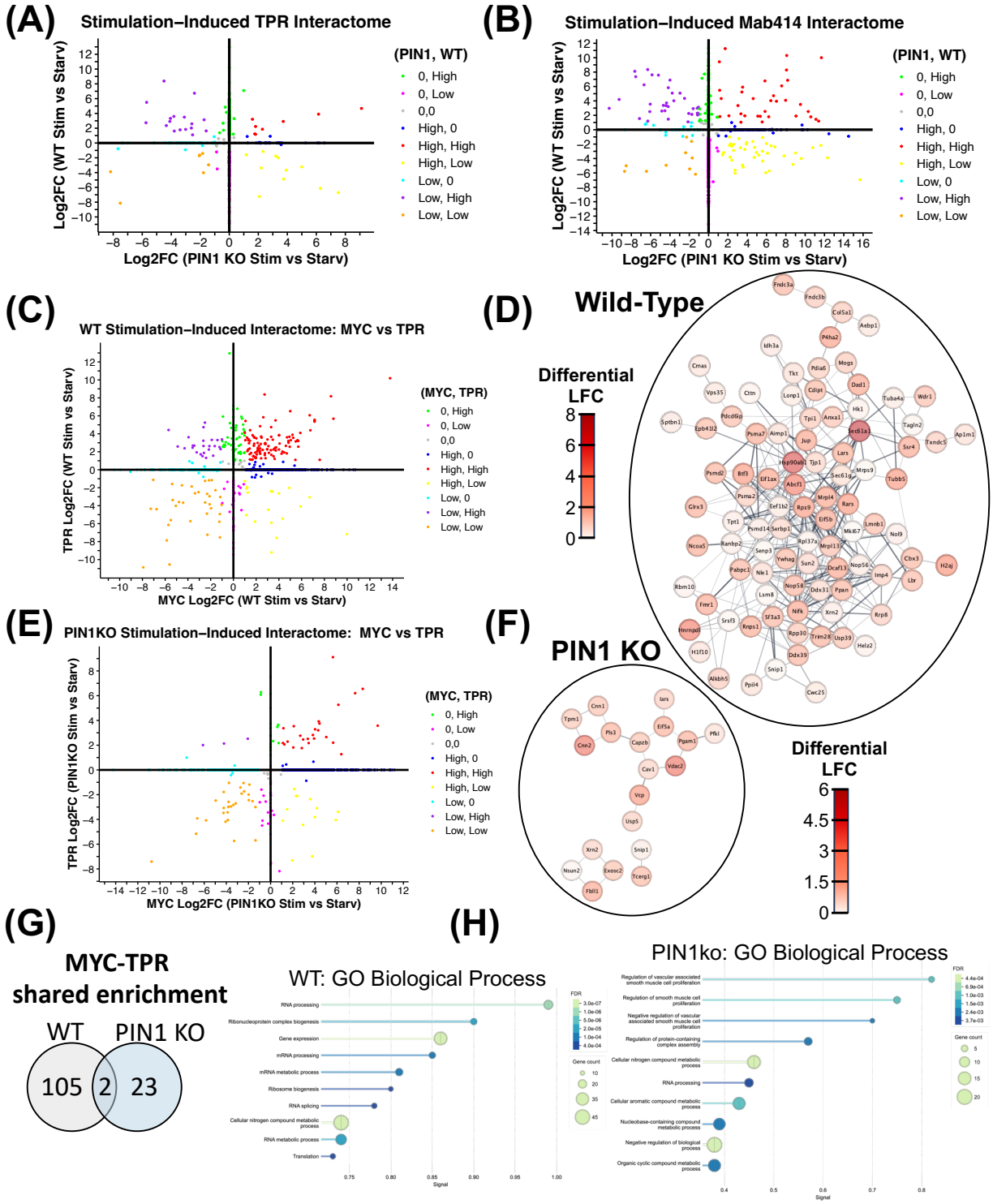

Figure 2.3.3. PIN1 is crucial for the overlap of MYC-NPC interactomes that drive MYC-mediated transcriptional responses to stimuli.

(A) Clustered classification following Log2FC of TPR interacting targets following serum stimulation in either WT or PIN1KO MEFs. Targets that had a FC between -1 and +1 were classified as “0”, otherwise a less than -1FC was classified as “Low” and a +1FC was

classified as “High”. (B) Clustered classification following Log2FC of Mab414 interacting targets following serum stimulation in either WT or PIN1KO MEFs. (C) Clustered classification following Log2FC of MYC and TPR interacting targets following serum stimulation in WT MEFs. (D) Cytoscape STRING analysis of shared MYC-TPR interacting targets in WT MEFs following serum-stimulation that were in the MYC=”High” and TPR=“High” (Red) cluster in (C). Darkness of red shading denotes differential in LFC with a larger value representing a greater serum-induced difference between MYC and TPR in WT MEFs. (E) Clustered classification following Log2FC of MYC and TPR interacting targets following serum stimulation in PIN1KO MEFs. (F) Cytoscape STRING analysis of shared MYC-TPR interacting targets in PIN1KO MEFs following serum-stimulation that were in the MYC=”High” and TPR=“High” (Red) cluster in (E). Darkness of red shading denotes differential in LFC with a larger value representing a greater serum-induced difference between MYC and TPR in PIN1KO MEFs. (G) Venn diagram of overlap between MYC-TPR shared interactions in WT and PIN1KO MEFs following serum stimulation. (H) Comparison between WT and PIN1KO MEFs of the top ten Gene Ontology Biological Process enrichment scores for MYC-TPR targets following serum-stimulation.

Development and validation of MYC- and NUP153-BioID2 system for studying protein interaction at the nuclear pore.

The RIME data suggests an overlap of serum-induced targets between MYC and the NPC in MEFs cells. To validate these findings in human cells, we developed a MYC- and NUP153-BioID2 system, which enables proximity-dependent biotinylation to study protein-protein interactions (Figure 2.3.4A). Given the extensive literature supporting NUP153’s role in gene regulation at the nuclear pore, we selected the NUP153-BioID2 system in place TPR[267, 268]. BioID2 technology offers several advantages over traditional co-IP mass spectrometry, particularly for studying MYC-induced interactions at the nuclear pore. These advantages include the ability to capture weak, transient interactions and to identify non-direct interactions with larger protein complexes [269, 270]. Plasmids were constructed to attach BioID2 connected to the N-terminus of either MYC or NUP153 using a five-glycine linker. Plasmids, along with a HA-BioID2 control, were transiently transfected into HEK293 cells and treated with 50μM biotin for 18 hours.

Biotinylated proteins were then isolated using streptavidin-agarose beads, and the input, supernatant, and eluted proteins were analyzed via immunoblot. Despite some none-specific bands, MYC-BioID2 was detected at approximately 80 kDa, which aligns with the expected size, considering MYC is detected at 55 kDa and BioID2 is 27 kDa (Figure 2.3.4B). No MYC was detected in the eluate of HA-BioID2 only. Furthermore, the addition of biotin enhanced the abundance of MYC-BioID2 in the eluate, indicating predicted auto-biotinylation. Similarly, NUP153-BioID2 was detected only in the eluate biotin-treated cells, with an estimated size of approximately 180 kDa, and no NUP153 was detected in the HA-BioID2 control (Figure 2.3.4C). To validate the functionality of the BioID2 constructs, we tested the eluates for abundance of isolated biotinylated proteins with a streptavidin-conjugated immunoblot (Figure 2.3.4D). The HA-BioID2 control appeared to only include known endogenously biotinylated proteins. Both the MYC- and NUP153-BioID2 exhibited robust biotin-induced streptavidin-detecting smears, indicating BioID2 activity and successful isolation of their respective interactomes in the eluate. To test whether a shared interactome could be detected between MYC and NUP153, the biotinylated-induced eluates were probed for SENP1 and PIN1 (Figure 2.3.4E). Previously, SENP1 was shown to interact with and stabilize MYC around the nuclear periphery[271]. Consistent with this finding, SENP1 was detected in both the NUP153- and MYC-BioID2 eluates but was absent in the HA-BioID2 control. Interestingly, the MYC-interacting SENP1 ran higher on the gel, possibly indicating post-translation modifications such as ubiquitination or SUMOylation. PIN1 was faintly detected in all three eluates, with slight enrichment in the MYC-BioID2 eluate. Since PIN1's promotion of MYC activity and localization to the NPC is serum-responsive, biotinylation followed by immunoblotting in

asynchronous cells may not fully capture a robust interaction[108, 116]. A more effective approach might be serum induction followed by mass spectrometry of the eluates to observe a stronger interaction of PIN1 with MYC and NUP153. This data demonstrates the functionality of the MYC- and NUP153-BioID2 system to isolate and study protein interactions at the nuclear pore. Future experiments involving serum induction followed by mass spectrometry may provide a more comprehensive analysis of the dynamic interaction between MYC and the NPC which contribute to MYC-driven transcription in response to stimuli.

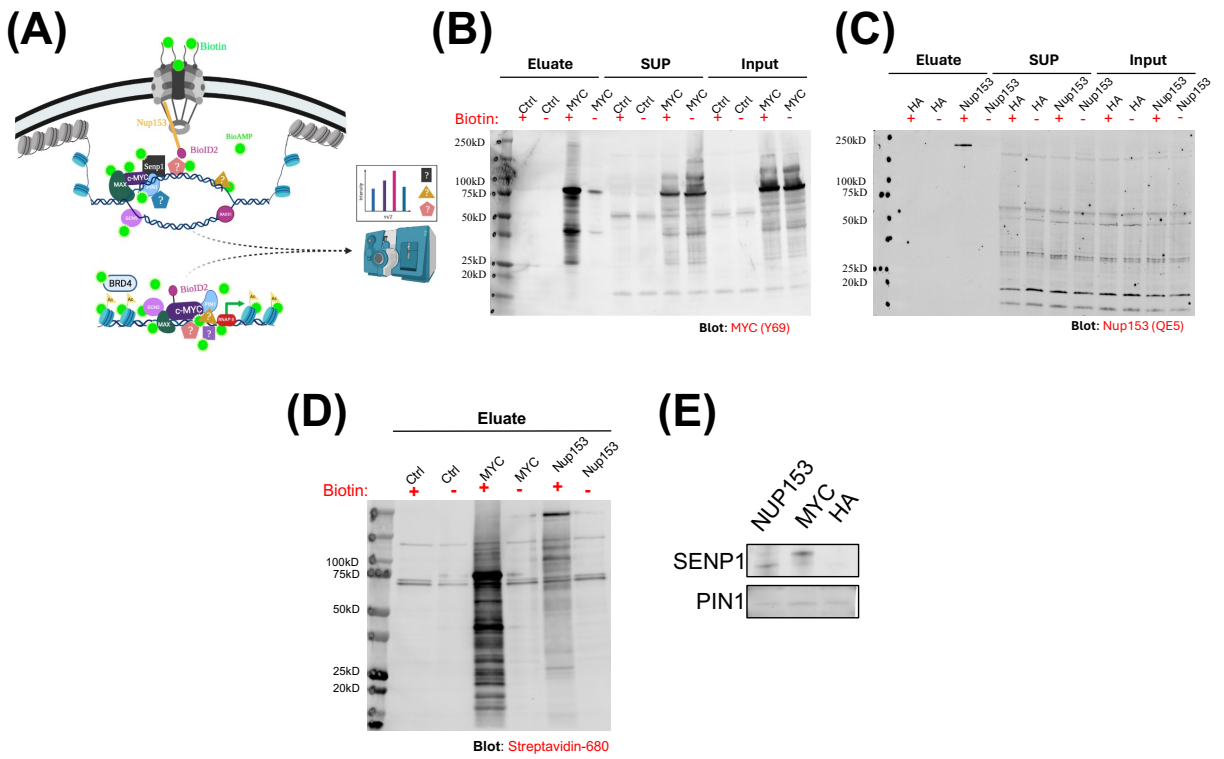

Figure 2.3.4 Development and validation of MYC- and NUP153-BioID2 system for studying protein interaction at the nuclear pore.

(A) Schematic of proposed MYC- and NUP153-BioID2 experiment to identify overlapping factors via mass spectrometry. (B) Validation Western Blot of MYC-BioID2 or HA-BioID2 (Ctrl) fusion proteins following 48-hours transfection in HEK293T cells and 18 hours 50μM biotin incubation. Eluate was products eluted from streptavidin-agarose beads. (C) Validation Western Blot of NUP153-BioID2 or HA-BioID2 (Ctrl) fusion proteins following 48-hours transfection in HEK293T cells and 18 hours 50μM biotin incubation. (D)

Streptavidin smear of eluate from streptavidin-agarose beads following 48-hours transfection of either HA-BioID2 (Ctrl), MYC-BioID2, or NUP153-BioID2 in HEK293T cells and 18 hours 50μM biotin incubation. (E) Bead elution of known MYC interacting proteins, SENP1 and PIN1, from either HA-BioID2 (Ctrl), MYC-BioID2, or NUP153-BioID2 in HEK293T cells and 18 hours 50μM biotin incubation.

2.4 Discussion

In this study, we demonstrate that PIN1 plays a critical role in regulating MYC's binding to target genes and its association with the nuclear pore complex (NPC) in human PDAC cells. Our results show that loss of PIN1 reduces both NPC and MYC's association and shared target gene engagement. Using RIME, we show a reliance on PIN1 in the shared serum-responsive interactome of MYC and the NPC, particularly in functional targets related to gene expression and RNA processing, suggesting PIN1-mediated isomerization is required for MYC's function at the NPC.

Understanding the regulatory dynamics of MYC is critical for elucidating the pleiotropic effects on the genome and its control of diverse cellular phenotypes. Early studies in the 1980s first described MYC associating with nuclear matrix laminae in cultured cells [141], while potentially suggesting that MYC might play a role in nuclear structural organization. A decade later, research on the nuclear-to-cytoplasm exchange of MYC, c-Fos, and PCNA demonstrated that serum stimulation leads to the rapid association of MYC with the nuclear pore complexes, eluding to a MYC-driven function at the nuclear periphery in response to stimuli[142]. In 2015, the first mechanistic study of MYC's localization to the nuclear periphery was conducted, linking this function to MYC's potent oncogenic role in driving regenerative proliferation[140]. The described mechanism shows that downstream of growth stimuli, MYC is phosphorylated at serine 62 (pS62-MYC) and accumulates on Lamin A/C-associated nuclear structures which is required for MYC-driven proliferation and intestinal regeneration following DNA damage.

Furthermore, this mechanism was not observed in normal crypts and was dependent on the functional protein phosphatase 2A (PP2A) inhibitor protein CIP2A, which prevents the removal of the stabilizing phosphorylation of pS62-MYC by PP2A. This highlights the importance of pS62-MYC and its trafficking to the nuclear periphery in regulating the cell's response to growth stimuli. This mechanism was further explored, revealing that the phosphorylation-directed peptidyl-prolyl isomerase, PIN1, is required for the rapid association of pS62-MYC's with the inner basket of the nuclear pore complex (NPC) under serum stimulation conditions in mouse embryonic fibroblasts (MEFs), during wound healing, and in cancer cell lines[108]. In agreement with these findings, we demonstrate here that in pancreatic ductal adenocarcinoma (PDAC) cells, MYC robustly interacts with PIN1 and components of the NPC (Figure 2.3.1). Furthermore, we show that MYC's association with the basket NPC protein, NUP153, is increased in response to serum stimulation in MIA PaCa-2 cells and following Olaparib treatment in a patient-derived cell line ST-00013312 (Figure 2.3.1F,I). PIN1 also prolongs the DNA-binding "on-time" of MYC to its target genes in MCF10A cells[116], and we confirm that MYC binding to E2F2 and NCL1 genes is decreased following PIN1-knockdown in MIA PaCa-2 cells Figure (2.3.1A,B).

The functional consequences of PIN1-depenent MYC recruitment to the NPC were suggested by Su et al., who found that serum-responsive MYC target genes lost chromatin accessibility and gene expression in $PIN1^{-/-}$ MEFs when compared to WT[108]. PIN1 is also essential for recruiting MYC co-activators, including histone acetyltransferases p300 and GCN5, to target genes, enhancing chromatin accessibly and gene activation [116]. In concordance, our RIME experiment revealed a large

redistribution of MYC's serum-responsive interactome when comparing PIN1-knockout to WT (Figure 2.3.2). The targets that lost MYC interaction following serum stimulation in PIN1-knockout MEFs were involved in growth-related pathways, including ribosome biogenesis and gene expression. Interestingly, Lamin B1, a component of the nuclear lamina, was detected and is known to alter chromatin architecture and regulates transcription [272]. Additionally, GCN5 was previously shown to traffic to the NPC in a PIN1-dependent manner as well[108]. Together with our observation of MYC and NPC sharing overlapping target gene binding (Figure 2.3.1J,K,L), these findings suggest a mechanism in which PIN1 regulates pS62-MYC, enhancing co-activator interaction and target gene engagement at the nuclear pore following stimulation.

The nuclear periphery is generally transcriptionally silent, except for heterochromatin exclusion zones (HEZs), which form when euchromatin tether to nuclear pore basket proteins such as TPR[144]. Actively transcribed genes traffic to the nuclear pores through gene gating, a well-established process that couples rapid gene transcription, nuclear export, RNA splicing, and translation for efficient gene expression[260]. Gene gating is an evolutionarily conserved mechanism that enables cells to mount a rapid transcriptional response to stimuli and is essential for cell survival. Additionally, induced genes remain tethered to the NPC in a transcriptionally permissive state, known as epigenetic memory, which allows for robust re-activation in response to future stimuli[148]. This process was first described in yeast, where a previously induced GAL1, which remained tethered to the NPC, re-activated much more rapidly than GAL1 in the nucleoplasm[273]. Whether MYC is directly involved in gene gating remains to be investigated. However, in colon cancer driven by abnormal WNT signaling, the expression

of the *Myc* gene super enhancer is dramatically increased through trafficking to the NPC, promoting MYC-driven pathological cell growth[274]. Following IFN-gamma stimulation, MYC's transcriptional activity is influenced, in part, by its dynamic association with promyelocytic leukemia (PML) bodies[275]. We demonstrate that both MYC and TPR lose their interaction with PML when PIN1 is lost (Figure 2.3.3C,D). Furthermore, target genes associated with PML bodies participate in transcriptional memory[276], suggesting that MYC is involved in establishing a shared NPC-interactome with PML protein and other factors to regulate gene expression at the NPC. Further investigation is required to determine whether the interaction between MYC and PML at the NPC is associated with the formation or regulation of PML bodies. In addition to phosphorylation, which regulates the stability and activity of MYC, SUMOylation and ubiquitination are key regulatory mechanisms[277]. We detected both SENP3 and SENP1 associating with MYC and the NPC (Figure 2.3.3D, Figure 2.3.4E). These enzymes are known to remove SUMOylation from both PIN1 and MYC[136, 271], enhancing their stability and activity, suggesting SUMOylation regulation may be involved in reinforcing MYC's transcriptional activity at the NPC.

NPC-driven mechanisms have been implicated in cancer progression and have been explored as a potential target for therapeutic interventions[146, 147]. In several cancer cells, the nuclear pore numbers increase, and gene gating-related transcription also rises as the cancer cell becomes more dependent on efficiently driving proliferation and responding to environment signals. Since PIN1 drives the relocation of MYC to stimuli-responsive gene programs at the nuclear pore, therapeutically inhibiting PIN1 could indirectly target MYC-driven tumors. In support of this idea, Sulfopin, a covalent

inhibitor of PIN1, has been shown to directly block MYC-driven tumors in vivo[278]. We show that in MIA PaCa-2 cells, Sulfopin decreased MYC's binding to E2F2 to a level comparable to PIN1 knockdown; however, did not appear to affect binding to NCL1 in preliminary experiments (Figure 2.3.1A,B). In contrast, another PIN1 inhibitor, PiB, was able to decrease MYC's binding to both targets, consistent with similar reports in MCF10A cells[116]. PIN1 knockdown also reduced the binding of MYC, pS62-MYC, and the NPC to a target gene (Figure 2.3.1L), suggesting that PIN1 loss could disrupt MYC-driven transcription involved in gene gating.

In conclusion, our study reveals that PIN1 is a critical regulator of MYC's binding to target genes and its association with the nuclear pore complex, particularly in response to serum stimulation and chemotherapy in PDAC cells. We show that PIN1 and MYC may play a role in gene gating, which is a key process for efficient gene expression. By utilizing techniques such as qChIP, RIME, and PLA, we uncover a mechanism where PIN1 is required for the serum-induced, shared interactome between MYC and the NPC, influencing MYC's interaction with coactivators and target genes. In addition, we provide evidence that PIN1 loss disrupts MYC-driven gene gating, supporting our previous study in MEFs[108], which could have a significant implication for cancer progression and response to therapies. Together with prior work utilizing a catalytic mutant of PIN1, we hypothesize that pS62-MYC proline isomerization creates an active conformation of MYC that associates with the NPC to provide gene gating function. PIN1 therapeutic targeting may offer a potent approach for treating MYC-driven cancers, especially since PIN1 null mice are viable, suggesting limited toxicity. Overall, this study highlights the intricate

relationship between PIN1 and the NPC in MYC's regulation and function and underscores the potential for targeting PIN1 in cancer therapies.

2.5 Materials and Methods

Cell Lines

Generation and characterization of PIN1 knockout MEF cells and the serum stimulation experiments were performed as previously described[131]. For serum stimulation, WT or $PIN1^{-/-}$ MEF cells were grown till density arrest then split into 50% confluence in 0.2% FBS medium and starved for two days. Cells were then stimulated with 20% FBS medium for 4 hours. HPAFII and MIA PaCa-2 cells were maintained in DMEM supplemented with 10% characterized fetal bovine serum (FBS), 2mM L-glutamine, and 1X penicillin/streptomycin at 37°C and 5% CO_2. Patient derived cell line ST-00013312 was generated as previously described[279].

Quantitative Chromatin Immunoprecipitation Assay

Cells were cross-linked with a final concentration of 1% formaldehyde in media and incubated at room temperature for 10 minutes. Cells were then collected in PBS-1mM EDTA and centrifuged to collect pellet. Pellets were then lysed by resuspension in 700μL ChIP lysis buffer (0.1% SDS, 0.5% Triton X-100, 20mM Tris-HCl [pH 8.1], and 150mM NaCl). Lysates were then sonicated six times with 10 pules per round (output = 3.5, 30% duty cycle). Lysate were then cleared by centrifugation at 14,000 rpm for 15 minutes at 4°C. Cell lysates were first pre-cleared by incubating with 50μL of a 50% protein A bead slurry for 1 hour at 4°C with rotation. Following a second clearance step via centrifugation at 14,000 rpm for 5 minutes at 4°C, immunoprecipitations were carried out by incubating

the lysates with 2μg of each specific antibody overnight at 4°C; 2μg of normal rabbit or mouse IgG (Santa Cruz Biotechnology) served as the negative control. The resulting immunoprecipitates were washed six times with ChIP lysis buffer and twice with Tris-EDTA (TE) buffer, with each wash involving a 15-minute rotation at 4°C. Subsequently, the complexes were eluted from the beads using an elution buffer containing 0.1M $NaHCO_3$ and 1% SDS for 15 minutes at room temperature; the eluates were then transferred to new tubes, adjusted with 5M NaCl to a final concentration of 0.2M, and incubated overnight at 65°C. Finally, the DNA was purified using the QIAquick PCR purification kit (Qiagen, Hilden, Germany) and subjected to quantitative PCR (qPCR) analysis with the primers listed below. The internal control of GAPDH was used as a reference control. The ΔCt values were calculated by the following equation: ΔCt = Ct(Target) - Ct(GAPDH). The $\Delta\Delta$Ct values were generated with the following equation: $\Delta\Delta$Ct = ΔCt(Target) - ΔCt(IgG). Relative enrichment then calculated by $2^{-\Delta\Delta Ct}$ for each experiment and graphed in GraphPad Prism. Antibodies used for pulldown are as follows: MYC (Santa Cruz, 764), pS62-MYC (Abcam, 78318), Mab414 (Abcam, 24609), IgG (Santa Cruz).

	Forward	Reverse
Nucleolin	5'-TTGCGACGCGTACGAGCTGG-3'	5'-ACTCCGACTAGGGCCGATAC-3'

E2F2	5'-TCACCCCTCTGCCATTAAAGG-3'	5'- AGCAGTGTATTCCCCAGGCC-3'
SYT1	5'-GGCGAACCCACACACATCG-3'	5'-GCTAGTTTTCCCGTTTTCCCTGG -3'
GAPDH	5'-TGGAGTCCACTGGCGTCTTC-3'	5'-TTCACACCCATGACGAACATG-3'

Proximity Ligation Assay

Proximity Ligation Assay was performed without deviation from manufacturer's instructions (DUO92008). Single-antibody controls were performed to ensure specificity of antibodies. Coverslips were washed in a 0.5mL volume and reactions were performed by inverting the coverslip onto a 35μL drop on parafilm. Following the proximity ligation reaction, cells stained with DAPI (0.2ug/mL) for 3 minutes followed by one wash in PBS and one water wash. The cells were then inverted and mounted on glass coverslips with 15μL of prolong gold mounting media (LifeTech, P36934) & were cured overnight in the dark at room temperature. A minimum of 30 cells were imaged per replicate at 63X on a Zeiss LSM880 confocal microscope and analyzed with CellProfiler. Antibodies used are as follows: MYC (Abcam, 32072), pS62-MYC (Abcam, 78318), PIN1 (Santa Cruz, 46660), NUP153 (Abcam, 24700), TPR (Santa Cruz, 121094), NUP98 (Santa Cruz, 74578), Lamin A/C (Santa Cruz, 6215).

Rapid Immunoprecipitation Mass Spectrometry of Endogenous Proteins (RIME)

RIME experiment was performed following the original published protocol[263]. WT or PIN1$^{-/-}$ MEF cells were grown till density arrest then split into 50% confluence in 0.2% FBS medium and starved for two days. Cells were then stimulated with 20% FBS medium for 4 hours. Antibodies used for immunoprecipitation are as follows: MYC (Santa Cruz, 764), Mab414 (Abcam, 24609), TPR (Santa Cruz, 121094), IgG (Santa Cruz). Protein intensities were then scale normalized to the total intensities detected. IgG intensities were then subtracted from the rest of the antibodies. A pseudo count of the global 5th percentile intensity was added prior to Log2 fold change analysis. Log2 fold change analysis was performed between the conditions and manually clustered into either 0, low, or high based off degree of fold change. Interaction network of identified proteins was then analysis using StringApp in Cytoscape[264-266]. Gene Ontology analysis of identified targets was analyzed using STRING v10[266, 280, 281].

BioID2 Analysis

BioID2 sequence with a five-glycine linker (Addgene: 74224) was cloned at the N-terminus of C-MYC (Addgene: 16011) or NUP153 (NM_005124). Cloning was performed and validated by GenScript. HA-BioID2 was used as a control (Invitrogen: 74224). HEK293 cells were plated on two 10-cm dishes per condition to achieve 80% confluency upon treatment. Each plasmid was independently transfected using Lipofectamine 3000 (Thermo Fisher Scientific L3000-015) and incubated for 24-hours. For biotinylation, cells were treated with 50μM biotin (Millipore Sigma: B4501) for 18 hours. After treatment, cells were washed twice with PBS and were then lysed with lysis buffer (50 mM Tris-Cl, pH

7.4, 150 mM NaCl, 1% Triton X-100, 0.1% SDS; 1 mM DTT, protease inhibitor (Millipore Sigma: 5892791001), and phosphatase inhibitor (Millipore Sigma: 4906837001), and incubated on ice for 10 minutes. Lysates were scraped, pooled, and sonicated with a Branson Sonifier 450 for two 30-pulse sessions at a 30% duty cycle and 1.5 output, with a 2-minute ice interval. Samples were diluted with pre-chilled 50 mM Tris-Cl (pH 7.4) and sonicated for an additional 30 pulses. Lysates were centrifuged at 16,500 x g for 10 minutes at 4°C to remove debris. Streptavidin-agarose beads (Millipore Sigma: 69203-3) were equilibrated in a 1:1 mixture of lysis buffer and 50 mM Tris-Cl (pH 7.4) and briefly spun down at 8,000 rpm for 2 minutes. Supernatants were transferred to the beads and incubated overnight on a rotator at 4°C. After incubation, beads were washed twice with wash buffer 1 (50 mM HEPES pH 7.5, 400 mM NaCl, 1% Triton X-100, 0.1% deoxycholic acid, 1 mM EDTA) for eight minutes, twice with wash buffer 2 (10 mM Tris-Cl pH 7.4, 500 mM LiCl, 0.5% NP-40, 0.5% deoxycholic acid, 1 mM EDTA) at room temperature. Beads were washed once in 50 mM Tris-Cl (pH 7.4) followed by three washes with 100mM ammonium bicarbonate. Beads were resuspended in 100 µL of 1X SDS buffer (50mM Tris-Cl pH 6.8, 2%SDS, 6% glycerol, 5% 2-mercaptoethanol) and boiled for 10 minutes to isolate eluate. Samples were loaded into a 4-12% Bis-Tris Citerion Gel (BioRad: 345-0123) and run for 1.5 hours at 180V on ice in XT-MOPS (BioRad: 161-0788). The gel is then transferred onto an Immobilin PVDF membrane (Fisher Scientific: IPFL00010) for 90 minutes at 400mA. Membrane is then blocked for 1 hour at room temperature in Aquablock (Arlington Scientific: NC2580736) then incubated overnight with primary antibody. The following day, the membrane is washed for three times with TBST and incubated with secondary Licor antibody for 1 hour in the dark room temperature and

imaged on a Licor Odyssey scanner. Antibodies used are as follows: MYC (Abcam, 32072), PIN1 (Santa Cruz, 46660), NUP153 (Abcam, 24700), SENP1 (Abcam, 108981), Licor IRDye 680RD Streptavidin (Fisher, NC0337633).

2.6 Acknowledgements

The authors acknowledge expert technical assistance by the OHSU Advanced Light Microscopy Core (RRID:SCR_009961), supported by the OHSU Knight Cancer Institute (NIH P30 CA069533). In addition, we'd like to thank OHSU's shared proteomics core for support and guidance on this project. Thank you to Dr. Eda Yildirim from Duke University for sharing the NUP153 plasmid.

2.7 Author Contributions

GMC and RCS contributed to the project design; GMC performed and analyzed all experiments unless otherwise stated; DFL and GMC performed and analyzed the qChIP experiments; YS and HM performed RIME experiment while GMC analyzed the data. GMC wrote the manuscript with edits and revisions from RCS.

2.8 Supplementary Materials

gene_ID	LFC_N262_PIN1	LFC_N262_WT	Cluster_Label	delta_LFC
Tuba1c	0.819543502	10.18456737	0, High	9.365023863
Igf2bp2	-0.499634103	7.533621669	0, High	8.033255772
Prdx2	-0.496798718	7.415044198	0, High	7.911842916
Anxa2	0.464701555	8.220728021	0, High	7.756026466
Lmnb1	0	7.14474648	0, High	7.14474648
Tubb2a	0.088979933	6.823417007	0, High	6.734437074
Snd1	0	6.709084788	0, High	6.709084788
Arpc4	0	6.55982443	0, High	6.55982443
Brix1	0	6.307211636	0, High	6.307211636
Srsf10	-0.246222586	6.013982798	0, High	6.260205384
Dpysl2	0	6.229803044	0, High	6.229803044
Ftsj3	-0.917951721	5.229954719	0, High	6.147906441

Dync1h1	0.423918079	6.3201493	0, High	5.896231221
Flna	-0.740256313	5.040628053	0, High	5.780884366
Mrpl4	0	5.699611754	0, High	5.699611754
Plec	-0.265865865	5.379331548	0, High	5.645197413
Dad1	0	5.629314237	0, High	5.629314237
Rab18	0	5.439100275	0, High	5.439100275
Eif5b	-0.97356509	4.318513774	0, High	5.292078864
Ufd1	0	5.249809943	0, High	5.249809943
Mogs	-0.303375237	4.930920206	0, High	5.234295443
Txndc17	-0.247798797	4.890282499	0, High	5.138081296
Vps26a	0	5.118012748	0, High	5.118012748
Ddx39	0.81312909	5.886532054	0, High	5.073402964
Wdr1	0	5.005811635	0, High	5.005811635
Pin1	0	4.932849066	0, High	4.932849066
Dazap1	0	4.883751804	0, High	4.883751804
Coro1c	0.945959984	5.822385377	0, High	4.876425393
Lbr	0	4.834212377	0, High	4.834212377
Atp8b4	0	4.81562295	0, High	4.81562295
Faf2	0	4.813679321	0, High	4.813679321
Fscn1	0.95137001	5.761895869	0, High	4.810525859
Srp72	-0.031802394	4.765226989	0, High	4.797029383
Stat1	-0.755067818	3.961654713	0, High	4.716722531
Prdx5	0.233463354	4.921386097	0, High	4.687922744
Atp5o	-0.625241338	3.987467414	0, High	4.612708752
Ndufs3	0	4.473883097	0, High	4.473883097
Upf1	0	4.463514915	0, High	4.463514915
Esyt2	0	4.457039593	0, High	4.457039593
Ddx5	0	4.399440416	0, High	4.399440416
Mnd1	0	4.341606	0, High	4.341606
Fkbp3	0.275849374	4.601139098	0, High	4.325289725
Cybc1	0	4.23946403	0, High	4.23946403
Cap1	-0.777282608	3.420349918	0, High	4.197632526
Hsd17b10	0	4.185618938	0, High	4.185618938
Mrpl49	0	4.152557249	0, High	4.152557249
Srp54b	-0.662685384	3.443939883	0, High	4.106625267
Atp5md	0	4.070382861	0, High	4.070382861
Fndc3a	0	4.013005193	0, High	4.013005193
Lcp1	0	4.00869919	0, High	4.00869919
Wdr75	0	4.006008805	0, High	4.006008805

Eif1	0	4.002209782	0, High	4.002209782
Atp6v1h	0	3.91322487	0, High	3.91322487
Eef1b2	-0.573800832	3.323341691	0, High	3.897142523
Anxa4	0	3.877863473	0, High	3.877863473
Csnk2a1	0	3.785170968	0, High	3.785170968
Nop2	0	3.755959954	0, High	3.755959954
Pes1	0	3.74368845	0, High	3.74368845
Epb41l2	0	3.73127099	0, High	3.73127099
Vat1	0	3.690033161	0, High	3.690033161
Acadsb	0	3.660982104	0, High	3.660982104
Txndc5	-0.829359899	2.760365758	0, High	3.589725657
Mrps5	-0.706569749	2.867319909	0, High	3.573889657
Prrx1	0	3.533800218	0, High	3.533800218
Hsp90ab1	-0.764025485	2.743365226	0, High	3.507390711
Plrg1	-0.728777661	2.764987746	0, High	3.493765406
Lyz1	0.471048777	3.938454683	0, High	3.467405906
Arcn1	0	3.429076885	0, High	3.429076885
Psma7	0.114536775	3.533898032	0, High	3.419361257
Tcp1	0	3.391005382	0, High	3.391005382
Ddx42	0	3.372971525	0, High	3.372971525
Snrpd1	0	3.353660655	0, High	3.353660655
Ahsa1	0	3.321725101	0, High	3.321725101
Rab1a	0	3.304737912	0, High	3.304737912
Gmps	0	3.287618549	0, High	3.287618549
Llph	0	3.287533096	0, High	3.287533096
Mtpn	-0.50892149	2.734433239	0, High	3.243354729
Mtch2	0	3.209871996	0, High	3.209871996
Ppia	-0.567099052	2.625281699	0, High	3.192380751
Stat3	0	3.15896173	0, High	3.15896173
Abcf2	-0.76090725	2.373835317	0, High	3.134742567
Alkbh5	0	3.121690518	0, High	3.121690518
Cyfip1	0	3.103642963	0, High	3.103642963
Nans	0	3.070308974	0, High	3.070308974
Mtdh	0.950033331	3.992634895	0, High	3.042601563
Pdia5	0	3.040331217	0, High	3.040331217
Dnpep	0	3.017861146	0, High	3.017861146
Ube2n	0	3.016858991	0, High	3.016858991
Trap1	0	2.975878352	0, High	2.975878352
Nle1	0	2.965111616	0, High	2.965111616

Zfp622	0	2.94866168	0, High	2.94866168
Dcaf13	-0.563142678	2.352297384	0, High	2.915440062
Eif4a1	-0.85045892	1.993176971	0, High	2.843635891
Actr1a	0	2.830428031	0, High	2.830428031
Wdr43	-0.442528325	2.382650502	0, High	2.825178827
Tjp1	0	2.767759798	0, High	2.767759798
Ddx46	0	2.765570256	0, High	2.765570256
Senp3	0.135448234	2.819510701	0, High	2.684062467
Hnrnpc	0	2.657662331	0, High	2.657662331
Actr1b	0	2.650388098	0, High	2.650388098
Hnrnpul2	-0.838953959	1.690827642	0, High	2.529781601
Helz2	-0.722018746	1.778422167	0, High	2.500440913
Rbm3	0.712013236	3.211535442	0, High	2.499522206
Tut7	0	2.471128158	0, High	2.471128158
Aldh2	-0.467799919	1.999985644	0, High	2.467785563
Idh3a	0	2.40467264	0, High	2.40467264
Rbm28	0	2.388366506	0, High	2.388366506
Psmc6	0.697453169	3.07902296	0, High	2.381569791
Mecp2	0.731362831	3.082271271	0, High	2.35090844
Ap2a2	0	2.33300593	0, High	2.33300593
Ranbp2	0	2.330222516	0, High	2.330222516
Utp14a	-0.742933449	1.583305033	0, High	2.326238482
Ppp1cc	0	2.316930627	0, High	2.316930627
Taf15	0.15737721	2.465659565	0, High	2.308282355
Katnal2	0	2.255979277	0, High	2.255979277
Tuba4a	0	2.254099631	0, High	2.254099631
Rab8a	0	2.185111119	0, High	2.185111119
Wdr36	0	2.176723657	0, High	2.176723657
Ddx31	0	2.134464114	0, High	2.134464114
Hnrnpa2b1	-0.303326138	1.817167465	0, High	2.120493602
Lonp1	0	2.063381704	0, High	2.063381704
Ddx3x	0	2.01403112	0, High	2.01403112
Ap1m1	0	1.981584777	0, High	1.981584777
Surf6	-0.733985112	1.245563254	0, High	1.979548366
Ndufs7	0	1.957385745	0, High	1.957385745
Trim28	-0.152034793	1.799919809	0, High	1.951954602
Mrps9	0	1.937303728	0, High	1.937303728
Vps35	0	1.876289655	0, High	1.876289655
Fads3	0	1.860453794	0, High	1.860453794

Ppig	0	1.834002854	0, High	1.834002854
Tpi1	0.632449534	2.447489019	0, High	1.815039486
Srsf3	0.32297508	2.135561674	0, High	1.812586594
Hnrnph1	-0.151933387	1.634168023	0, High	1.78610141
Sbds	0	1.783723468	0, High	1.783723468
Serbp1	-0.203943294	1.431297861	0, High	1.635241155
Rpl27a	0	1.63507578	0, High	1.63507578
P4hb	-0.39212801	1.235697376	0, High	1.627825387
Hnrnpk	0.587682588	2.213332774	0, High	1.625650186
Ncoa5	0.074028404	1.684901616	0, High	1.610873212
Rpa1	0	1.580174282	0, High	1.580174282
Aimp1	0.392627566	1.961107262	0, High	1.568479696
Rps8	0.257437159	1.819006125	0, High	1.561568966
Rpf1	0	1.53199667	0, High	1.53199667
Aco2	0.011635896	1.509242814	0, High	1.497606919
Myh14	-0.371187387	1.102844203	0, High	1.47403159
Coro1a	0.394895574	1.867204097	0, High	1.472308523
Tpt1	-0.019956748	1.437322212	0, High	1.45727896
Sf3a3	0	1.453772799	0, High	1.453772799
Nol9	0	1.453085379	0, High	1.453085379
Txn1	0	1.437388669	0, High	1.437388669
Utp4	0	1.409122555	0, High	1.409122555
Pdcd6ip	0	1.379434785	0, High	1.379434785
Vrk2	0	1.377337439	0, High	1.377337439
Ak1	0	1.377183314	0, High	1.377183314
Rtraf	0	1.356414449	0, High	1.356414449
Man2a1	0.448503569	1.783488283	0, High	1.334984714
Srp68	0	1.303961021	0, High	1.303961021
Hsp90b1	-0.040196079	1.262227134	0, High	1.302423213
G3bp1	0	1.294858771	0, High	1.294858771
Ddx27	0	1.272997782	0, High	1.272997782
Lyar	0	1.256567462	0, High	1.256567462
H4c11	0.834331658	2.076642635	0, High	1.242310977
Rbm39	-0.046411308	1.16460656	0, High	1.211017868
Calml3	0.015131996	1.219757665	0, High	1.204625669
Fdps	0	1.164527215	0, High	1.164527215
S100a4	0	1.14009421	0, High	1.14009421
Fam98b	0	1.134079192	0, High	1.134079192
Pdap1	0	1.11577401	0, High	1.11577401

Fkbp11	0	1.072709555	0, High	1.072709555
Sf1	0	1.063222117	0, High	1.063222117
Ilk	0	1.060828719	0, High	1.060828719
Pafah1b2	0.679721008	1.739776454	0, High	1.060055446
Usp14	0	1.03063793	0, High	1.03063793
Celf2	0	1.027426714	0, High	1.027426714
Cpne3	0.772020554	1.791081079	0, High	1.019060524
Copb2	0.928548349	1.945996875	0, High	1.017448526
Btf3	0	1.007212185	0, High	1.007212185
Atp2a2	0.662890887	1.4722405	0, High	0.809349613
Eno1b	0.871024906	1.521216856	0, High	0.650191949
Slc25a5	0.430604153	1.011805023	0, High	0.58120087
Hnrnpdl	0.652956527	1.06967056	0, High	0.416714033

Supplementary Table 2.8.1. Table of MYC-interacting proteins within the serum-responsive, PIN1-dependent cluster (0,High). This table contains 181 MYC-interacting targets that were enriched in WT but markedly reduced in the PIN1$^{-/-}$ condition following serum-stimulation. Log fold change (LFC) between serum stimulation and starvation was calculated for each target in both the WT and PIN1$^{-/-}$ (PIN1) conditions. The absolute difference in LFC between the two conditions was used to quantify the magnitude of change in MYC interactome upon stimulation.

gene_ID	LFC_WT_MYC	LFC_WT_TPR	Cluster_Label	delta_LFC
Mki67	2.348034207	2.369963153	High, High	0.021928947
Mrps9	1.937303728	1.910763055	High, High	0.026540673
Snip1	2.204191786	2.23583741	High, High	0.031645624
Senp3	2.819510701	2.851248568	High, High	0.031737867
Lsm8	2.094507293	2.029532317	High, High	0.064974976
Srsf3	2.135561674	2.211789431	High, High	0.076227757
Tagln2	3.463009588	3.343342165	High, High	0.119667423
Rbm10	2.765003692	2.906065141	High, High	0.141061449
Rpl37a	2.81250701	2.966359463	High, High	0.153852453
Cttn	4.021467189	3.86275133	High, High	0.158715859
Hk1	4.013833107	3.822614356	High, High	0.191218751
Pafah1b2	1.739776454	1.505208691	High, High	0.234567763
Helz2	1.778422167	1.532491389	High, High	0.245930777
Ranbp2	2.330222516	2.070981752	High, High	0.259240764
Abracl	2.149950927	2.423412411	High, High	0.273461484
Tpt1	1.437322212	1.73251533	High, High	0.295193118
Nol9	1.453085379	1.151196108	High, High	0.301889271

Xrn2	1.561491084	1.86568329	High, High	0.304192206
Eef1b2	3.323341691	3.669293278	High, High	0.345951587
Lonp1	2.063381704	1.702409177	High, High	0.360972527
Psmd14	2.998960733	3.366997885	High, High	0.368037151
Nfib	2.57732954	2.206895892	High, High	0.370433648
Tuba4a	2.254099631	2.654739754	High, High	0.400640123
Nop56	8.583972451	8.181553263	High, High	0.402419188
Cwc25	2.325683595	1.87147925	High, High	0.454204345
Sptbn1	3.086400284	2.628563417	High, High	0.457836867
Idh3a	2.40467264	2.871557848	High, High	0.466885208
Vps35	1.876289655	1.407451803	High, High	0.468837852
Cmas	1.610830431	1.106580265	High, High	0.504250166
Aebp1	1.688478936	1.149870598	High, High	0.538608338
H1f10	2.359775656	1.779450389	High, High	0.580325266
Ppil4	1.970182744	1.374216857	High, High	0.595965887
Ap1m1	1.981584777	1.342432571	High, High	0.639152206
Tkt	6.71424362	6.063007009	High, High	0.651236611
Aimp1	1.961107262	1.286115935	High, High	0.674991327
Sec61g	2.984609397	2.290052964	High, High	0.694556433
Nle1	2.965111616	2.267560681	High, High	0.697550935
Zfp326	1.2387077	2.079001191	High, High	0.840293491
Ddx31	2.134464114	2.983156522	High, High	0.848692408
Sun2	1.80398562	2.677743854	High, High	0.873758233
Serbp1	1.431297861	2.358285003	High, High	0.926987142
Tjp1	2.767759798	1.83314415	High, High	0.934615648
Ppp3cb	1.301788256	2.253204632	High, High	0.951416376
Imp4	1.827621252	2.896940162	High, High	1.06931891
Rab2a	2.473834984	3.570383164	High, High	1.096548181
Cyb5r3	4.724305569	3.611045332	High, High	1.113260237
Txndc5	2.760365758	1.637420701	High, High	1.122945057
Rrp8	3.30037022	2.175540744	High, High	1.124829476
Psma2	4.065339486	2.913455561	High, High	1.151883925
Pdia6	2.441777222	1.268323582	High, High	1.173453639
Alkbh5	3.121690518	1.87773953	High, High	1.243950988
Fndc3b	3.694496889	2.448162302	High, High	1.246334587
Col5a1	3.656382515	2.407728361	High, High	1.248654153
Tpi1	2.447489019	3.696214662	High, High	1.248725642
Mogs	4.930920206	3.674398339	High, High	1.256521868
Cpne1	3.756056756	2.48569181	High, High	1.270364947

Prrx1	3.533800218	2.258293467	High, High	1.275506752
Rpp30	5.200518876	3.891472211	High, High	1.309046666
Anxa1	3.32174626	4.742448039	High, High	1.420701779
Usp39	2.019389869	3.499424217	High, High	1.480034348
Wdr1	5.005811635	6.520240189	High, High	1.514428554
Mrpl13	2.827883018	1.281355437	High, High	1.546527581
Pdcd6ip	1.379434785	2.951374437	High, High	1.571939652
Epb41l2	3.73127099	2.146010524	High, High	1.585260466
Lmnb1	7.14474648	5.55713937	High, High	1.587607111
Lbr	4.834212377	3.20221885	High, High	1.631993527
Cdipt	3.342830193	1.653440183	High, High	1.689390011
Ywhag	7.143895298	5.437254095	High, High	1.706641203
Cbx3	5.260693804	3.550342824	High, High	1.710350981
Krt71	1.853099132	3.567081312	High, High	1.71398218
Ppan	5.047699448	3.291063712	High, High	1.756635737
Fndc3a	4.013005193	2.25407101	High, High	1.758934182
Sf3a3	1.453772799	3.226897568	High, High	1.773124769
Pabpc1	7.137212685	5.357230021	High, High	1.779982664
Ddx39	5.886532054	4.100719342	High, High	1.785812712
Nop58	3.711948958	5.498215752	High, High	1.786266794
Psmd2	4.853891879	3.004775157	High, High	1.849116723
Trim28	1.799919809	3.67420858	High, High	1.874288771
Lars	1.317411077	3.266456329	High, High	1.949045252
Glrx3	4.61615837	2.658953664	High, High	1.957204706
Psma7	3.533898032	1.498185517	High, High	2.035712516
Rnps1	1.315862652	3.405563416	High, High	2.089700764
Ncoa5	1.684901616	3.85051267	High, High	2.165611055
Fmr1	1.047487277	3.290673393	High, High	2.243186116
Eif5b	4.318513774	2.022039395	High, High	2.296474379
Ssr4	5.484525046	3.151223936	High, High	2.333301109
Ufl1	5.640715289	3.284737299	High, High	2.35597799
Nifk	6.768777821	4.394922702	High, High	2.373855119
Eif1ax	1.193811849	3.581628837	High, High	2.387816988
Ifi205	4.954265143	2.555178842	High, High	2.399086301
Dad1	5.629314237	3.214787212	High, High	2.414527025
Jup	3.626068496	1.210658123	High, High	2.415410373
Cybc1	4.23946403	1.789854793	High, High	2.449609236
Dcaf13	2.352297384	4.848267061	High, High	2.495969678
Mrpl4	5.699611754	3.201832268	High, High	2.497779486

Tecr	4.463501793	1.921569284	High, High	2.541932508
P4ha2	4.695324695	1.822367601	High, High	2.872957094
Atp2a2	1.4722405	4.399275885	High, High	2.927035385
Btf3	1.007212185	4.123324446	High, High	3.11611226
Rps9	8.801095466	5.682000834	High, High	3.119094632
Rars	5.709928451	2.568443868	High, High	3.141484583
Tubb5	2.63195571	5.838517354	High, High	3.206561645
H2aj	13.78614706	10.19073719	High, High	3.59540987
Abcf1	5.452056559	1.096763206	High, High	4.355293354
Hnrnpdl	1.06967056	5.428131775	High, High	4.358461215
Hsp90ab1	2.743365226	8.378269482	High, High	5.634904255
Sec61a1	7.594173404	1.102675544	High, High	6.49149786

Supplementary Table 2.8.2. Table of MYC-TPR co-interacting proteins in WT cells within the serum-responsive cluster (High,High). This table includes 107 targets identified to interact with both MYC and TPR following serum stimulation in the WT condition. Log fold change (LFC) between serum stimulation and starvation was calculated for each target, and the absolute difference in LFC was used to quantify the magnitude of change in interaction with either MYC or TPR upon stimulation.

gene_ID	LFC_PIN1KO_MYC	LFC_PIN1KO_TPR	Cluster_Label	delta_LFC
Nsun2	2.684360469	2.764786918	High, High	0.08042645
Snip1	2.052746169	1.81482342	High, High	0.237922748
Akr1b3	4.357712345	3.925161958	High, High	0.432550388
Pfkl	2.947317455	2.459973356	High, High	0.487344099
Gnai2	4.42526077	3.749606905	High, High	0.675653865
Cav1	4.020949315	3.284689996	High, High	0.736259319
Xrn2	1.538216282	2.28739803	High, High	0.749181749
Usp5	1.244072205	2.065537251	High, High	0.821465046
Iars	3.362779143	2.513191471	High, High	0.849587672
Hmga1	6.131982557	5.263930517	High, High	0.86805204
Tpm1	3.828684424	2.822548375	High, High	1.006136049
Capzb	1.12290132	2.172732051	High, High	1.049830731
Exosc2	2.826103723	1.764828689	High, High	1.061275034
Cnn1	4.300422338	3.206184023	High, High	1.094238315
Tcerg1	3.442814048	2.170799154	High, High	1.272014893
Pls3	3.932570285	2.534461275	High, High	1.39810901
Eif5a	7.640692168	6.203528612	High, High	1.437163557
Pgam1	2.098027221	3.535733032	High, High	1.437705812
Fbll1	8.331409959	6.551074489	High, High	1.78033547

Carhsp1	1.163561368	3.368479856	High, High	2.204918488
Vcp	5.03446668	2.656772097	High, High	2.377694583
Cnn2	5.656464914	2.200760408	High, High	3.455704506
Vdac2	5.634501914	9.114577295	High, High	3.480075381
Acin1	6.396831467	1.270637525	High, High	5.126193942
H3f3a	9.682126154	3.573533371	High, High	6.108592784

Supplementary Table 2.8.3. Table of MYC-TPR co-interacting proteins in PIN1$^{-/-}$ cells within the serum-responsive cluster (High,High). This table includes 25 targets identified to interact with both MYC and TPR following serum stimulation in the PIN1$^{-/-}$ condition. Log fold change (LFC) between serum stimulation and starvation was calculated for each target, and the absolute difference in LFC was used to quantify the magnitude of change in interaction with either MYC or TPR upon stimulation.

Chapter 3: MYC Serine 62 phosphorylation promotes its binding to DNA double strand breaks to facilitate repair and cell survival under genotoxic stress.

Gabriel M. Cohn[1], Colin J. Daniel[1], Jennifer R. Eng[1], Xiao-Xin Sun[1], Carl Pelz[1,2], Koei Chin[3,4], Alexander Smith[2], Charles D. Lopez[2,5,6], Jonathan R. Brody[2,6,7,8], Mu-shui Dai[1], Rosalie C. Sears[1,2,6]

[1]Department of Molecular and Medical Genetics, School of Medicine, Oregon Health and Science University, Portland, OR, USA

[2]Brenden-Colson Center for Pancreatic Care, Oregon Health and Science University, Portland, OR, USA

[3]Center for Early Detection Advanced Research, Oregon Health and Science University, Portland, OR, USA

[4]Department of Biomedical Engineering, Oregon Health and Science University, Portland, OR, USA

[5]Department of Hematology and Oncology, Oregon Health and Science University, Portland, OR, USA

[6]Knight Cancer Institute, Oregon Health and Science University, Portland, OR, USA

[7]Department of Surgery, Oregon Health and Science University, Portland, OR, USA

[8]Department of Cell, Developmental and Cancer Biology, Oregon Health and Science University, Portland, OR, USA

Corresponding Author:

Rosalie C. Sears

Oregon Health & Science University

searsr@ohsu.edu

3.1 Abstract

Genomic instability is a hallmark of cancer, driving oncogenic mutations that enhance tumor aggressiveness and drug resistance. MYC, a master transcription factor that is deregulated in nearly all human tumors, paradoxically induces replication stress and associated DNA damage while also increasing expression of DNA repair factors and mediating resistance to DNA-damaging therapies. Emerging evidence supports a non-transcriptional role for MYC in preserving genomic integrity at sites of active transcription and protecting stalled replication forks under stress. Understanding how MYC's genotoxic and genoprotective functions diverge may reveal new therapeutic strategies for MYC-driven cancers. Here, we identify a non-canonical role of MYC in DNA damage response (DDR) through its direct association with DNA breaks. We show that phosphorylation at serine 62 (pS62-MYC) is crucial for the efficient recruitment of MYC to damage sites, its interaction with repair factors BRCA1 and RAD51, and effective DNA repair to support cell survival under stress. Mass spectrometry analysis with MYC-BioID2 during replication stress reveals a shift in MYC's interactome, maintaining DDR associations while losing transcriptional regulators. These findings establish pS62-MYC as a key regulator of genomic stability and a potential therapeutic target in cancers.

3.2 Introduction

MYC is a master transcriptional regulator that impacts all cellular pathways involved in proliferation, differentiation, and response to cellular signals [45, 75]. Due to its participation in anabolic and stress-responsive biology, MYC deregulation is found in virtually all human cancers, is prognostic for patient survival, and is often responsible for

chemotherapy resistance[44, 282-284]. To prevent MYC's oncogenic effect in normal cells, MYC protein abundance and activity is tightly regulated with a half-life of about 15-30 minutes under physiological conditions[285]. MYC's stability is primarily regulated through sequential phosphorylation events within MYC's transactivation domain, Thr58 (pT58-MYC) and Ser62 (pS62-MYC) which impact its degradation through the ubiquitin-proteosome system[259, 286, 287]. Upon cell growth stimulation, MYC becomes transiently stabilized by RAS-induced and/or cyclin-dependent kinase-mediated phosphorylation at Ser62 resulting in increased MYC stability and activity[116, 288]. To trigger MYC's degradation, subsequent phosphorylation at Thr58 by GSK3 or BRD4 initiates MYC's engagement with the ubiquitin-proteosome system [126, 289].

Mechanistically, MYC canonically functions as a transcription factor that enables potent transcriptional amplification, intensifying the recruitment and assembly of multiple protein complexes at each stage of transcription[77]. MYC-driven transcriptional amplification is accompanied by genomic burdens such as increased torsional stress, R-loop formation, Transcriptional-Replication Conflicts (TRCs), among others[161]. To mitigate this increase in genomic stress, emerging and non-canonical functions of MYC have recently been described. Along with recruiting transcriptional machinery to active promoters, MYC nucleates a "topoisome" complex between topoisomerase 1 & 2 to relieve DNA torsional stress produced by the elevated transcription[203]. MYC has also been shown to facilitate the transfer of polymerase associated factor 1c (PAF1c) to stalled RNA polymerase, activating several chromatin modifying complexes and DNA repair to ensure high fidelity elongation[194]. In response to a variety of cellular stressors including transcriptional stress, replication stress, and proteolytic stress, MYC proteins have been

described to multimerize and protect replication-fork stability, decrease R-loop formation, and terminate transcription, all to protect genomic stability in the presence of stress[196, 199]. Accompanying these MYC multimers were DNA maintenance proteins which aligns with previous findings that the neuronal MYC paralog, MYCN, and MYC are capable of recruiting critical components of DNA repair such as BRCA1, the TRRAP-containing NuA4 complex, and the p400 helicase to active promoters[84, 195, 196, 290, 291]. Although these studies have highlighted emerging roles of MYC in safeguarding the genome under cellular stress, a direct role for MYC in mediating DNA repair has not been explored.

In this study, we investigated a direct role of MYC in DNA repair in cancer cells with a focus on pancreatic ductal adenocarcinoma (PDAC). Our previous research demonstrated that MYC pathway activity is high in a subset of patients with aggressive, liver metastatic PDAC, characterized by elevated replication stress and DNA repair signatures[292]. We performed further analyses and confirmed a strong correlation between MYC and the tumor's response to genomic instability, both at the transcriptional and tissue levels. To investigate the cellular mechanisms behind this strong correlation, we employed a DNA double-strand break (DSBs)-specific proximity ligation assay to discover that MYC associates with DSBs and that genomic stress enhances MYC's association with DSBs as well as repair proteins such as BRCA1 and RAD51. Furthermore, using a MYC-BioID2 proximity-dependent proteomic approach, we observed a shift in MYC's interactome under replication stress, marked by a notable enrichment of DNA repair machinery. Mechanistically, we discovered that MYC's association with DSBs is dependent on the phosphorylation at serine 62 (pS62-MYC).

Blocking this phosphorylation with a phosphorylation-deficient MYC mutant (S62A-MYC) disrupts BRCA1 and RAD51 recruitment to DSBs, resulting in a reduction in DNA repair and overall cell survival. Together, our findings reveal a novel direct role for MYC in DNA damage repair, offering new insights into MYC's involvement in genome maintenance that could be leveraged for new therapeutic strategies.

3.3 Results

MYC Activity Positively Correlates with Genomic stress, DNA repair and Poor Patient Survival in PDAC

Our recent study demonstrated that pancreatic ductal adenocarcinoma (PDAC) patients with tumors exhibiting higher molecular signatures of tolerance to replication stress are more likely to develop liver metastasis and experience poorer overall survival[292]. Furthermore, this study demonstrated that elevated MYC activity was associated with a tumor survival advantage under conditions of high replication stress and DNA damage. To explore this dataset of 218 primary tumors and 71 metastases further, we generated a replication stress gene set based on the intersection between known cell cycle, check point, and DNA replication genes. We found a significant positive correlation between this replication stress signature score and the hallmark MYC-V1 target pathway score (Figure 3.3.1A). Since tumor cells experiencing high proliferation and transcriptional activity are often deficient in biosynthetic activity, they face stalled and collapsed replication forks leading to DSBs and genomic damage [293, 294]. In agreement with the replication stress signature, elevated hallmark MYC-V1 targets pathway activity significantly positively correlated with the hallmark DNA repair pathway score in our patient PDAC tumor samples, suggestive of MYC's emerging non-canonical

function involved in maintaining genomic integrity (Figure 3.3.1B). We then stratified our PDAC tumor dataset into either high or low hallmark MYC-V1 pathway score cohorts and performed Virtual Inference of Protein-Activity Enrichment Regulon (VIPER)[295, 296] analysis. Comparing common replication stress response and DNA damage repair regulons from the VIPER analysis revealed a robust enrichment in tumors with high MYC-V1 pathway scores compared to those with lower MYC-V1 pathway scores (Figure 3.3.1C). In PDAC, patient survival and efficacy of treatment is impacted, in part, by somatic alterations in DNA damage response (DDR) genes[292, 293]. To investigate whether DDR alteration status affects MYC's impact on patient survival, we separated our cohort into four categories that stratify based on high/low Hallmark MYC V1 target score and whether a patient has a detected somatic DDR alteration in their tumor. Patients with MYC-high tumors had poor survival regardless of tumor DDR status (Figure 3.3.1D, red vs blue lines); however, patients with DDR-altered MYC-low tumors have a significantly better survival probability over MYC-high DDR-altered tumors (Figure 3.3.1D). This suggests that high MYC activity promotes tolerance to the presence of DDR alterations, supporting aggressive tumors and poor patient outcome including resistance to DNA damaging chemotherapy, as 24% of our patients in our cohort received neoadjuvant and/or adjuvant chemotherapy[292].

To investigate these findings at the protein level within human PDAC, we performed cyclic immunofluorescence (cycIF) on a patient-derived PDAC tissue microarray (TMA) with antibodies detecting markers of post-translationally active MYC (phospho-Ser62), cell proliferation, and DNA damage response. Consistently, we observed cytokeratin-19 positive tumor cells with overlapping staining for the activated

pS62-MYC[297, 298] and DNA damage markers RAD51, pRPA, and γH2AX (Figure 3.3.1E,F). When per cell intensities were quantified and ranked by correlation with pS62-MYC in tumor cells, in addition to the DNA damage proteins RAD51, pRPA, γH2AX and 53BP1, we observed significant correlation with cell cycle proteins PCNA and Ki67, suggestive of coupled proliferate and DNA repair (Figure 3.3.1G,H). However, when quantifying all 54 cores across 34 patients, the correlation between pS62-MYC and proliferation markers is not as strong while the correlation with DNA damage markers remain robust and significant (Figure 3.3.1I). Together, this data indicates that MYC

expression correlates with markers for DNA damage response in PDAC tumors and impacts overall patient survival, particularly with patients with somatic DDR alterations.

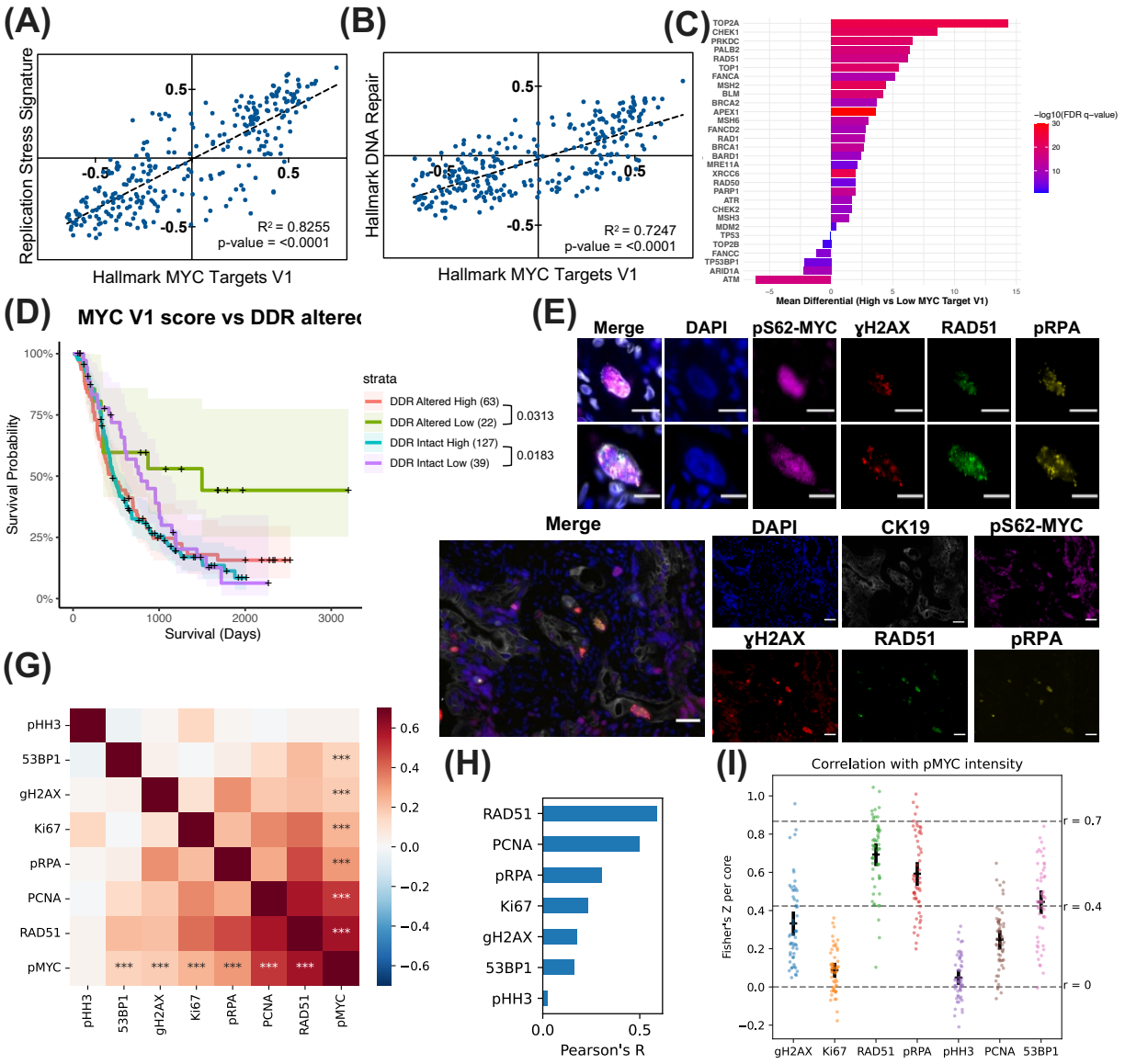

Figure 3.3.1. MYC Activity Positively Correlates with Genomic Damage and Poor Patient Survival in PDAC.

(A) Pearson correlations of RNA expression of 289 primary and metastatic PDAC tumors comparing GSVA scores of hallmark MYC-V1 targets and a replication stress gene signature (B) as well as hallmark DNA repair pathway. (C) Mean differential VIPER regulon activity for DNA maintenance factors between tumors with high or low hallmark MYC-V1 target score, with coloring indicating FDR q-values from a one-way ANOVA. (D) K-M graph of overall survival for patients with high or low hallmark MYC-V1 target score stratified by tumors with (DDR altered) or without (DDR intact) known somatic alterations in DNA damage response-related genes. Shaded regions represent 95% CI. All P-values

not shown are greater than 0.05. (E) Two close-up images of pS62-MYC positive and DNA damage marker positive cells. Scale bar, 26μm. (F) Representative images of cyclic immunofluorescence analysis of a single core from a PDAC tissue microarray. Scale bar, 32.5μm. (G) Pearson correlation (two-sided) of mean antibody intensities (***)FDR <0.001. (H) Ranked Pearson's R correlation of mean antibody intensity. (I) Fisher's Z transformed Pearson correlation r value per core of single cell mean intensity correlation with pS62-MYC intensity for all 54 cores across 34 patients. Error bars represent the 95% confidence interval. Dotted lines represent Pearson r value of 0, 0.4 and 0.7, respectively.

MYC is Detected in Proximity to DNA Double-Strand Breaks

To explore whether MYC plays a direct role in the molecular regulation of DNA breaks, we performed DNA Damage in situ Proximity Ligation Assay (DI-PLA) [299], wherein a biotinylated DNA probe was ligated to DSBs, and proximity ligation assay (PLA) was conducted between biotin and MYC (Figure 3.3.2A). We treated an early passage patient-derived cancer cell line (ST-00024058), isolated from a resected PDAC tumor, with bleomycin and conducted DI-PLA. Bleomycin treatment resulted in a significant increase in DI-PLA puncta compared to DMSO control, indicating an enhanced proximity between MYC & DSBs in a patient-derived cancer cell line following DNA-damaging chemotherapy (Figure 3.3.2B). In a more precisely controlled system, we leveraged site-specific cleavage with a cas9 transfection with RNA guides targeting the 28S ribosomal DNA (rDNA) [300]. Targeting rDNA allows for signal amplification since there are approximately 400 copies of rDNA per cell. DI-PLA revealed a robust increase in association between MYC and cas9-induce DSBs compared to non-targeting control (NT) (Figure 3.3.2C). This suggests that MYC associates with DSBs generated by both chemotherapy and site-specific cleavage.

As replication stress is a driver of DSBs and MYC expression correlates with pRPA expression, a marker of stalled replication forks (Figure 3.3.2D-G), we sought to

determine whether MYC localization to DSBs is increased under high levels of replication stress in cells. To induce replication stress, cells were treated with aphidicolin (APH), an inhibitor of DNA polymerases α, δ, and ε, leading to the formation of vulnerable regions of single-stranded DNA, replication fork collapse, and the subsequent generation of DSBs[294]. Consistent with direct DSB generation, APH treatment for 5-hours in HEK293, U2OS, MIA PaCa-2, and HeLa cells revealed a significant and robust increase in MYC's association with replication stress-induced DSBs (Figure 3.3.2D). In agreement, the MYC-γH2AX PLA signal also increased following APH treatment in these cell lines, together highlighting the presence of MYC at DSBs following replication stress across multiple conventional cell lines (Figure 3.3.2E). To begin to understand the influence of MYC's localization to DSBs on DNA repair, we tested whether APH induced an enrichment between MYC and known DNA repair proteins. BRCA1 binds DSBs and promotes homologous recombination directed repair and has been shown to bind to MYC, however, the mechanistic impact of this interaction remains to be clarified [301-303]. We observed a robust association between MYC and BRCA1 following 5-hour APH treatment, suggesting that this interaction is responsive to increased genomic damage (Figure 3.3.2F). Furthermore, we detected an APH-induced increase in association between the post-transcriptionally stable form of MYC (pS62-MYC) and RAD51 (Figure 3.3.2G); an interaction not previously reported in the literature. Taken together, our data suggests that MYC has a conserved capability of associating with DSBs and is able to interact with DNA repair proteins in response to DNA damage.

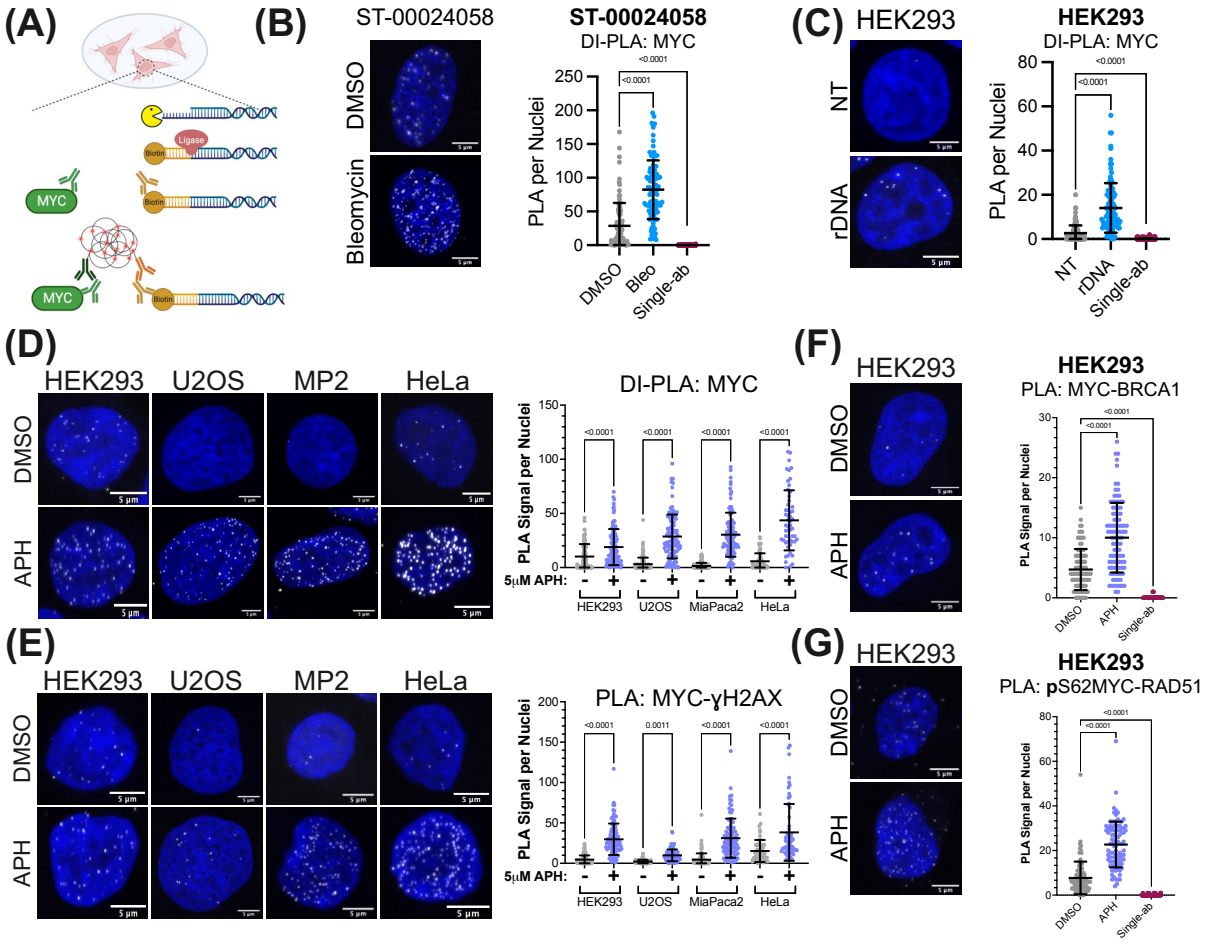

Figure 3.3.2. MYC is Detected in Proximity to DNA Double-Strand Breaks.

(A) Schematic of DNA Damage in situ Proximity Ligation Assay (DI-PLA). (B) Left: Merged DI-PLA between MYC and biotin in a patient-derived PDAC cell line treated for 1 hour with 100 μg/mL bleomycin or DMSO. PLA puncta pseudo-colored in white. Right: quantification from three biological replicates of DI-PLA. Single antibody control combines PLA counts for both primary antibodies alone treated with bleomycin. The error bars show mean ±s.d. Statistical significance was determined by unpaired two-tailed t-test. (C) Left: Merged DI-PLA between MYC and biotin in HEK293 cells transfected with Cas9 protein and guide RNAs (sgRNA) targeting the 28S rDNA or non-targeting control (NT) for 8 hours. Right: quantification of DI-PLA. (D)Left: Representative images of DI-PLA between MYC and biotin in HEK293, U2OS, MIA PaCa-2, and HeLa cells treated with either 5μM APH or DMSO for 5-hours. PLA signal pseudo-colored in white. Left: Quantification of three biological replicates. (E) Left: Representative images of PLA between MYC and γH2AX. Right: Quantification of MYC and γH2AX PLA. (F) Left: Merged representative images of PLA between MYC and BRCA1 in HEK293 cells treated either DMSO or 5μM APH for 5-hours. Right: quantification of PLA. Single antibody control combines PLA counts for both primary antibodies alone treated with 5μM APH. (G) Left: PLA between pS62-MYC and RAD51 in HEK293 cells treated either DMSO or 5μM APH for 5-hours.

Right: quantification of PLA. Note, MYC or pS62-MYC antibodies were chosen for PLA with RAD51 & BRCA1 antibodies based off cross-species compatibility.

MYC's Interactome is Enriched for DNA Repair Proteins Under Replication Stress

To survey a broader and more unbiased enrichment of MYC's interactions under replication stress, we generated stably expressed, doxycycline-inducible MYC-BioID2 in HEK293 cells for proximity-dependent labeling (Figure 3.3.3A). We treated these cells with either DMSO or APH and detected a total of 1,648 targets (Figure 3.3.3B). Our aim was to detect shifts in MYC's interactome following 24-hour APH treatment. However, there were no statistically significant interactors enriched in APH treatment versus DMSO treatment following false discovery rate (FDR) correction (Figure 3.3.3C). This limited differential is likely attributed to a technical limitation of the BioID2 system, which requires an 18-hour incubation for biotinylation of proteins, whereas DNA damage response occurs on a much shorter timescale. Nevertheless, after background subtraction of the BioID2-only control and applying a ³2-fold differential abundance threshold and p=0.25 a shift in MYC protein target interactions in response to APH treatment is observed (Figure 3.3.3D). To better understand the functional differences of MYC interactors between DMSO and APH conditions, we conducted Gene Ontology (GO) enrichment using the BinGO tool in Cytoscape [264, 265, 304]. The interconnections of the enriched gene ontologies for MYC interactors under DMSO emphasize mechanisms which align with MYC's canonical functions involved in gene expression, chromatin remodeling, and metabolism (Figure 3.3.3E). The APH-enriched MYC interactor ontologies highlight proteins involved in response to genomic damage, cell cycle regulation, and DNA repair (Figure 3.3.3F). These findings are consistent with recent studies demonstrating that under stress conditions, MYC shifts away from driving transcriptional processes to

promoting DNA stability[196, 199]. In agreement, when GO terms are ranked by adjusted p-value, we see the most significant terms for DMSO include processes involved in nucleotide metabolism and gene regulation while top terms for APH-induced MYC interactions pertain to genomic maintenance (Figure 3.3.3G). This data indicates that MYC's interactome becomes more enriched for DNA damage response proteins under replication stress.

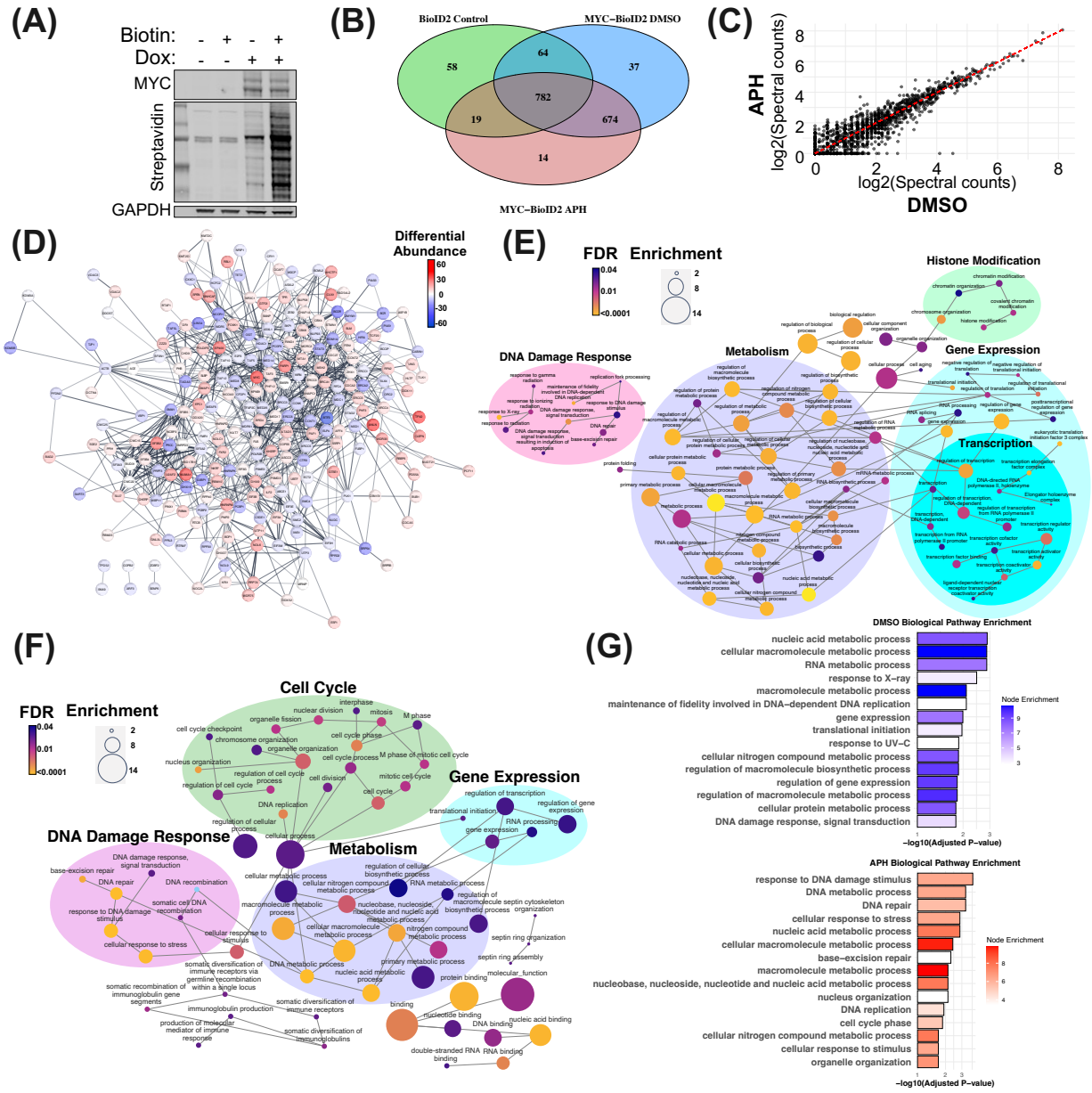

Figure 3.3.3. MYC Interactome is Enriched for DNA Repair Proteins Under Replication Stress.

(A) Western Blot validation of inducible MYC-BioID2 construct in HEK293 cells treated with 1 μg/mL doxycycline for 24-hours and 50 μM biotin for 18-hours. (B) Venn diagram of biotinylated proteins detected in the different conditions, BioID2-only control (n=3), MYC-BioID2 treated with 24-hours of DMSO (n=3) or 5μM APH (n=2). (C) Scatter plot showing mean log2 value for the DMSO and APH conditions following background subtraction of BioID2-only. (D) Cytoscape interaction network analysis of MYC-BioID2 targets that pass a threshold of ≥2-fold differential abundance. Nodes colored based off mean spectral count differential abundance between APH (Red) and DMSO (Blue).

BiNGO analysis showing the Gene Ontology (GO) enrichment network of DMSO (E) and APH (F). (G) Top 15 significantly enriched GO Biological pathway terms for DMSO (top) and APH (bottom).

Serine 62 Phosphorylation of MYC Promotes its Association with DSBs

To begin to investigate whether post-translational modification of MYC could play a role in the functional switch in MYC activity upon genomic insult and its localization to DSBs and interaction with repair proteins, we investigated the impact of MYC's phosphorylation status on this mechanism. Phosphorylation of MYC, particularly at threonine 58 and serine 62, have been shown to regulate its stability, target gene promoter binding, and spatial localization within the nucleus[108, 305]. In response to growth signals, MYC is transiently stabilized by the phosphorylation of serine 62, enhancing its engagement with target genes, including those poised at the nuclear periphery[108, 116, 125, 306]. Processive phosphorylation at threonine 58 (pT58-MYC) destabilizes MYC, initiating its degradation via the proteosome[130, 307]. To examine whether these phosphorylation sites in MYC could also affect its association with DSBs, we used doxycycline-inducible HEK293 cells which express hemagglutinin (HA) tagged wild-type MYC (WT-MYC), serine-to-alanine mutant MYC (S62A-MYC), or the threonine-to-alanine mutant MYC (T58A-MYC). Given the sequential nature of phosphorylation at these sites, with S62 phosphorylation preceding the phosphorylation of T58 by the processive GSK3 kinase [126], S62A-MYC lacks phosphorylation at both sites, whereas T58A-MYC exhibits robust phosphorylation at S62 but lacks phosphorylation at T58 (Figure 3.3.4A). We performed HA-tagged DI-PLA following cas9-directed cleavage of the 28S rDNA. Consistent with endogenous MYC, we observed a robust increase in the association of ectopic WT-MYC and cas9-induced DSBs (Figure 3.3.4B). In contrast,

S62A-MYC showed no statistically significant difference between non-targeting (NT) control and cas9-induced DSBs, while T58A-MYC exhibited a similar or even greater induction of MYC associated with DSBs compared to WT. Similar induction patterns were observed in a PLA between HA-tag and γH2AX (Figure 3.3.4C), demonstrating that serine 62 phosphorylation is a key determinant of MYC's association with cas9-induced DSBs. To confirm these findings under replication-stress induced DSBs, we treated the MYC mutant cells with APH. WT-MYC showed a strong increased association with APH-induced DSBs compared to the DMSO control (Figure 3.3.4D). Likewise, T58A-MYC demonstrated a robust increase in association with APH-induced DSBs. While the S62A-MYC mutant also showed some increased association with DSBs, this was significantly less than WT-MYC and T58A-MYC. T58A-MYC retains persistent serine 62 phosphorylation due to resistance to PP2A-mediated dephosphorylation, unlike WT-MYC [127, 306]. Notably, T58A-MYC displayed elevated association with DSBs even prior to APH treatment. Collectively, these data indicate that serine 62 phosphorylation plays an important role in MYC's efficient association with DSBs in response to cas9- and APH treatment-induced DSBs. To verify that the difference in association with DSBs was not due to differences in expression levels, whole cell lysates of the three cell lines showed equal expression of the HA-tag MYCs (Figure 3.3.4E). In agreement with past findings of negative autoregulation [308], the lower molecular weight band of endogenous MYC was nearly undetectable when ectopic MYC is expressed, supporting that endogenous MYC did not compensate for the phosphorylation mutants. Furthermore, a neutral comet assay demonstrated that the levels of DSBs induced by 5-hour APH treatment was not significantly different between cells expressing WT-, S62A-, and T58A-MYC, confirming

that the number of DSBs is equivalent across the conditions (Figure 3.3.4F,G). Taken together, these data underscore the critical role of serine 62 phosphorylation in MYC's efficient association with DSBs.

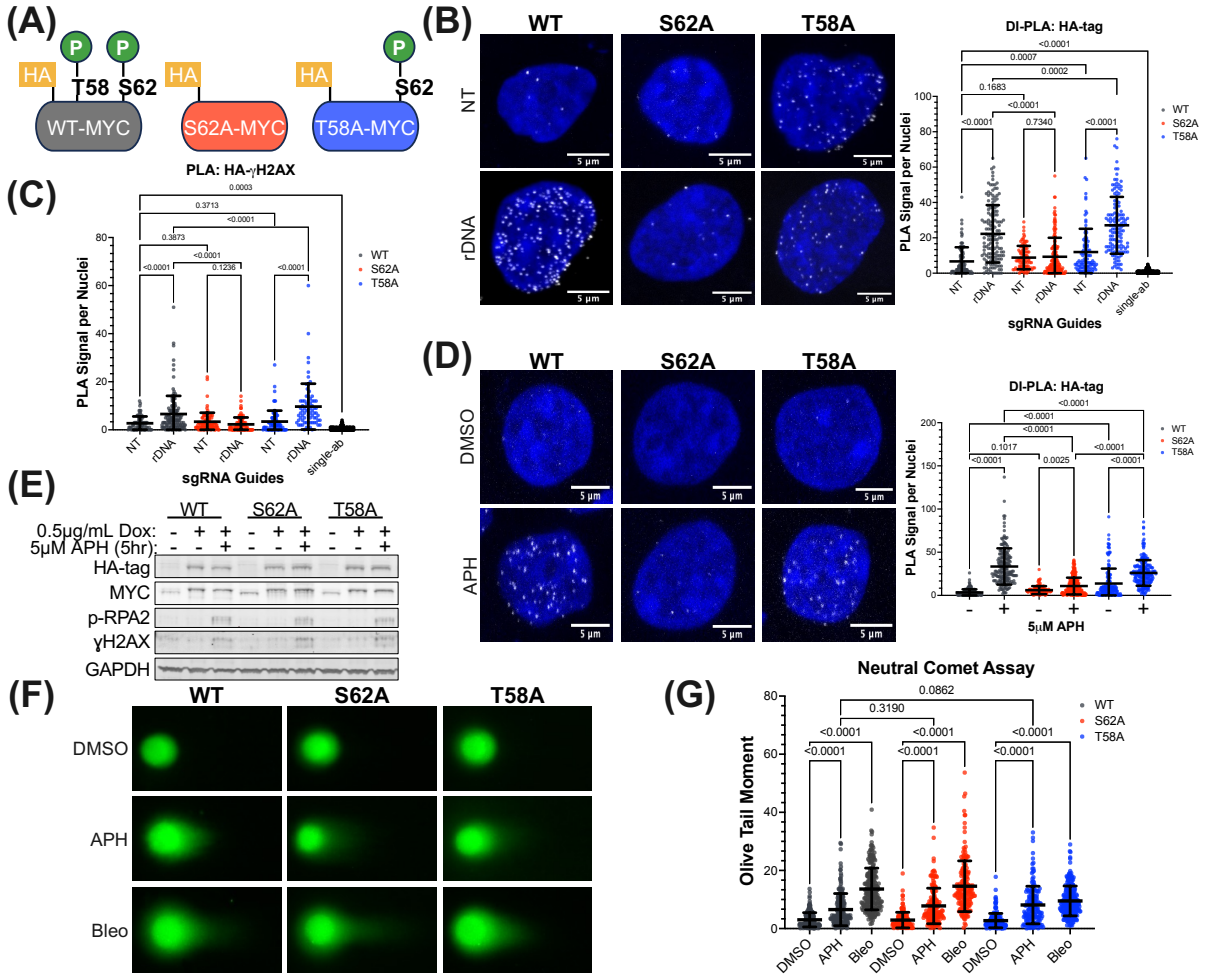

Figure 3.3.4. Serine 62 Phosphorylation of MYC Promotes its Association with DSBs.

(A) Schema of phosphorylation status of HA-tagged WT-MYC, S62A-MYC, and T58A-MYC in doxycycline inducible HEK293 cells. (B) *Left:* Merged DI-PLA between HA-tag and biotin treated for 18-hours with 0.5μg/mL doxycycline followed by an 8-hour transient transfection with Cas9 protein and guide RNAs (sgRNA) targeting the 28S rDNA or non-targeting control (NT). PLA puncta pseudo-colored in white. *Right:* Quantification of three biological replicates of DI-PLA in. Single antibody control combines PLA counts for both primary antibodies alone treated with rDNA guides. The error bars show mean ±s.d. Statistical significance was determined by ANOVA. (C) Quantification of three biological replicates of PLA between HA-tag and γH2AX. (D) *Left*: Merged representative single-cell images of DI-PLA between HA-tag and biotin treated for 18-hours with 0.5μg/mL doxycycline followed by 5μM APH (+) or DMSO (-) for 5 hours. Right: Quantification of three biological replicates with error bars showing mean ±s.d. and statistical significance was determined by ANOVA. (E) Western Blot analysis of WT-, S62A-, and T58A-MYC in HEK293 cell lines treated with 0.5μg/mL doxycycline for 18-hours followed by 5μM APH (+) or DMSO (-) for 5 hours. (F) Neutral comet assay following the same treatment as (E). 1-hour 100 μg/mL bleomycin treatment was positive control. (G) Quantification of (F)

showing the Olive Tail Moment of three biological replicates. The error bars show mean ±s.d. Statistical significance was determined by ANOVA.

Serine 62 Phosphorylation of MYC Regulates the Efficient Recruitment of BRCA1 and RAD51 to DSBs

To assess whether MYC could influence the recruitment of repair factors to DSBs, we initially evaluated the impact of MYC phosphorylation status on its association with BRCA1 & RAD51 as shown in Figure 2F & G. Both WT & T58A-MYC exhibited strong and comparable association with BRCA1 following APH treatment, while S62A-MYC showed a weaker induction, significantly reduced compared to WT & T58A-MYC (Figure 3.3.5A). Similarly, WT-MYC demonstrated a pronounced APH-induced increase in RAD51 association, T58A-MYC association was also significantly increased, while S62A-MYC did not show a significantly increased interaction with RAD51 (Figure 3.3.5B). Co-immunoprecipitation of flag-tagged WT-, S62A-, or T58A-MYC in APH-treated HEK293 cells confirmed the reduced interaction between MYC and RAD51 when serine 62 phosphorylation is blocked (Figure 3.3.5C). Given S62A-MYC's diminished association with DSBs, we next examined whether serine 62 phosphorylation of MYC and its efficient recruitment to DSBs might be important for the localization of BRCA1 and RAD51 to DSBs. DI-PLA analysis of BRCA1 in WT-MYC expressing cells demonstrated a robust APH-induced increase in BRCA1 association with DSBs (Figure 3.3.5D,E). However, this induction was not observed in S62A-MYC expressing cells, with no significant difference in BRCA1 association with DSBs between DMSO and APH treatment in these cells. A similar pattern was observed with cas9-induced DSBs (Figure 3.3.5F), with the unexpected finding that BRCA1's association with DSBs falls below NT control in S62A-MYC expressing cells, an observation that warrants further experimentation to draw a

definitive conclusion. S62A-MYC expressing cells also had a marked reduction in RAD51 localization to APH-induced DSBs compared to WT-MYC expressing cells (Figure 3.3.5G,H). These results collectively demonstrate that efficient recruitment of BRCA1 and RAD51 to DSBs as well as their association with MYC is reliant on serine 62 phosphorylation of MYC.

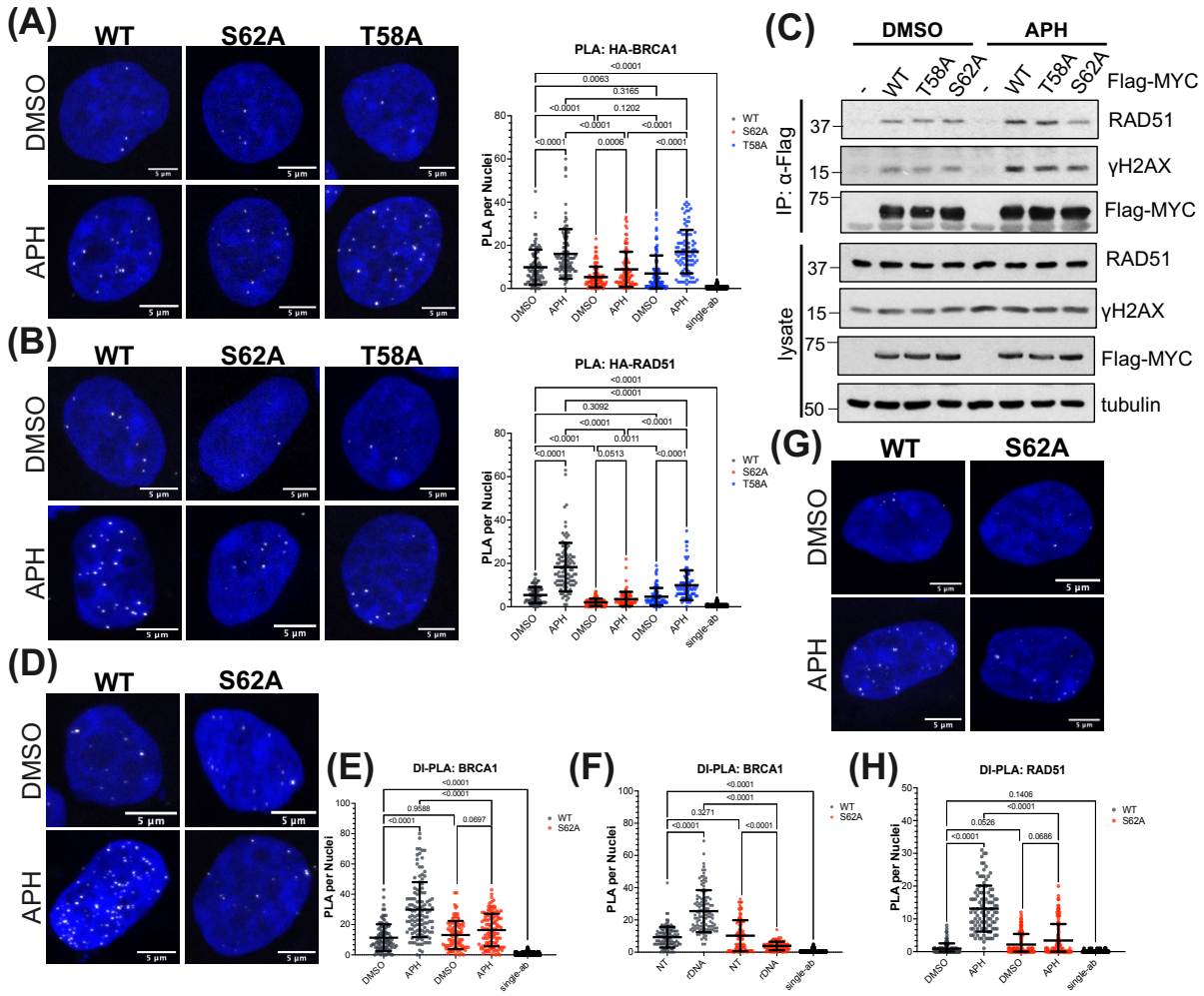

Figure 3.3.5. Serine 62 Phosphorylation of MYC Regulates the Efficient Recruitment of BRCA1 and RAD51 to DSBs.

(A) Merged PLA between HA-tag and BRCA1 treated for 18-hours with 0.5μg/mL doxycycline followed by 5 hours of either DMSO or 5μM APH. PLA pseudo-colored in white. (B) Quantification of (A) experiment. Single antibody control combines PLA counts for both primary antibodies alone treated with 5μM APH for 5-hours. The error bars show mean ±s.d. Statistical significance was determined by ANOVA. (C) Merged PLA between HA-tag and RAD51 treated for 18-hours with 0.5μg/mL doxycycline followed by 5 hours of either DMSO or 5μM APH. PLA pseudo-colored in white. (D) quantification of (C). (E) Co-immunoprecipitation of transiently transfected Flag-tagged WT, T58A, or S62A-MYC in HEK293 cells followed by 5-hour treatment with either DMSO or 5μM APH. Anti-Flag antibody for precipitation followed by Western Blot analysis. (F) Merged DI-PLA experiment between BRCA1 and biotin in WT or S62A-MYC expressing HEK293 cells treated with 0.5μg/mL doxycycline for 18-hours followed by 5-hour treatment with either DMSO or 5μM APH. (G) Quantification of (F). (H) Merged DI-PLA experiment between RAD51 and biotin in WT or S62A-MYC expressing HEK293 cells treated with 0.5μg/mL

doxycycline for 18-hours followed by 5-hour treatment with either DMSO or 5μM APH. (I) Quantification of (H).

Phosphorylation of MYC at Serine 62 is Critical for DNA Damage Repair and Cell Survival in Response to APH-induced Stress.

To investigate the biological implications of MYC's association with DSBs and DNA repair machinery, we performed a 3-hour washout experiment following APH treatment. Consistent with Figure 3.3.4F & 3.3.4G showing equivalent levels of DNA damage in WT- and S62A-MYC expressing cells, APH treatment produced comparable γH2AX puncta in both WT- and S62A-MYC expressing cells (Figure 3.3.6A,B). However, while WT-MYC efficiently resolved many of those γH2AX puncta during the 3-hour washout, the number of puncta increased in S62A-MYC expressing cells. Since γH2AX is not an exclusive marker of DSBs, we performed a neutral comet assay of pre- and post-washout. In agreement, WT-MYC successfully resolved APH-induced DSBs, while S62A-MYC comet tails showed longer comet tails post-washout compared to the pre-washout (Figure 3.3.6C,D). To assess whether the deficiency in DNA damage repair observed in S62A-MYC expressing cells impacted cell survival, we conducted a 10-day colony formation assay following a 5-hour APH treatment at varying concentrations. T58A-MYC exhibited a similar number of colonies to WT-MYC, whereas S62A-MYC showed a significant reduction and an impaired ability to recover from APH-induced DNA damage (Figure 3.3.6E,F). Altogether, these findings suggest that MYC serine 62 phosphorylation impacts its association with DSBs, the recruitment of DNA repair machinery, and the promotion of DNA repair and cell survival.

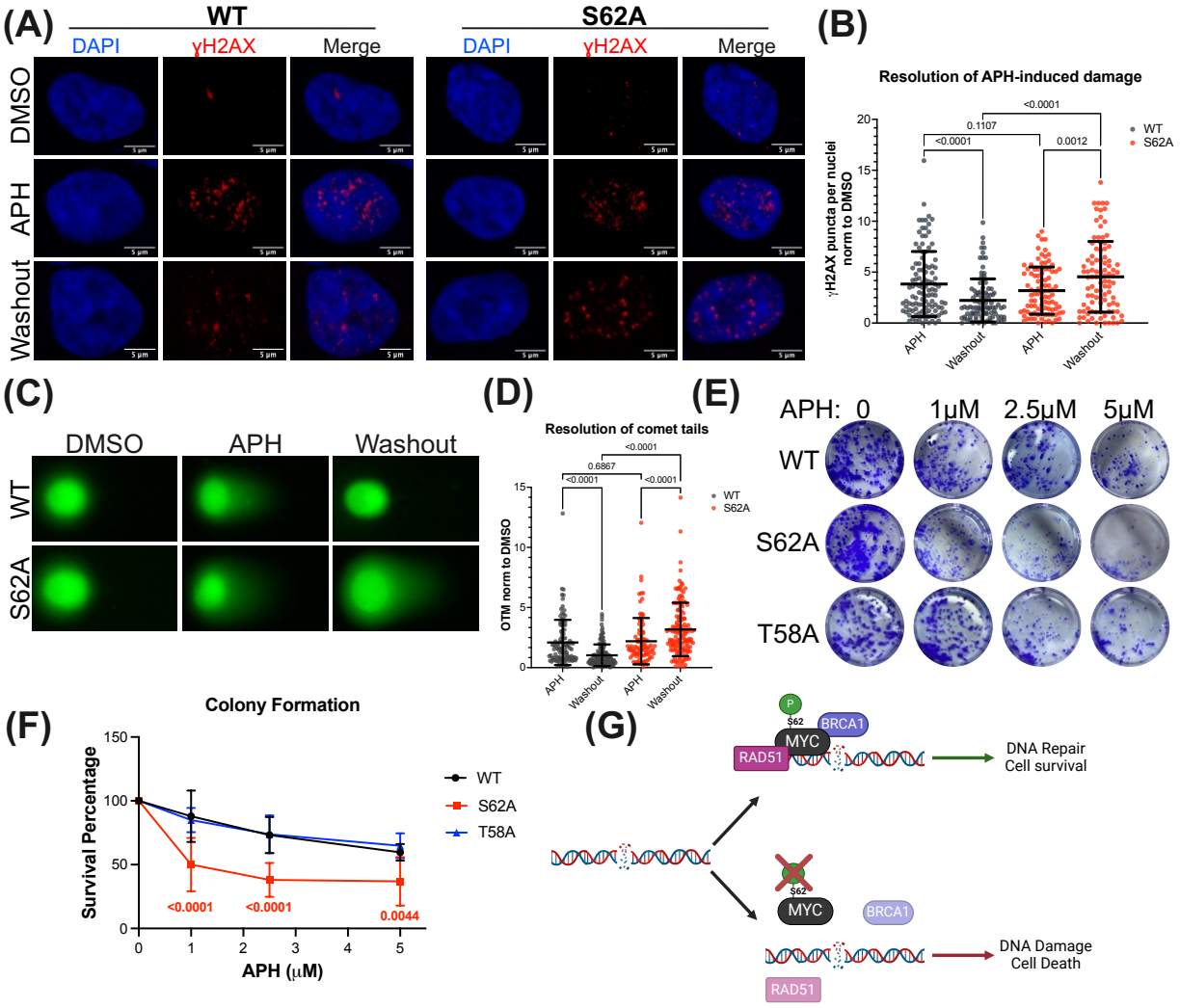

Figure 3.3.6. Phosphorylation of MYC at Serine 62 is Critical for DNA Damage Repair and Cell Survival in Response to APH-induced Stress.

(A) Representative immunofluorescence images showing γH2AX puncta. WT- or S62A-MYC were induced by 18-hour 0.5μg/mL doxycycline treatment followed by either 5-hours of either DMSO or 5μM APH. Washout represents coverslips which were treated with 5μM APH for 5-hours followed by a media change with doxycycline for 3-hours. Statistical significance was determined by ANOVA. (B) Quantification of (A) comparing γH2AX puncta for 5-hour APH and 3-hour washout. Puncta were normalized to respective 5-hour DMSO or DMSO-washout condition. (C) Neutral comet assay of 3-hour washout post 5-hour DMSO or 5μM APH treatment in WT- or S62A-MYC HEK293 cells. (D) Quantification of (C) where washout APH treatment was normalized to washout DMSO. Statistical significance was determined by ANOVA. (E) 10-day Colony formation assay following 5-hour DMSO or APH in increasing concentrations. (F) Quantification of (E) showing the survival percentage of WT-, S62A-, and T58A-MYC expressing cells following 5-hour

APH treatment. Statistical significance was determined by ANOVA. (G) Graphical summary of findings.

3.4 Discussion

In this study, we explored the non-canonical role of MYC in DDR and its association with DSBs to elucidate new mechanisms through which MYC drives oncogenesis and cancer cell survival. Our findings underscore a role for MYC in maintaining genomic integrity through mechanisms involving a direct role in DNA repair, and we reveal that MYC's phosphorylation at serine 62 is critical for its proximity to DSBs, recruitment of repair proteins like BRCA1 and RAD51, and overall effectiveness of DNA repair (Figure 3.3.6G).

Transcriptionally, MYC has been shown to promote genomic maintenance by regulating transcription of several DNA repair proteins including RAD50, RAD51, XRCC2, BRCA1, BRCA2, DNA-PKcs, HUS1, and Ku70 [183]. Furthermore, during S-phase, MYC upregulates expression of homologous recombination-directed repair proteins, RAD51 and HUS1 [189]. In our large expression dataset from 289 human PDAC tumors, we demonstrated a positive correlation between MYC target pathway activity and both replication stress and DNA repair pathway activity (Figure 3.3.1A,B). Furthermore, high versus low MYC target pathway activity showed increased VIPER activity score for DNA repair proteins and an increase in overall survival for patients who harbor somatic DDR mutations when MYC activity is low, consistent with prior findings that heightened MYC and DDR pathways drive a subset of aggressive PDAC tumors[292]. This connection may not be exclusive to PDAC given that prior clinical findings have shown that MYC amplification and increased genomic instability drive breast cancer progression and aggressiveness in BRCA1-mutated tumors [309]. The positive correlation between MYC-

target pathway activity and replication stress signature, supports the idea that MYC upregulates factors to mitigate the MYC-driven stress induced by accelerated cell cycle progression [227]. In agreement, MYC, along with MYCN, compensates for heightened replication stress by increasing transcription of components that address stalled replication forks and facilitate DNA repair, including the MRN complexes [184, 185], Cohesin components [250], TRIM33 [254], and MCM10 [253]. In addition, MYC expression induces nucleotide biosynthesis genes to sustain nucleotide balance to reduce replication stress [191].

Beyond MYC's transcriptional role in genomic maintenance, emerging evidence suggests that MYC protein can directly influences DNA damage prevention and repair. In a study by Cui et al., pS62-MYC colocalized with gH2AX and DNA-PKcs/S2056 foci in irradiated HeLa cells and that MYC silencing reduced DNA repair [182]. In neuroblastoma, MYCN is found at sites of heightened transcription which have a greater propensity to accumulate DNA damage. At these genomically stressed sites, the ubiquitin-specific protease USP11 was shown to preferentially bind to and stabilize de-phosphorylated threonine 58 MYCN which mediated the recruitment of BRCA1 to stalled RNAPII complexes, preventing the accumulation of deleterious R-loops [195]. In agreement, we showed that MYC's association with DSBs and BRCA1 was greatest in T58A-MYC and diminished in S62A-MYC when compared to WT-MYC (Figure 3.3.4, Figure 3.3.5). Emphasizing that serine 62 phosphorylation is important for MYC's association with DSBs and repair factors.

MYC elicits its cellular activity through its interactome and by recruiting and concentrating multiprotein complexes at genomic sites across the genome[77, 310]. Our

MYC-BioID2 proteomic screen detected a functional shift in MYC's interactome under replication stress (Figure 3.3.3). Under DMSO conditions, MYC-BioID2 biotinylated more interactions with proteins involved in canonical MYC functions that drive gene expression and metabolism while APH-enriched MYC interacting proteins aligned more with DDR pathways. MYC's interactome under cellular stress aligns with observations that MYC forms stress-induced higher-order multimeric structures around stalled replication forks, shielding them from RNAPII [199]. These MYC multimers were also reported to encompass repair proteins such as FANCD2, ATR, and BRCA1, to mitigate transcription-replication conflicts and subsequent DSBs during S-phase. In addition, it was recently shown that MYCN exists in two distinct physical states depending on the phase of the cell cycle. During G1, MYCN heterodimerizes with MAX to drive transcription, whereas during S-phase, MYCN interacts with nuclear exosome targeting complexes responsible for preventing transcription-replication collisions and eliminating genotoxic RNA-structures [196, 311]. These functionally distinct physical states of MYC align with numerous observations that post-translational modifications (PTMs) and protein-protein interactions partition MYC into functionally distinct "MYC-pools" which impacts its stability [79, 312, 313]. Since pS62-MYC, but not pT58-MYC, was shown to be essential for the spatial partitioning of MYC within the nucleus [108], it is plausible that phosphorylation at threonine 58 and serine 62 regulates functionally distinct MYC-pools under different cellular contexts. For example, MYC assembles and recruits a topiosome composed of topoisomerases 1 and 2 to alleviate transcription-induced topological stress [203]. However, in the presence of excessive DNA damage in cell lines, MYC is degraded and replaced with a p53-mediated topiosome, leading to proficient DDR and repair [204]. MYC

also requires ubiquitination and degradation for the transfer of PAF1c to RNAPII to couple transcriptional elongation with DSB repair [194]. The notion that MYC-pools are independently regulated spatially, could help explain reports that MYC is degraded in response to DNA damage [237, 242, 314], since a subset of more stable MYC pools, such as pS62-MYC, could allow for prolonged repair. Furthermore, since pS62-MYC is required for the efficient recruitment of BRCA1 and RAD51 to DSBs, MYC may play a role in directing homologous-directed repair. Future studies will investigate the consequences of MYC-directed repair in PDAC.

In conclusion, this study provides novel mechanistic understanding into the non-canonical role of MYC in DSB repair, demonstrating that serine 62 phosphorylation is critical for directing MYC's efficient association with DSBs and subsequent recruitment of repair factors necessary for productive DNA repair and cell survival under stress. These insights advance our understanding of MYC's function beyond transactional regulation, highlighting additional contributions to MYC-driven oncogenesis and resistance to DNA damaging chemotherapy.

3.5 Materials and Methods

Cell Lines

MIA PaCa2, U2OS, HeLa, HEK293 and MYC-mutant HA-tag HEK293TR cells were maintained in DMEM supplemented with 10% characterized fetal bovine serum (FBS), 2mM L-glutamine, and 1X penicillin/streptomycin at 37°C and 5% CO_2. Patient derived cell line ST-00024058 was generated as previously described [279].

Generation of stable inducible 293TR-MYC cells

293TR-MYC inducible cells were generated using a technique as previously described [116]. Briefly, HEK293 cells were infected with lentivirus encoding the Tet repressor, pLenti6/TR (Invitrogen) for 12 hours. Stable clones were maintained at 5μg/mL blasticidin (Invitrogen). Clones were then infected with lentivirus expressing HA-MYC (pLenti4/TO/CMV-HA-MYC). Cells were selected with 200 μg/mL Zeocin (Invitrogen) for 10 days until clones grew out. Clones were screened for HA-MYC when treated with 1μg/mL doxycycline for 24 hours. Stable 293TR-MYC^{T58A} and 293TR-MYC^{S62A} cells were similarly constructed except with pLenti4/TO/CMV-HA-MYC^{T58A} or pLenti4/TO/CMV-HA-MYC^{S62A} respectively.

Tissue acquisition and patient consent

Patient blood, tissues, and data were acquired with inform consent aligned with the Declaration of Helsinki and were obtained through the Oregon Pancreas Tissue Registry under Oregon Health & Science University IRB protocol #3609.

RNA-sequencing of patient PDAC

Detailed methods for RNA preparation and sequencing can be found in Link et al [315]. OHSU supplied formalin-fixed paraffin-embedded tissue sections to Tempus as part of a contract agreement. Tempus performed whole-transcriptome RNA sequencing as previously described [316].

Gene Set Variation Analysis (GSVA)

GSVA analysis[317] along with the MSigDB database v7.5.1 Hallmark gene set collection [318] was used to calculate Hallmark scores for all primary tumors. The replication stress gene set was derived from replication stress-induced gene expression patterns observed in Dreyer et al [293]. We compiled this composite gene set from all genes the appeared

in 3 or more of the 21 gene sets identified by Dreyer et al as being activated in replication stress and DNA damage response. Pearson's correlation coefficient and p-values were calculated using the cor.test() function in R.

VIPER analysis of high vs low Hallmark MYC-V1 score

Transcriptional regulon enrichment was analyzed using VIPER alongside the ARACNe-inferred TCGA PAAD network[295, 296]. Before running VIPER, gene expression data were normalized by median centering and scaling, and the resulting regulon scores from all primary samples were used for cohort comparisons. For the Gene Ontology (GO)[319, 320] enrichment analysis of regulons elevated for the high Hallmark MYC-V1 target pathway cohort, we utilized the R package ClusterProfiler (v.4.6.2)[321]. Primary tumors were ranked based on the HALLMARK_MYC_TARGETS_V1 GSVA score to produce quartiles. We then compared the top quartile to the bottom quartile and calculated multiple test corrected p-values (q-values) and difference in means between these quartiles for all Viper features. The enrichGO function was configured to assess GO biological process terms, with both p-value and q-value thresholds set to 0.05, and all regulons used as the background. Jaccard similarity was computed using the default setting of the pairwise_termsim.

Cyclic Immunofluorescence multiplex imaging analysis

A PDAC tissue microarray (TMA) was created at OHSU using FFPE blocks from tumors with 1-2 cores per tumor from 34 primary tumors, totaling 55 cores. Immunofluorescence preparation and analysis conducted as previously described[322]. Briefly, images were scanned with Zeiss Axioscan Z1, acquired, stitched, and exported as TIFF format with Zeiss Zen Blue software (v.2.3). Image registration was performed using MATLAB

(v.9.11.0), and cellular segmentation was carried out using either Cellpose[323] or Mesmer[324]. Unsupervised clustering of individual cell mean fluorescence intensity was used to classify cell types, using the Leiden algorithm implemented in scanpy (v.1.9.3)[325]. Pearson correlation r of tumoral single-cell mean intensity of DNA damage and proliferation markers with pMYC was calculated in each core. For hypothesis testing, Pearson's r values were transformed with Fisher's Z and 95% confidence intervals calculated.

DNA Damage In Situ Ligation followed Proximity Ligation Assay (DI-PLA)

This protocol is adapted from Galbiati et al [299]. Cells are grown on 13mm coverslips and fixed in 4% PFA for 10 minutes at room temperature followed by two washes with PBS.

DI-PLA: Blunting

Coverslips are washed twice for 5 minutes with NEB2 buffer (50mM NaCl, 10mM Tris-HCl pH 8, 10mM $MgCl_2$, 1mM DTT, 0.1% Triton X-100) and twice for 5 minutes with Blunting buffer (50mM NaCl, 10mM Tris-HCl pH 7.5, 10mM $MgCl_2$, 5mM DTT, 0.025% Triton X-100). Coverslips are then inverted onto a 35μL drop on parafilm of NEB Blunting Reaction (NEB, E1201): (1mM dNTPs, 1X Blunting Buffer, 0.2mg/mL BSA, 1X Blunting Enzyme). Coverslips are incubated in a dark humidity chamber for 1hr at room temperature.

DI-PLA: Ligation

Coverslips are washed twice for 5 minutes with NEB2 buffer (50mM NaCl, 10mM Tris-HCl pH 8, 10mM $MgCl_2$, 1mM DTT, 0.1% Triton X-100) the twice for 5 minutes with ligation buffer (50mM Tris-HCl pH 7.5, 10mM $MgCl_2$, 10mM DTT, 1mM ATP). Coverslips are then

inverted onto a 50μL drop on parafilm of Ligation Reaction (0.1μM DI-PLA Linker, 1X T4 Ligation Buffer (NEB, B0202), 1mM ATP, 0.2 mg/mL BSA, 1X T4 Ligase (NEB, M0202)) overnight at 4°C in dark humidity chamber followed by proximity ligation assay between biotin and protein of interest.

DI-PLA Linker:

5'-TACTACCTCGAGAGTTACGCTAGGGATAACAGGGTAATATAGTTT[BtndT]

TTTCTATATTACCCTGTTATCCCTAGCGTAACTCTCGAGGTAGTA -3'

Proximity Ligation Assay

Proximity Ligation Assay was performed without deviation from manufacturer's instructions (DUO92008). Single-antibody controls were performed to ensure specificity of antibodies. Coverslips were washed in a 0.5mL volume and reactions were performed by inverting the coverslip onto a 35μL drop on parafilm. Following the proximity ligation reaction, cells stained with DAPI (0.2ug/mL) for 3 minutes followed by one wash in PBS and one water wash. The cells were then inverted and mounted on glass coverslips with 15μL of prolong gold mounting media (LifeTech, P36934) & were cured overnight in the dark at room temperature. A minimum of 30 cells were imaged per replicate at 63X on a Zeiss LSM880 confocal microscope and analyzed with CellProfiler. Statistical significance was performed using two-tailed student's t-test or one-way ANOVA with multiple comparisons. Antibodies used are as follows: MYC (Abcam, 32072), pS62-MYC (Abcam, 78318), Biotin (Sigma, B7653), Biotin (Abcam, 53494), RAD51 (Abcam, 133534), HA-tag (ABM, G036), pRPA2 (Novus, NB100-544), γH2AX (Invitrogen, MA12022), γH2AX (Cell Signaling, 9718S), BRCA1 (Santa Cruz, 6954), BRCA1 (Sigma, 07-434-MI).

Cas9-Transfection

Cells were cultured on glass coverslips and transiently transfected using Lipofectamine CRISPRMAX (Thermo, #CMAX00015) with TrueCut Cas9 Protein v2 (Thermo, #A36499) and synthetic guide RNA from Invitrogen TrueGuide Synthetic sgRNA (Cat#: 35514) or Negative Control (Cat#: A35526) following manufacturer's instructions. After 8-hour incubation, cells were fixed in 4% paraformaldehyde for 10 minutes at room temperature, washed three times with PBS, and stored at 4°C. The following two rDNA guides were used in a 1:1 ratio of rDNA guide 1: CGAGAGAACAGCAGGCCCGC and rDNA guide 3: GATTTCCAGGGACGGCGCCT.

Western Blot

MYC-Mutant expressing HEK293 cells were seeded into 6-well chamber well. The next day, cells were treated with 0.5μg/mL doxycycline for 18 hours then treated with 5μM aphidicolin for 5 hours. Cells were then washed three times with DPBS and flash frozen at -70°C. Cells were then thawed and scraped in lysis buffer (20mM Tris-HCl pH7.5, 50mM NaCl, 0.5% Triton X-100, 0.5% DOC, 0.5% SDS, 1mM EDTA, protease inhibitor (Millipore Sigma: 5892791001), and phosphatase inhibitor (Millipore Sigma: 4906837001). Lysates were then sonicated with a Branson Sonifier 450 for 10 pulses, Duty factor of 20, and an output of 2. Protein content was then quantified and 25μg of protein was boiled in 1X SDS buffer (50mM Tris-Cl pH 6.8, 2%SDS, 6% glycerol, 5% 2-mercaptoethanol). Samples were loaded into a 4-12% Bis-Tris Citerion Gel (BioRad: 345-0123) and run for 1.5 hours at 180V on ice in XT-MOPS (BioRad: 161-0788). The gel is then transferred onto an Immobilin PVDF membrane (Fisher Scientific: IPFL00010) for 90 minutes at 400mA. Membrane is then blocked for 1 hour at room temperature in Aquablock (Arlington Scientific: NC2580736) then incubated overnight with primary

antibody. The following day, the membrane is washed for three times with TBST and incubated with secondary Licor antibody for 1 hour in the dark room temperature and imaged on a Licor Odyssey scanner. Antibodies used are as follows: MYC (Abcam, 32072), HA-tag (ABM, G036), pRPA2 (Novus, NB100-544), γH2AX (Invitrogen, MA12022), GAPDH (Fisher, AM4300). Anti-rabbit IgG 800CW (VMR, 102673-330), Anti-mouse IgG 680RD (LI-COR, 926-68072), Anti-mouse IgG 800CW (Fisher, NC9401841).

BioID2 Cloning

BioID2 sequence with a five-glycine linker (Addgene: 74224) was cloned at the N-terminus of C-MYC (Addgene: 16011) and inserted into pcDNA4/TO (Invitrogen: V102020) via HindIII (NEB: R0104T) and NotI (NEB: R0189L). The HA-BioID2 only control sequence (Invitrogen: 74224) was cloned into pcDNA4/TO via HindIII and BspeI (NEB: R0540) Each plasmid was independently transfected using Lipofectamine 3000 (Thermo Fisher Scientific L3000-015) into HEK293 cells which contained pcDNA6/TR (Invitrogen: V102520) under blasticidin selection at 20ug/mL. Single cell clones were isolated after several days of Zeocin selection at 200ug/mL. MYC-BioID2 positive clones were identified by western blot for biotin and MYC expression upon doxycycline induction (1ug/mL for 24 hours) with Strepavidin 680 (LI-COR Biosciences 926-68079) and Y69 (Abcam ab32072). HA-BioID2 positive clones were screened using a HA-tag antibody (Applied Biological Materials G036).

MYC-BioID2 Assay

Cells were plated on two 15-cm dishes per condition to achieve 80% confluency upon treatment. Cells were treated for 24-hours with 1 μg/mL doxycycline in combination with either 5 μM APH or DMSO vehicle control. For biotinylation, cells were treated with 50

μM biotin (Millipore Sigma: B4501) for 18 hours. After treatment, cells were washed twice with PBS and frozen at -70°C and stored until three biological replicates were obtained. Cells were then lysed with 1.5 mL/dish of lysis buffer (50 mM Tris-Cl, pH 7.4, 150 mM NaCl, 1% Triton X-100, 0.1% SDS; 1 mM DTT, protease inhibitor (Millipore Sigma: 5892791001), and phosphatase inhibitor (Millipore Sigma: 4906837001), and incubated on ice for 10 minutes. Lysates were scraped, pooled, and sonicated with a Branson Sonifier 450 for two 30-pulse sessions at a 30% duty cycle and 1.5 output, with a 2-minute ice interval. Samples were diluted with 2.6 mL pre-chilled 50 mM Tris-Cl (pH 7.4) and sonicated for an additional 30 pulses. Lysates were centrifuged at 16,500 x g for 10 minutes at 4°C to remove debris. 150 μL/condition of Streptavidin-agarose beads (Millipore Sigma: 69203-3) were equilibrated in a 1:1 mixture of lysis buffer and 50 mM Tris-Cl (pH 7.4) and briefly spun down at 8,000 rpm for 2 minutes. Supernatants were transferred to the beads and incubated overnight on a rotator at 4°C. After incubation, beads were washed twice with wash buffer 1 (50 mM HEPES pH 7.5, 400 mM NaCl, 1% Triton X-100, 0.1% deoxycholic acid, 1 mM EDTA) for eight minutes, twice with wash buffer 2 (10 mM Tris-Cl pH 7.4, 500 mM LiCl, 0.5% NP-40, 0.5% deoxycholic acid, 1 mM EDTA) at room temperature. Beads were washed once in 50 mM Tris-Cl (pH 7.4) followed by three washes with 100mM ammonium bicarbonate. Beads were resuspended in 100 μL of 100mM ammonium bicarbonate (pH 8) and underwent trypsinization with the addition of 15μL of 80ng/μL trypsin (1.6ug) in 50mM Triethyl ammonium bicarbonate and incubated for 17 hours at 37°C with shaking. After trypsinization, beads were isolated, supernatant removed and filtered with 0.22μm Millipore filter. Filtered sample was dried and dissolved in 20μL of 5% formic acid and injected into Thermo QExactive HF mass

spectrometer and run with the 90min LC/MS method. Survey mass spectra were acquired over m/z 375−1400 at 120,000 resolution (m/z 200) and data-dependent acquisition selected the top 10 most abundant precursor ions for tandem mass spectrometry by HCD fragmentation using an isolation width of 1.2 m/z, normalized collision energy of 30, and a resolution of 30,000. Dynamic exclusion was set to auto, charge state for MS/MS +2 to +7, maximum ion time 100ms, minimum AGC target of 3 x 106 in MS1 mode and 5 x 103 in MS2 mode. Mass spectrometry data from all samples was processed using COMET/PAWS against Uniprot Human database. Comet (v. 2016.01, rev. 3)[326] was used to search MS2 Spectra against a January 2024 version of canonical FASTA protein database containing human uniprot sequences, and concatenated sequence-reversed entries to estimate error thresholds. Comet searches for all samples were performed with trypsin enzyme specificity with monoisotopic parent ion mass tolerance set to 1.25 Da and monoisotopic fragment ion mass tolerance set at 1.0005 Da and a variable modification of +15.9949 Da on Methionine residues.

Protein interaction ontology analysis

BioID2-only detected spectral counts were subtracted from MYC-BioID2 to remove background biotinylation and spectral counts from MYC-BioID2 samples treated with either DMSO or APH were normalized by scaling the average total spectral counts across samples. Log2 fold changes were computed between APH- and DMSO-treated samples, and statistical significance was assessed using two-sided t-test followed by

a Benjamini-Hochberg correction. Ontological analysis of targets which pass the 2-fold differential abundance threshold was determined with the BinGO tool in Cytoscape[264, 265, 304].

Neutral comet assay

Cells were plated in 6-well plate and treated with either DMSO control or 5mM aphidicolin for 5-hours. A positive control of 1-hour 100mg/mL bleomycin was included. Glass slides were pre-coated in 1% normal melting point agarose and dried at room temperature. Cells were trypsinized, counted, and resuspended in PBS to 0.35 × 10^6 cells/mL on ice. Cell suspensions were combined with molten 1% low-melting-point agarose at a 1:10 (v/v) ratio, then 200 µL of this mixture was applied to pre-coated slides labeled in pencil. Coverslips were added for even distribution, and slides were solidified at 4 °C for 10 minutes in the dark. Slides were then submerged in 4°C lysis buffer (2.5 M NaCl, 100 mM EDTA, 10 mM Tris, 200 mM NaOH, 1% sarcosinate, and 1% Triton X-100, pH 10) for 18-hours. Slides were equilibrated in neutral electrophoresis buffer (100mM Tris and 300mM sodium acetate, pH 9) at 4°C for 30 minutes and transferred to an electrophoresis chamber with chilled buffer. Electrophoresis was conducted at 1 V/cm for 30 minutes at 4 °C. Slides were immersed in DNA precipitation solution (1M ammonium acetate in 80% ethanol) for 30 minutes, followed by a 30-minute rinse in 70% ethanol at room temperature. Slides were dried at 37 °C, then stained with SYBR Green (1:2000, Thermo cat#: S33102) for 15 minutes in the dark. Following a brief rinse in dH2O, slides were dried partially and stored. Images were acquired at 10x using a BioTek Cytation 5 microscope. Comets analyzed using ImageJ software plugin, OpenComet[327]. Olive Tail Moment (OTM) was calculated using the following equation.

$$OTM = \frac{Tail.mean - Head.mean}{100} \times Tail\%DNA$$

Co-Immunoprecipitation

HEK293 cells were transfected with plasmids using Lipofectamine 2000 (Life Technologies) following the manufacturers' protocols. The cells were harvested at 36–48 h post-transfection, washed with PBS and then lysed in ice-cold lysis buffer consisting of 30 mM Tris-HCl (pH 8.0), 0.5% Nonidet P-40, 1 mM EDTA, 1 mM EGTA, 200 mM NaCl, 1 mM phenylmethylsulfonyl fluoride, 1 mM DTT, 1 μg/mL pepstatin A, and 1 mM leupeptin and 1mM β-Glycerophosphate with sonication. Equal amounts of clear cell lysate were incubated with anti-Flag M2 agarose beads for 5 hours at 4°C. The beads were washed 5 times with lysis buffer. Bound proteins were detected by immunoblot using antibodies, as indicated in Figure legends.

Immunofluorescence staining

HEK293 cells with either HA-MYC or S62A-MYC were plated on poly-D-lysine treated glass coverslips and incubated for 24-hours. Expression was induced with 0.5μg/mL doxycycline for 18-hours then treated with 5μM APH or DMSO for 5-hours. Cells were then either fixed with 4% paraformaldehyde for 10 minutes or media change with dox for 3-hours followed by fixation. Coverslips were then permeabilized with 0.25% Triton X-100 for 10 minutes followed by a 1-hour block (10% goat serum, 0.1% Triton X-100). Coverslips were then incubated in primary antibody (gH2AX, Cell Signaling, 9718S) overnight at RT. Cells were then washed in three times in 1X PBS for 10 minutes and incubated in secondary antibody (Jackson Immuno, 111-565-144) for 2 hours at RT. Coverslips are washed again for three times in 1X PBS and stained with 0.2μg/mL DAPI for 3 minutes, mounted (LifeTech, P36934), and cured overnight in the dark at room temperature. Coverslips were imaged at 63X on a Zeiss LSM880 confocal microscope and puncta were analyzed with CellProfiler (www.cellprofiler.org) [328].

Colony formation assay

Cells were treated in a 6-well plate then trypsinized, counted, and plated at 1,000 cells/well of a 12-well plate. Media was changed every three days with the addition of 0.5μg/mL doxycycline. After 10 days, the media was removed and stained with 0.5% crystal violet in 50% ethanol for 30 minutes. The excess dye was then gently washed away with slow-running water. The plates were then dried at RT and colonies were counted.

3.6 Acknowledgements

The authors acknowledge expert technical assistance by the OHSU Advanced Light Microscopy Core (RRID:SCR_009961), supported by the OHSU Knight Cancer Institute (NIH P30 CA069533). In addition, we'd like to thank OHSU's shared proteomics core for support and guidance on this project. The authors would also like to acknowledge and thank Drs. Moriah R. Arnold and Vivek K. Unni for assistance in the Cas9-induced DNA damage experiments. This manuscript was financially supported by the following: NCI U01CA224012 (RCS & JRB), U01CA278923 and R01s CA186241, CA196228 and DoD PA210068, R01CA287672 (JRB), R01 CA212600 (JRB), R21 CA263996 (RCS & JRB); the Brenden-Colson Center for Pancreatic Care and the Krista L. Lake Endowed Chair. GMC was supported, in part, by the Knight Cancer Institute stipend award.

3.7 Author Contributions

GMC and RCS contributed to the project design; GMC performed and analyzed all experiments unless otherwise stated; CP analyzed RNA-sequencing data; KC stained tumor microarray and JE analyzed tumor microarray; CDL is the principal investigator of the clinical trial which lead to the created of PDAC patient-derived cell lines; JRB

developed technology for deriving patient-derived cell lines; AS assisted in the generation and classification of the patient-derived PDAC cell line, ST-00024058; CJD & GMC designed and executed MYC-BioID2 experiments and analysis with bioinformatic help from CP; XXS & MD performed Co-Immunoprecipitation experiment. GMC wrote the paper with edits and revisions from RCS and CJD. All authors have approved the current version of the manuscript.

3.8 Supplementary Materials

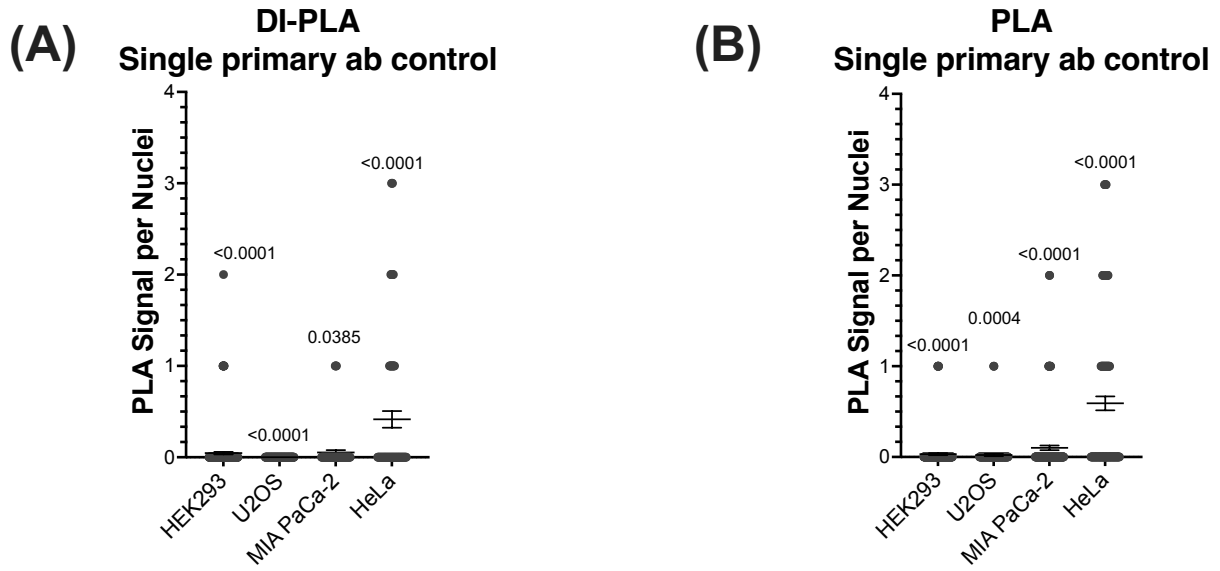

Supplementary Figure 3.8.1. Negative controls to determine technical specificity for proximity ligation assays. (A) Quantification of three replicate experiments of combined single antibody controls for MYC DI-PLA experiment (MYC- and Biotin-only) for HEK293, U2OS, MIA Paca-2, and HeLa cells. Statistical significance was determined by a two-tailed t-test between single antibody control and the DMSO condition in Figure 3.3.2D. (B) Quantification of three replicate experiments of combined single antibody control for MYC-γH2AX PLA (MYC- and γH2AX-only) for HEK293, U2OS, MIA Paca-2, and HeLa cells. Statistical significance was determined by a two-tailed t-test between single antibody control and the DMSO condition in figure 3.3.2E.

Gene_ID	pVal	log2FC	qVal	mean_delta
MYC	0.071843128	0.394886406	0.956754079	56.28372347
ANLN	0.006753242	1.544067109	0.675757944	17.90434988
TPX2	0.010943698	0.797980269	0.771168725	16.59380109
KI67	0.004843363	0.581667448	0.602760553	15.34510067
ARI1B	0.006423572	0.749156209	0.665272059	15.2378424
PRC2B	0.003517831	1.042246334	0.526922891	13.68222764
NUMA1	0.111029341	1.579730702	0.971583383	13.25554902
EP400	0.186649597	0.095415053	0.982899372	10.35706773
PARP1	0.149893547	2.441271128	0.978794972	10.1727512
SF3B2	0.015991904	0.347397805	0.831211958	9.735371166
MYBB	0.070716131	0.560670889	0.956095132	9.41188982
CUX1	0.00054521	0.632143985	0.218521791	8.922042142
SMRC1	0.04674273	0.968444896	0.935039978	8.839783695
CLSPN	0.018327778	1.065747663	0.849486124	6.973828773
RBL1	0.128947307	0.329752874	0.975435036	6.608193097
TERA	0.001572679	0.351723915	0.399137431	6.555713599
HNRPM	0.022231054	0.697497143	0.872544754	6.328807315
UBP11	0.010436367	0.921434826	0.762684691	6.295635038
MINT	0.018389136	0.832489537	0.849912961	6.006067909
GTSE1	0.03726795	1.651550801	0.919848636	5.965615939
ELYS	0.032439762	1.713919426	0.909004782	5.820370864
PP1RA	0.111659509	0.552245723	0.971739224	5.729434449
NUCL	0.233258719	0.385596106	0.986269456	5.726527963
DPOD1	0.108519251	0.792789427	0.970945194	5.626120603
SPDLY	0.035932045	0.38051227	0.917115704	5.588436485
NOL6	0.178817763	0.381809253	0.98216376	5.587625031
WDR33	0.062349414	1.097901802	0.950495168	5.455833137
TOPB1	0.087841346	0.511976017	0.964349507	5.368205283
TCP4	0.13307792	0.667303988	0.976179347	5.104471235
GTF2I	0.104560516	0.182126783	0.969878293	4.997544866
ACL6A	0.031639844	0.274934182	0.90691838	4.986218575
EPC1	0.16603734	0.185003934	0.980817184	4.906666845
SMCA5	0.029475259	1.615090079	0.900761078	4.753441494
FA83H	0.24958961	0.993877891	0.98715632	4.671404553
TF3C5	0.039849718	0.428276687	0.924650172	4.481597211
BLM	0.086656478	0.616288294	0.963879659	4.279651112
DHX9	0.144409886	0.422226061	0.978007465	4.248482126
RS7	0.082691523	1.576796243	0.962213178	4.083392358

FUBP2	0.139146326	0.853947848	0.977194514	4.076241155
RRP7A	0.129763196	0.883943777	0.975585718	4.008999249
INT12	0.081213106	0.514607319	0.961551748	3.997032151
DMAP1	0.153035751	0.194260437	0.979221317	3.941071634
ROA1	0.028607955	0.519319574	0.898059164	3.913059136
WDR75	0.047008361	0.632379759	0.93538333	3.853763707
RBM10	0.072627357	0.776248246	0.957201062	3.852137906
ARC	0.141711379	0.772516902	0.977598058	3.825665957
PHF3	0.121586981	0.364630942	0.973986667	3.631438484
RS10	0.028770818	1.176786817	0.898577693	3.531352005
ACLY	0.071786429	0.839178969	0.956721401	3.488160322
AP3D1	0.00711663	0.949196696	0.686669114	3.484112797
ZZZ3	0.198219699	0.275181406	0.983881448	3.477380177
KC1A	0.193896336	0.544265388	0.983527968	3.377073318
DDX11	0.195407324	0.805540718	0.983653256	3.28518239
FXR2	0.18382704	1.261503628	0.98264136	3.268865154
ATAD5	0.072487516	2.287805199	0.957122036	3.23978647
ZN687	0.024075297	0.293818793	0.881147813	3.217784438
FOXK1	0.112510127	0.541868782	0.971946892	3.120031501
PDIP3	0.115917322	0.359097239	0.972748996	3.098556501
RBBP6	0.091183578	0.438204834	0.965611299	3.09198675
BAG2	0.234107359	1.233166285	0.986318548	3.072730413
BRCA1	0.002934237	0.537398391	0.501123717	3.031693012
NKRF	0.086159755	1.255465962	0.963678984	2.964829524
WRIP1	0.185333247	0.656508016	0.982780004	2.939057885
PAF1	0.151276384	0.448760956	0.978984736	2.935064977
PDS5A	0.030002593	0.432958151	0.902334977	2.925086569
RLA2	0.130478124	1.3570447	0.975716242	2.913476945
DCNL4	0.076663165	1.022031652	0.959362583	2.86177714
RBM4	0.12804442	0.80844263	0.975266104	2.85315827
TPR	0.026457664	0.53176356	0.890679858	2.844684801
RS15	0.128214922	1.366867984	0.975298183	2.832063307
RPA2	0.184953734	1.373969197	0.98274528	2.831630271
AT7L2	0.076333405	0.526110952	0.959194193	2.815031399
RLA0	0.176611979	1.237631722	0.981945017	2.793996866
UTP11	0.007030168	2.130917913	0.684033168	2.786166927
BRD4	0.120656111	0.498300977	0.973791233	2.772754785
MSH2	0.111699177	0.5486957	0.971748977	2.76067826
KI18B	0.020185148	1.126798678	0.861416563	2.71875791

TCOF	0.044584425	0.152156449	0.932108798	2.712637316
RL27	0.136013966	1.076060498	0.976681558	2.710907111
RL7	0.247963082	2.055854195	0.98707316	2.681399497
PGAM5	0.125304736	1.181713629	0.974738979	2.674768929
EIF3B	0.054119166	1.052134139	0.943392819	2.656977292
SLU7	0.008885146	0.597223567	0.732342362	2.607854727
NOLC1	0.200199172	0.517546718	0.984038277	2.606238643
RANB9	0.049341893	1.454577201	0.938250552	2.59717702
ESF1	0.249286189	0.815782439	0.987140888	2.596425997
SUPT3	0.228430021	0.122848818	0.985983279	2.545419147
TCF20	0.227676315	0.40940028	0.98593753	2.537326035
RU2A	0.056539179	2.578448177	0.945684139	2.486484381
UNG	0.067709796	1.099567444	0.954234957	2.458973387
GNL3L	0.072937332	1.647356744	0.957375199	2.449367584
SMRD1	0.132544492	0.640612161	0.976085773	2.443440784
ERCC5	0.207589463	0.335444036	0.98459777	2.442580346
CHERP	0.220566655	0.159304532	0.985490823	2.385366635
CDCA2	0.121227974	0.708847603	0.973911641	2.3852018
PCF11	0.238080174	0.282158186	0.986543777	2.371991224
ILF2	0.128059367	1.217086719	0.975268919	2.345942594
MTA1	0.209241877	0.186433289	0.984717545	2.335880403
ROA0	0.026365816	0.869780676	0.890340791	2.316722228
DLGP5	0.147705628	1.178850291	0.978487625	2.282960869
CBX8	0.030434139	1.908132869	0.903586314	2.256861526
EIF3A	0.164895002	0.731918906	0.980686859	2.25437937
RL17	0.032922025	1.942211549	0.910218064	2.254176819
TFP11	0.169548033	0.260556656	0.981206922	2.23740208
CRTC2	0.027378081	1.885112159	0.893965364	2.23270597
ZN622	0.159158268	1.893955032	0.980004651	2.226775087
UBF1	0.051309894	0.772164912	0.940477991	2.198626624
SSRP1	0.188005256	1.968064801	0.983020587	2.114964493
TAD2A	0.17827645	0.494431835	0.982110572	2.081024487
CARF	0.169946108	0.685287227	0.981250117	2.076916532
YJU2B	0.078592277	2.361929096	0.960320483	2.070286351
ERLN2	0.049777752	1.339271256	0.938758124	2.069850984
RPC3	0.130045014	0.343119739	0.975637337	2.063438682
ZNF24	0.167866165	0.585929708	0.981022206	2.050877618

Supplementary Tabel 3.8.1. Table of identified targets in MYC-BioID2 screen. Targets are filtered by a ≥2 differential mean spectral count abundance between DMSO and APH and a p-value ≤0.25.

Chapter 4: Discussion

4.1 Summary

This body of work presents a multiscale examination of MYC's innate biological functions and how these are altered and exploited throughout the course of oncogenesis. At the tissue level, MYC drive rapid cellular proliferation necessary for establishing proper tissue architecture and morphology during embryonic development[61]. In adult mammals, MYC's primary role remains the promotion of cellular proliferation, but it is tightly regulated and becomes activated only in response to growth promoting signals, such as during tissue regeneration following injury[57, 63]. In Chapter 2, we focus on PIN1 as a necessary regulator of MYC, enabling robust transcription and subsequent proliferation in response to extrinsic signals. We broaden our understanding of PIN1's regulation of MYC by investigating its interactome at the NPC, which may support gene gating and may contribute to epigenetic memory. Our findings show that PIN1 inactivation reduces both the overlap between MYC and NPC interactomes and their shared binding to target genes. Through these mechanisms, we proposed that following extrinsic growth-promoting signals, PIN1 acts as a required MYC co-activator, facilitating the interactome necessary to boost transcriptional amplification at the NPC.

During oncogenesis, the accumulation of genetic mutations disrupts the tight regulation of MYC, promoting unchecked proliferation and creating a strong selective pressure for the emergence of prosurvival mechanisms. The resulting MYC driven tumors exhibit high levels of replication stress and increased genomic instability, yet they are able to survive and even evade DNA damaging chemotherapies. In Chapter 3, we explore a novel mechanism in which MYC associates with replication stress induced DNA damage and enhances DNA repair efficiency. We find that under replication stress, MYC's

interactome becomes enriched with DNA repair factors and facilitates the efficient recruitment of key repair proteins such as BRCA1 and RAD51 to sites of DNA damage. These mechanisms depend on MYC's phosphorylation at serine 62, and prevention this modification impairs DNA repair and reduces cell survival.

Taken together, this manuscript details a holistic understanding of MYC's enigmatic functions both in physiological and oncogenic conditions. MYC's diversity of functions arise from alterations to its post-translational modifications and interactome which impact its activity and subnuclear localization. We detail the emergent growth and survival promoting mechanisms driven by serine 62 phosphorylation and proline-directed isomerization, highlighting a targetable axis to cripple MYC-driven cancers.

4.2 PIN1 is a Conduit Linking Extrinsic Signals to MYC-Driven Cellular Growth

PIN1 is a master mediator of signal transduction. While asynchronously growing PIN1$^{-/-}$ MEFs appear similar to WT, they exhibit a significant delay in cell cycle reentry when stimulated with mitogens[107]. Past findings have linked PIN1 to the regulation of MYC's stability and DNA binding, both of which are essential for the effective activation of genes involved in of cell growth and proliferation[116]. In Chapter 2, we explore the crosstalk between MYC and PIN1 in greater detail, investigating how PIN1 influences MYC's interactome following serum stimulation (Figure 2.3.2). Through the RIME analysis, we show that in serum stimulated MEFs, knockout of PIN1 leads to a loss of serum-induced MYC interactions with co-activators involved in gene expression, metabolism, and cell cycle progression. Furthermore, activated genes localize to the nuclear pores to engage in gene gating, a process in which transcription, nuclear export,

and translation are coupled to maximalize the efficiency of signal induced gene expression[260]. MYC and PIN1 appear to participate in gene gating, as PIN1 is required for MYC's trafficking to the nuclear pore in response to growth-promoting signals in MEFs[108]. In cancer cells, the loss of regulation over growth-promoting pathways allows for their activation independent of external stimuli. In line with this, MYC was found to localized robustly to the nuclear pore in several conventional cancer cell lines. We show that this phenomenon extends to pancreatic cancer cell lines, where pS62-MYC robustly associates with PIN1 and NUP153, a component of the nuclear pore basket protein complex implicated in gene gating (Figure 2.3.1)[267, 268]. MYC's interaction with NUP153 increased following either serum stimulation or Olaparib treatment, suggesting that MYC driven transcription at the NPC is enhanced in response to diverse stimuli in PDAC cell lines. In these PDAC cell lines, therapeutic inhibition or genetic silencing of PIN1 dramatically reduces promoter binding of target genes shared between MYC and the NPC, highlighting PIN1 as a potential target to suppress MYC driven transcription at the NPC.

In addition to facilitating MYC's trafficking to the NPC, PIN1 also influences MYC's interactome by promoting the recruitment of the HAT GCN5 to the NPC, thereby enhancing MYC driven chromatin acetylation and transcriptional activity[108, 200]. In our RIME analysis, we found that PIN1 is crucial for efficiently establishing MYC's interactome at the NPC following serum stimulation in MEFs (Figure 2.3.3). The overlap of interacting proteins between MYC and the NPC showed a nearly threefold reduction following serum stimulation in the absence of PIN1. Among the shared MYC-NPC interacting proteins that were lost, Gene Ontologies analysis revealed enrichment in biological pathways of gene

expression, anabolism, and ribosome biogenesis, all processes that are required for MYC's response to growth promoting signals. Given that most of MYC's interactions have been shown to be weak and transient[79, 132], we developed a MYC- and NUP152-BioID2 system to more robustly capture MYC's interactome at the NPC (Figure 2.3.4). Initial findings in asynchronously growing HEK293T cells show that both MYC and NUP153 interact with SENP1, a SUMO protease known to stabilize and promote the activation of both MYC and PIN1[136, 271]. This technology will enable us to characterize MYC's interactome at the nuclear pore across various cell types and stimuli, providing insight into MYC's role in gene gating and its potential involvement in epigenetic memory.

Taken together, our findings in Chapter 2 implicate PIN1 as the conduit which connects extrinsic growth promoting stimuli involved in tissue regeneration, to MYC driven cellular growth and proliferation. Our data further suggest that MYC's subnuclear localization shapes its response to extrinsic stimuli by directing it to the nuclear pore, where it likely participates in amplifying gene expression linked to gene gating. During oncogenesis, gene gating and epigenetic memory at the NPC are coopted to perpetuate cellular growth gene expression independent of extrinsic stimuli, further promoting tumorigenic phenotypes[146, 147]. Thus, our data provides further therapeutic rationale for targeting PIN1 to indirectly suppress MYC driven gene amplification at the NPC in human tumors and will be discussed further in a later section.

4.3 The Balance Between MYC Regulation and Oncogenesis

The genomic instability that accompanies the proliferation required to establish and maintain multicellularity creates a constant tug-of-war between tissue regeneration and oncogenesis. The determinant factor that dictates the outcome of this tug-of-war lies

within the cells ability to mitigate genomic alterations through prevention and DNA repair. At the heart of this balance is the regulation of MYC, since it's a master regulator of proliferation whose activity is indispensable for regeneration and deeply implicated in oncogenesis[329]. In non-transformed cells that experience DNA damage, MYC is rapidly downregulated, presumably to reduce global transcriptional amplification and replication to allow time for effective DNA repair[234, 236, 237, 242]. This is further supported by the evidence showing that ectopic expression of MYC overrides cell cycle checkpoints[179, 180], acutely disrupts DNA repair[231], and leads to increased genomic instability[228, 330], often culminating in apoptosis[219, 221-223]. Ectopic expression disrupts the normal turnover of MYC, a process that is closely linked to its growth promoting activity. For example, MYC's ubiquitin-mediated degradation is required for the efficient recruitment of TRRAP, BRD4, and P-TEFb, which activate RNAPII elongation[331], highlighting the intimacy of MYC's turnover and function.

The fact that MYC overexpression alone is not sufficient for oncogenesis suggests that additional mutations such as loss of p53 and/or upregulation of DNA repair pathways are required to accommodate the genomic stress and enable tumor survival[243, 284]. To illustrate the connection between MYC regulation and DNA damage through oncogenesis, I propose three distinct scenarios (Figure 4.3.1) In normal cells, MYC is activated in response to growth signals but rapidly degraded if genomic damage accumulates. This degradation is largely mediated through crosstalk with p53, which, depending on the cellular context, will either promote cell cycle arrest or apoptosis. The next phase in oncogenesis is where MYC is dysregulated and increases genomic instability and promotes p53-mediated apoptosis. Under these conditions, MYC drives

the mutator phenotype, where elevated levels increase the tumor's mutational rate, creating an immense selective pressure for cells that harbor alterations that accommodate both high MYC activity and genomic instability[243, 244]. The ultimate phase for MYC-driven oncogenesis is the emergence of cancer cells that have dysregulated MYC and inactivated tumor suppressors such as p53, allowing for both high genomic instability and unchecked proliferation. It is at this phase where the tumor becomes increasingly reliant on the noncanonical functions of MYC involved in DNA repair, which accompany and support elevated MYC activity. Characterizing these compensatory mechanisms provides the potential for therapeutic intervention against MYC-driven tumors.

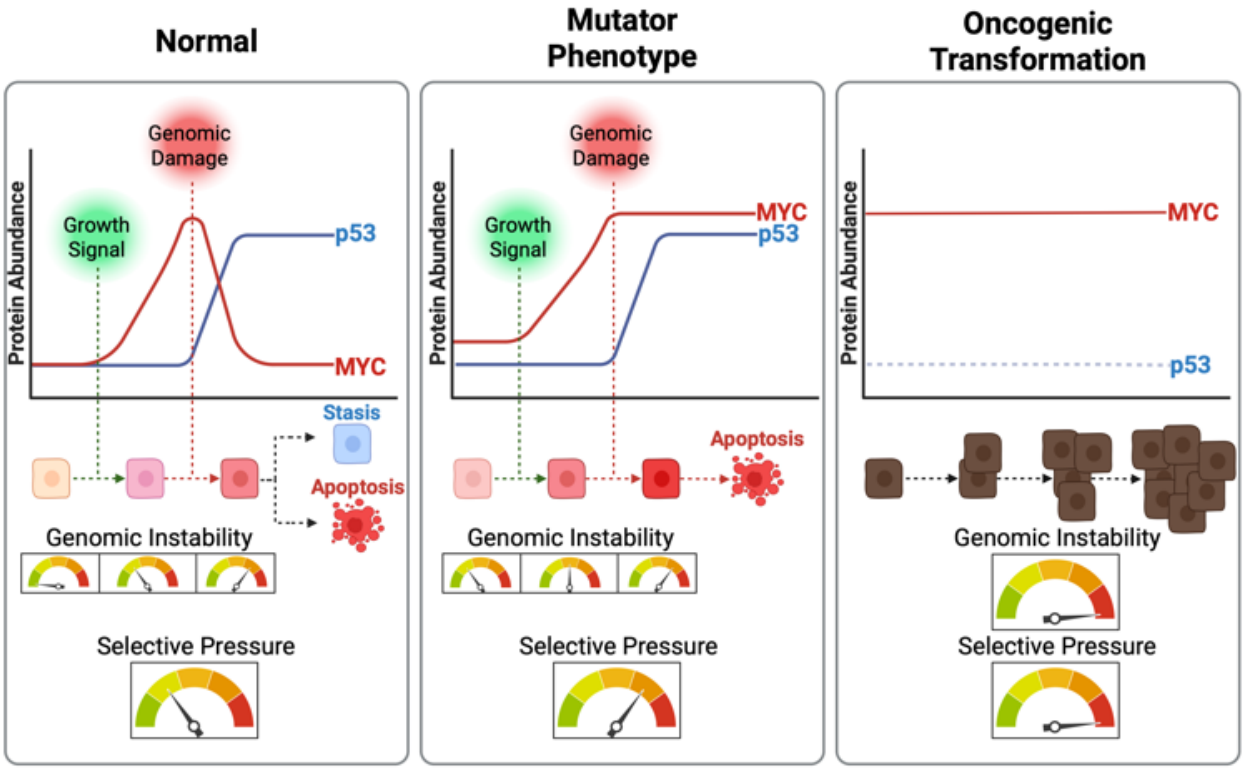

Figure 4.3.1 The Balance Between MYC Regulation and Oncogenesis.

The relationship between MYC regulation and cellular transformation can be conceptualized in three distinct phases. In normal cells, MYC is stabilized in response to growth signals (pink cell) but is rapidly degraded following genomic damage and activation of p53 signaling (red cell). When p53 is functional, the cellular response depends on the extent of damage and will either result in apoptosis or cell stasis to promote DNA repair. Under these conditions, there is minimal selective pressure, as cells with elevated MYC and genomic damage are efficiently eliminated from the tissue. The second phase, referred to as the mutator phenotype, arises in the context of additional mutations that stabilize MYC and increase its abundance. In these cells, MYC is no longer efficiently degraded following genomic damage. While functional p53 signaling promotes apoptosis in most cases, stabilized MYC activity creates a strong selective pressure for the emergence of cells that can sustain elevated MYC-driven proliferation. Under strong selective pressure, cells with altered p53 signaling and elevated MYC undergo oncogenic transformation marked by increased genomic instability (brown cells). In this context, selection favors cells that enhance MYC-driven DNA repair mechanisms, enabling aggressive tumorigenesis and resistance to chemotherapy. Figure created with BioRender.com

4.4 The MYCanic: MYC Promotes DNA Repair

To begin to understand MYC's connection to genomic instability in tumors, we analyzed gene expression profiles from 289 primary and metastatic PDAC tumors (Figure 3.3.1). Although there is no universal list of MYC target genes due to its variability in promoter binding cross different cell types and conditions[160, 332], we used the Hallmark MYC V1 score as a proxy for elevated MYC activity. Contrary to several studies suggesting that MYC regulates DDR gene programs[73, 183, 184], there is only a 4 percent (8/200) overlap between Hallmark MYC V1 and Hallmark DNA Repair pathway targets. This lack of overlap actually enables us to compare elevated MYC activity and DDR pathways activation in our large patient dataset without introducing correlation bias from shared gene programs. When comparing these GSVA scores, we found a strong correlation between the hallmark MYC Target V1 score and both replication stress and hallmark DNA Repair pathway signatures. We then stratified the tumors based on low versus high Hallmark MYC V1 activity score and performed VIPER analysis, which revealed that MYC high tumors showed enriched regulon activity for DNA maintenance

factors compared to MYC low tumors. Furthermore, tumors with low MYC activity and concurrent DDR deficiency exhibit a significant survival advantage compared to tumors with high MYC activity. This suggests that elevated MYC activity, in combination with DDR mutations, contributes to more aggressive tumors, a phenomenon that was also observed with a connection towards metastatic organotropism[292]. To visualize the correlation between MYC and genomic instability in tumor tissues, we performed cyclic immunofluorescence on patient samples and observed a strong co-occurrence between pS62MYC and DDR markers.

To begin uncovering the mechanism underlying this correlation, we conducted a series of PLA and DI-PLA experiments and observed a conserved association of MYC and DSBs, as well as key DDR proteins such as γH2AX, BRCA1, and RAD51 following genomic insult (Figure 3.3.2). Previously, immunofluorescence studies showed that MYC colocalizes with γH2AX foci following ionizing radiation; however, since γH2AX can propagate up to one megabase from the site of a DSB[333], our DI-PLA assay provides a more precise biochemical approach for assessing MYC's proximity to DSBs across various forms of genomic insults. Since all of MYC's functions are dictated by its interactome[78, 79], we generated a MYC-BioID2 fusion protein to identify its binding partners following 24-hour APH treatment in HEK293T cells (Figure 3.3.3). We identified 725 MYC interacting targets, with the majority, approximately 93 percent (674/725), shared between the DMSO and APH treatment conditions. The major difference observed in MYC's interactome was in the relative abundance of interactions, where replication stress markedly reduced MYC's association with proteins involved in gene expression and metabolism, while robustly increasing its interactions with DNA damage response

and cell cycle regulatory proteins. This suggests that MYC engages with DNA repair machinery in parallel with its canonical function in gene amplification and that this association is robustly enhanced under conditions of genomic stress. This notion is supported by findings that MYC couples transcriptional elongation with DSB repair at promoters through the transfer of PAF1c onto RNAPII[194]. In response to a variety of cellular stressors that increase the risk of genomic damage, MYC has been shown to multimerize to facilitate both effective transcriptional termination and DNA repair[334]. There multimers protect replication forks by reducing transcriptional replication conflicts and stabilize nascent RNA to prevent R-loop formation[195, 199]. Mechanistically, these multimers sequester DDR factors such as FANCD2, ATR, BRCA1, while reducing MYC's interaction with transcriptional promoting factors.

We show that the shift in MYC's interactome is reliant on pS62-MYC and preventing this phosphorylation significantly reduces MYC's association with DSBs, γH2AX, BRCA1, and RAD51 following genomic damage (Figure 3.3.4 and 3.3.5). The T58A-MYC mutant, which exhibits elevated serine 62 phosphorylation[126], consistently showed equivalent or greater association with DSBs and DDR proteins when compared to WT-MYC. Given that S62A-MYC and WT-MYC exhibited similar DSBs after 5 hours of APH treatment, we assessed the efficiency of repair using a 3-hour washout experiment. While WT-MYC reduced both γH2AX puncta and neutral comet tail following the 3-hour washout, expression of S62A-MYC resulted in increased DNA damage. Mechanistically, we showed that cells expressing S62A-MYC were deficient in BRCA1 and RAD51 recruitment to DSBs, highlighting serine 62 phosphorylation as a necessary regulatory step for enabling MYC driven DNA repair (Figure 3.3.4). In agreement, pS62-MYC was

found to colocalize with foci composed of γH2AX and phosphorylated DNA-PKcs in irradiated cells, and knockdown of MYC attenuated the repair of these DSBs[182]. Furthermore, we performed a 10-day survival assay following APH treatment and found that S62A-MYC reduced cell survival after DNA damage, while T58A-MYC closely resembled WT-MYC in promoting survival (Figure 3.3.5).

Taken together, these findings outline a MYC driven mechanism that augments DNA repair in the face of genomic instability to facilitate oncogenesis. This mechanism was characterized in the context of dysregulated MYC, either in cancer cell lines or through ectopic expression, mirroring the stabilized MYC observed in advanced human tumors. In normal cells, genomic instability triggers a rapid decrease in MYC levels, and failure to downregulate MYC under these conditions leads to apoptosis. Therefore, all the cell lines used to describe this mechanism carry co-occurring mutations bypass normal MYC regulation during genomic instability. For example, the patient derived PDAC tumors and cell lines all carry loss-of-function of p53, along with other cancer promoting mutations[292]. In the HEK293T cells used to study MYC phosphorylation mutants, p53 is considered inactive due to its interaction with the large T-antigen[335], highlighting the necessity of disrupted p53 signaling in MYC driven oncogenesis. Within this oncogenic cellular environment driven by constitutive MYC signaling, we show that the cell becomes increasingly dependent on MYC directed mechanisms of DNA repair to support survival and promote oncogenesis. Therefore, in MYC addicted tumors, MYC delivers the medicine for the poison it administers, and therapeutically targeting these compensatory mechanisms could turn survival into self-destruction.

4.5 Strategic Targeting of MYC Addicted Tumors

Given MYC's widespread role in tumorigenesis, it has been the focus of decades of research aimed at clinically targeting human cancers[4, 6, 45, 247, 332]. Notably, experimentally inactivation of MYC inhibits proliferation and induces sustained tumor regression across multiple cancer types originating from diverse tissues[174, 336]. However, clinically, MYC has long been considered "undruggable" due to its intrinsically disordered structure lacking a defined druggable pocket, along with the concern that silencing MYC would disrupt normal tissue regeneration and result in unacceptable toxicity[337]. Over the past 20 years, both of these notions have been heavily challenged by the development of Omomyc, a 91-amino acid synthetic miniprotein that mimics a mutated version of MYC's basic-loop-helix-leucine zipper domain[338-341]. Omomyc inhibits MYC's transcriptional activity by blocking its binding to gene promoters and forming homo- and heterodimers with MAX at E-boxes, resulting in the formation of a transcriptionally repressive complex. Omomyc showed strong promise in a phase 1 trial involving 22 patients with solid tumors, most of whom experienced limited adverse effects[342]. Notably, one patient was classified as having stable disease with a tumor reduction of 49% at the end of the trail. This phase 1 clinical trial, along with a thorough mouse model investigation into the tolerance of MYC inhibition[341], demonstrate that directly targeting MYC can preferentially impair tumor growth with relatively mild side effects on normal tissue function.

While direct inhibition of MYC with OmoMYC is showing strong clinical potential, indirect disruption of MYC activity has also demonstrated encouraging results[4]. In this manuscript, we outline two distinct mechanisms that contribute to MYC's function and role in oncogenesis, both converging on the post-translational regulation of MYC through

phosphorylation of serine 62. In Chapter 2, we explored how PIN1 stabilizes pS62-MYC and directs it to the nuclear pore, where it participates in gene gating to promote proliferation in response to serum stimulation. PIN1 is a promising indirect target in MYC-driven tumors, as it is frequently co-overexpressed in cancer and correlates with poor patient survival[101, 117]. Furthermore, although PIN1 knockout mice are stunted and infertile, they are viable and exhibit significantly delayed tumor formation when crossed with cancer driving mutants of HER2 or RAS[109, 110]. In our PIN1 knockout MEFs, we show that the serum stimulated MYC's interactome formation at the nuclear pore is abolished compared to WT, highlighting how loss of PIN1 diminishes MYC driven gene activation at the nuclear pore (Figure 2.3.3). In cancer, growth promoting mechanisms such as PIN1-directed MYC activity at the nuclear pore are constitutively active independent of extrinsic signals[108]. Since PIN1 knockout MEFs exhibit a similar proliferative rate to WT during asynchronous growth but show a significant delay in proliferation following mitogen stimulation[107], targeting PIN1 could hinder MYC's contribution to sustained proliferative signaling. To this point, we show that PIN1 knockdown in MIA PaCa-2 PDAC cell lines reduces both MYC, pS62MYC, and NPC promoter binding of target genes (Figure 2.3.1). We also show that that the PIN1 inhibitor, PiB, reduces MYC's promoter binding to E2F2 and NCL1 in HPAFII PDAC cells. This is consistent with previous findings that PiB reduces MYC's efficiency of DNA promoter binding in MCF10A breast cancer cells lines and diminishes its oncogenic potential[116]. Interestingly, we found that the covalent PIN1 inhibitor Sulfopin showed variable efficacy in reducing MYC target gene binding in HPAFII cells, despite previous reports demonstrating its ability to block MYC-driven tumors in vivo[278]. Further investigation is

needed to understand the mechanism underlying Sulfopin's variable inhibition of MYC activity. Taken together, therapeutically targeting PIN1 could uncouple constitutive growth promoting signals in cancer from MYC's gene amplification activity at the nuclear pore, thereby reducing tumor growth and proregression.

Beyond disrupting pS62-MYC's role in regulating growth promoting transcription at the nuclear pore, in Chapter 3 we propose that pS62-MYC also contributes to enhancing DNA repair genomic damage. Prevention of serine 62 phosphorylation results in reduced recruitment of BRCA1 and RAD51 to DSBs, hindering efficient DNA repair and leading to an overall decrease in cell recovery following DNA damage (Figures 3.3.4 and 3.3.5). Targeting serine 62 phosphorylation would disrupt both MYC's transcriptional activity and its role in DNA repair, highlighting a promising strategy for selectively targeting MYC tumors. One promising therapy is the small-molecule activator of PP2A, DT-061, which selectively stabilizes the B56α subunit of PP2A, a key mediator of serine 62 dephosphorylation of MYC[343, 344]. DT-061's stabilization of PP2A-B56α removes serine 62 phosphorylation and promotes MYC's degradation through the ubiquitin proteosome system[127]. Although DT-061 may reduce MYC driven oncogenesis, determining its direct impact on MYC's role in DNA repair would be challenging, as PP2A regulates multiple components of DNA damage response[345].

Another method we explored for reducing pS62-MYC as a cancer therapy was targeting the upstream activators of serine 62 phosphorylation. This project was carried out in collaboration a research assistant, Alex Smith, and with a talented high school student, Ariffin, whom I had the opportunity to mentor over two summers. This targeting approach involved the use of patient derived PDAC cell lines in a drug sensitivity assay,

coupled with Western Blot analysis (Figure 4.5.1A). In PDAC patients, four major genetic alterations are commonly observed: KRAS (~90%), TP53 (~65%), CDKN2A (~90%), and SMAD4 (~50%)[346-348]. The co-occurrence of overactivated KRAS signaling with the loss of these tumor suppressors promotes tumor cells with elevated MYC driven growth activity while disabling the oncogenic safeguards that would normally trigger apoptosis. The hotspot mutations that activate KRAS typically occur at the 12th glycine residue, resulting in G12D, G12V, G12R, and G12C variants. These point mutations impair KRAS GTPase activity and prevents the hydrolysis of guanosine triphosphate (GTP), leading to constitutive KRAS signaling. This persistent activation in turn drives continuous stimulation of the RAF-MEK-ERK and PI3L-AKT-MTOR phosphorylation cascades[349], all of which converge on MYC serine-62 phosphorylation (Figure 5.5.1B). Mutant KRAS inhibitors were historically difficult to develop due to the protein's lack of deep, druggable clefts. However, in 2013, Dr. Kevan Shokat and his laboratory discovered a druggable pocket within the switch II domain of KRAS-G12C, enabling the development of covalent small molecules that selectively target this mutation[350]. This groundbreaking discovery led to the creation of several KRAS-G12C inhibitors that have shown strong clinical promise in non-small cell lung cancer[351-353]. In PDAC, G12D mutations are more prevalent than G12C mutations [354], and covalent inhibitors that target KRAS-G12C have little-to-no effect on tumors harboring G12D mutations. Inactivation of KRAS-G12C depends on reactive amino acids near the switch II pocket that enable stable covalent bond formation between the inhibitor and cysteine-12[355, 356]. Structural analysis of KRAS-G12D proteins revealed an altered switch II pocket, further supporting the limited efficacy of KRAS-G12C inhibitors against G12D mutations[357]. In 2022, a study led by

Dr. James Christensen at Mirati Therapeutics reported promising preclinical data in PDAC using MRTX1133, a small molecule inhibitor, selectively targeting KRAS-G12D[358]. MRTX1133 is a non-covalent inhibitor that inactivates KRAS-G12D with over 1000-fold sensitivity compared to WT KRAS, making it a promising therapeutic candidate for PDAC [359, 360].

To investigate whether MYC serine 62 phosphorylation could be indirectly targeted through the direct inhibition of mutant KRAS in PDAC cells, Ariffin, Alexander Smith, and I established a drug screening approach using patient-derived pancreatic cancer cell lines (Figure 4.5.1A). Previously, these tumors and cell lines were subjected to whole exome sequencing to define their mutational profiles (data not included). Ariffin's summer project involved performing drug sensitivity screens in parallel with Western Blot analysis to correlate mutation profiles with sensitivity to specific KRAS pathway inhibitors that reduce pS62MYC. Although the conclusions from Ariffin's summer project require further validation through additional replicates and experiments, we observed varying degrees of sensitivity to both MRTX1133 and the MEK1/2 inhibitor Cobimetinib across patient-derived PDAC cell lines. Ariffin found that patient lines ST-00022683 and ST-00024058, both carrying G12D mutations, showed the greatest sensitivity to MRTX1133. In contrast, ST-00022939 and ST-00022975, which harbor G12R mutations, were less sensitive. Notably, ST-00013312 cells with the KRAS-G12C mutation were approximately five orders of magnitude less sensitive than the G12D cell lines, highlighting the specificality of MRTX1133 on KRAS-G12D PDAC tumor cell lines. In addition to harboring the KARS-G12C mutation, ST-00013312 also carries a loss of function mutation for the tumor suppressor PTEN, resulting in constitutive PI3K (Figure 4.5.1B). This may explain why

MRTX1133 treatment led to a decrease in pERK1/2 but did not translate into drug sensitivity. ST-00022683, which carries a G12D mutation, showed an MRTX1133-induced reduction in pERK1/2, a response that was absent in the G12R mutants. Surprisingly, pERK1/2 levels remained relatively unchanged in ST-00024058, despite the cell line's sensitivity to MRTX1133. Unfortunately, most of Ariffin's Western Blots for MYC following MRTX1133 treatment were unsuccessful, except for ST-00024058 which showed a dose-dependent decrease in both pS62-MYC and total MYC levels.

In addition to directly targeting mutant KRAS, we included Cobimetinib, which inhibits MEK1/2, a kinase activated downstream of KRAS (Figure 4.5.1B). As expected, the response to Cobimetinib was largely independent of the specific KRAS missense mutation (Figure 5.5.2). Most cell lines exhibited comparable GR50 values, with exception of ST-00013312, which carries the PTEN mutation as previously noted. Aside from ST-0013312 as an outlier to this trend, sensitivity to Cobimetinib correlated with the loss of both pS62-MYC and total MYC bands in the Western Blot, suggesting that upstream inhibition of MEK1/2 prevents serine-62 phosphorylation of MYC and promotes its degradation. Although these findings are preliminary and require further validation, Ariffin's work provides a proof of principal that indirectly targeting MYC through upstream pathway inhibition can impact its stability. This groundwork opens the door to future studies aimed at determining whether these therapies also impair MYC's role in gene gating and/or DNA repair in cancer.

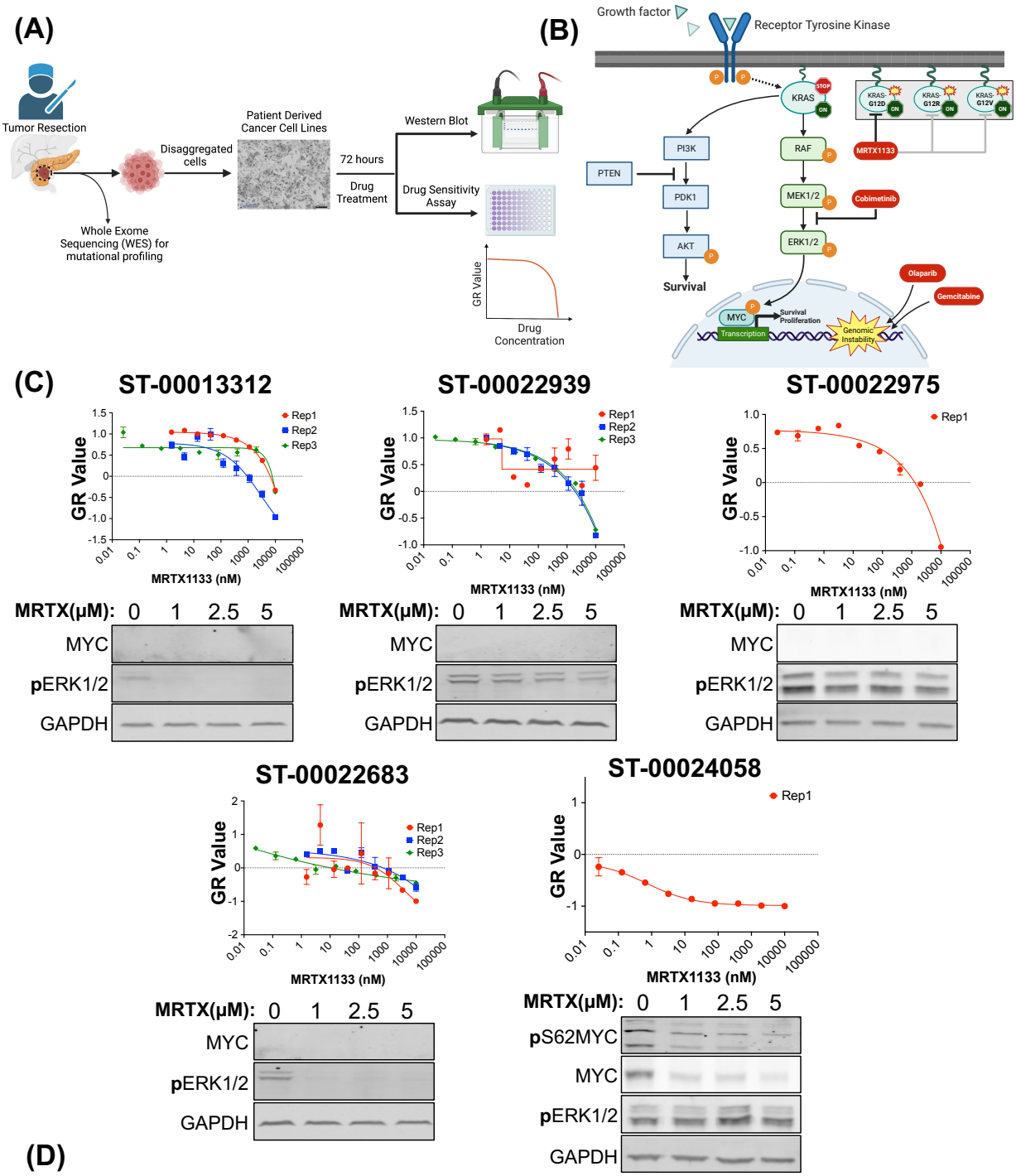

	ST-00013312	ST-00022939	ST-00022975	ST-00022683	ST-00024058
MRTX1133 average GR50 (nM):	1974.5	170.35	81.89	0.02	>0.02
KRAS Mutation:	G12C	G12R	G12R	G12D	G12D

Figure 4.5.1. A Drug Screen Approach in Patient-Derived Pancreatic Cell Lines to Optimize Personalized Therapeutic Strategies.

(A) Schema illustrating Ariffin's workflow. Patient tumor samples were resected, profiled for mutation status, and created into cell lines. Drug sensitivity assays and Western Blot analysis were performed on these cell lines. (B) Simplified MAPK signaling pathway showing therapeutic targets (red). Only MRTX1133 and Cobimetinib were included in this dissertation. (C) Drug sensitivity graphs showing the Growth Rate (GR value) of cells treated with MRTX1133 (nM) for 72hrs. In addition, Western Blot analysis displaying downstream MAPK activation. (D) Average GR50 values for each cell line with specific KRAS missense mutation identified.

(A)

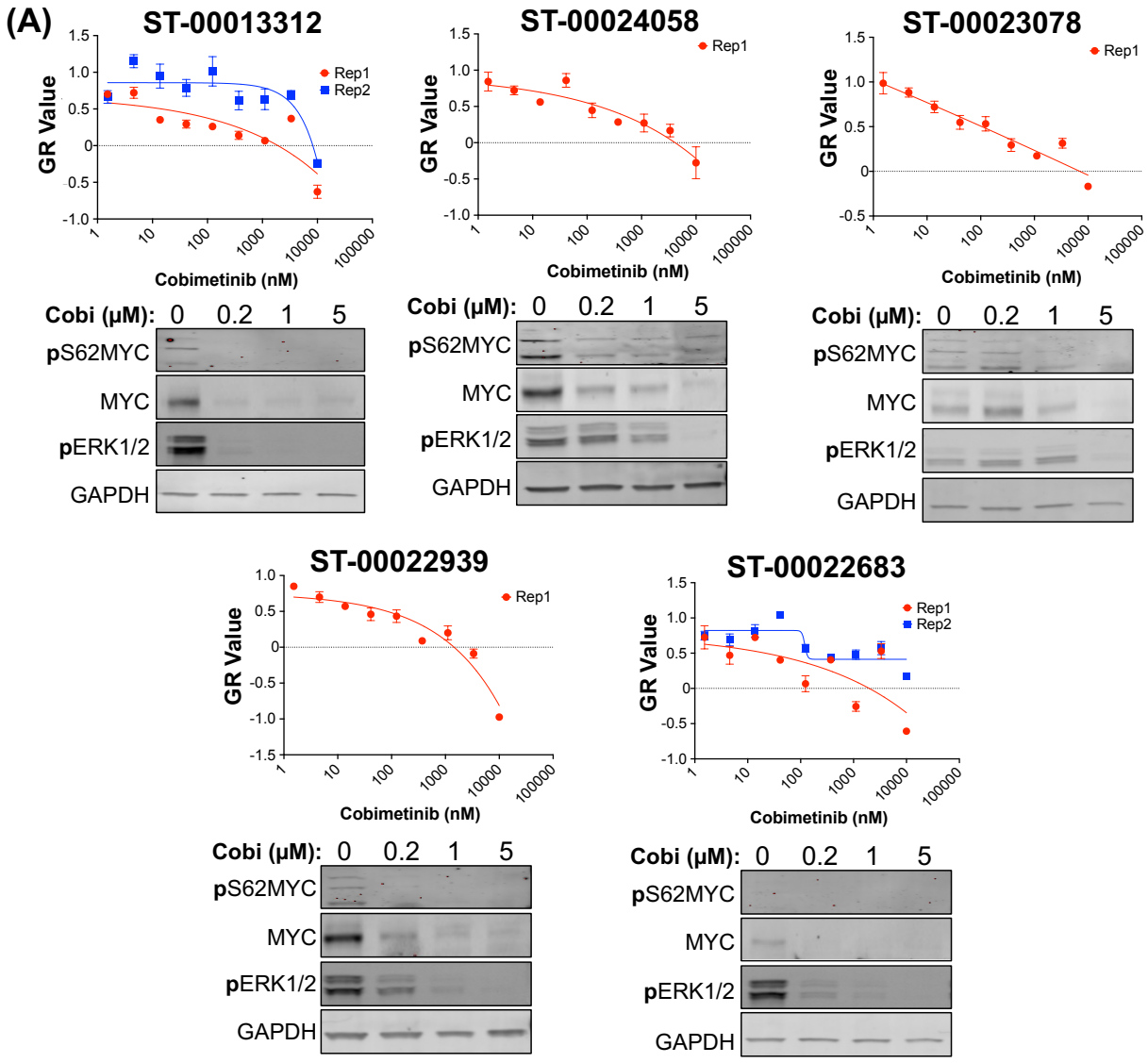

(B)

	ST-00013312	ST-00024058	ST-00023078	ST-00022939	ST-00022683
Cobimetinib average GR50 (nM):	2027.33	165.9	105.6	82.46	75.69
KRAS Mutation:	G12C	G12D	G12V	G12R	G12D

Figure 4.5.2. Patient-Derived Pancreatic Cell Lines Response to Cobimetinib.

(A) Drug sensitivity graphs showing the Growth Rate (GR value) of cells treated with Cobimetinib (nM) for 72hrs. In addition, Western Blot analysis displaying downstream MAPK activation. (B) Average GR50 values for each cell line with specific KRAS missense mutation identified.

4.6 MYC: The Molecular Prometheus

"Unlike Beowulf at the hall of Hrothgar, we have not slain our enemy, the cancer cell, or figuratively torn the limbs from his body. In our adventures, we have only seen our monster more clearly and described his scales and fangs in new ways – ways that reveal a cancer cell to be, like Grendel, a distorted version of our normal selves."

-Dr. Harold Varmus giving his Nobel Prize banquet speech in Stockholm (1989)[361]

In this dissertation, I sought to illuminate the duality of MYC's function, from its essential role in supporting multicellular growth required for the establishment and maintenance of tissues, to its dangerous potential to drive oncogenesis when dysregulated. This duality echoes the ancient Greek myth of the Titan Prometheus and his gift of fire to humanity. A force of both creation and destruction, fire gave rise to civilizations even as it held the power to consume them. This gift of fire brought warmth and prosperity but also served as a great arbiter of survival. Societies that mastered its use for cooking, metallurgy, warfare, or engines of industry often surpassed their neighbors in power and influence. So it is with MYC, cells that harness its power for growth and repair may flourish, but when unrestrained, its flame turns inward, fueling the chaos of oncogenesis. MYC was first revealed as a potent torchbearer of cellular survival through studies of a phenomena known as cell competition, initially observed in *Drosophila Minute* (M) mutants, which carry mutations in ribosomal protein genes[362]. Homozygous *Minute* (M/M) mutations were lethal, but heterozygous *Minute* (M/+) cells were viable, allowing flies to develop normally aside from slightly thinner bristles. Cell completion between WT and M/+ cells was observed in developing *Drosophila* wing discs, where neighboring WT cells displaced and eliminated small colonies of induced M/+ cells[363]. Subsequent research revealed that cell competition is a conserved mechanism

of tissue adaptability and fitness sensing across insects and mammals, wherein slower-dividing cells are designated as ‘losers’ and eliminated through apoptosis, allowing the more proliferative ‘winner’ cells to prevail[364-367]. Similar to the dynamics observed in *Drosophila Minute* mutants, differing protein levels of the *Drosophila* MYC ortholog, dMYC, also triggered cell competition, with dMYC-low cells being eliminated in the presence of WT neighbors[368]. Furthermore, mosaic overexpression of dMYC in the *Drosophila* wing disc transformed the dMYC-high cells into ‘supercompetitors,’ inducing apoptosis in neighboring WT cells and clonally outcompeting them for space and survival[369, 370]. Importantly, the replacement of WT cells by dMYC-high cells occurred without any morphological or developmental abnormalities, suggesting that this phenomenon is part of normal tissue homeostasis and may become corrupted or dysregulated during oncogenesis. This ‘supercompetitor’ phenotype appears to be a unique feature of MYC, as RAS- or Src-transformed cells in similar experiments were eliminated by delamination from the epithelial layer through a process known as epithelial defense against cancer (EDAC), leaving WT epithelial cells to dominate the tissue[371, 372].

As the MYC-high cells spread like wildfire, they not only outpace the neighboring WT cells in growth but also actively induce their apoptosis, clearing the path for their own expansion[373]. This non-cell autonomous tissue apoptotic response is distinct from MYC’s cell intrinsic role in apoptosis discussed in Chapter 1. For example, co-culture experiments revealed that conditioned media from dMYC-high cells could initiate MYC-driven cell competition, suggesting that these cells secrete soluble factors through paracrine signaling to induce apoptosis in their less fit neighbor cells[374]. In agreement,

Toll-related receptors and the *Drosophila* cytokine Spätzle were shown to activate NFκB-dependent apoptosis and are required for the elimination of WT cells by dMYC-high cells[375]. Furthermore, dMYC-high cells assert tissue dominance through direct interaction with their less fit neighboring cells, often resulting in a cannibalistic act of engulfing adjacent apoptotic WT cells[376]. The supercompetitor phenotype of MYC has also been documented in mammals, including the developing mouse embryo and human cancer cells in vitro, where MYC-high cells engulf neighboring WT cells that are undergoing JNK-driven apoptosis[377-379]. MYC's supercompetitor phenotype aligns with its strong correlation in driving aggressive and metastatic tumors[292, 380]. In the sequential events of cellular transformation, it remains unclear what systemic mechanisms allow MYC's supercompetitor phenotype to emerge while restraining its full oncogenic propensity. As discussed in the introduction, p53 plays a paramount role in counteracting the oncogenic potential of MYC. This is also true for MYC's supercompetitor phenotype, as loss of p53 impairs MYC's ability to outcompete its WT neighbors[381]. This further supports the notion that additional mutations are required to buffer the effect of supraphysiological levels of MYC in the absence of functional p53, ultimately enabling tumor formation.

The research presented in this dissertation outlines actionable mechanisms through which MYC enacts its cellular fitness ability. Post-translational modifications that govern MYC stability, such as serine-62 phosphorylation and PIN1-mediated isomerization, enable MYC to activate cell growth-promoting gene programs at the NPC and augment DNA repair to sustain elevated transcription and replication. These mechanisms are essential for tissue prosperity, but as oncogenic mutations accumulate,

they become corrupted, allowing the flames of MYC to burn without proper restraint and drive oncogenesis. An excess of MYC kindles a selfish cell, one that abandons the harmony of the tissue and consumes more than its share, thriving at the expense of its neighbors. To extinguish this fire, we must restore cellular balance through pharmacologically means and reclaim control of the flames of MYC.

Appendix A: Alpha-synuclein regulates nucleolar DNA double-strand break repair in melanoma

Moriah R. Arnold[1,2], **Gabriel M. Cohn[3]**, Kezia Catharina Oxe[4], Somarr N. Elliott[2], Cynthia Moore[5], Allison May Zhou[2], Peter V. Laraia[6], Sahar Shekoohi[7], Dillon Brownell[8], Rosalie C. Sears[3,9,10], Randall L. Woltjer[11], Charles K. Meshul[5,12], Stephan N. Witt[7,13], Dorthe H. Larsen[4], Vivek K. Unni*[2,14]

[1]Medical Scientist Training Program, Oregon Health and Science University, Portland, OR, USA.

[2]Department of Neurology and Jungers Center for Neurosciences Research, Oregon Health and Science University, Portland, OR, USA.

[3]Department of Molecular and Medical Genetics, School of Medicine, Oregon Health and Science University, Portland, OR, USA.

[4]Danish Cancer Institute, Nucleolar Stress and Disease Group, Strandboulevarden 49, 2100 Copenhagen, Denmark.

[5]Research Services, Neurocytology Laboratory, Veterans Affairs Medical Center, Portland, OR, USA.

[6]Independent Collaborator.

[7]Department of Biochemistry and Molecular Biology, Louisiana State University Health Sciences Center, Shreveport, LA, USA.

[8]Department of Molecular Microbiology and Immunology, Oregon Health and Science University, Portland, OR, USA.

[9]Brenden-Colson Center for Pancreatic Care, Oregon Health & Science University, Portland, OR, USA.

[10]Knight Cancer Institute, Oregon Health & Science University, Portland, OR, USA.

[11]Layton Aging & Alzheimer's Disease Research Center and Department of Pathology, Oregon Health and Science University, Portland, OR, USA.

[12]Departments of Behavioral Neuroscience and Pathology, Oregon Health and Science University, Portland, OR, USA.

[13]Feist-Weiller Cancer Center, Louisiana State University Health Sciences Center, Shreveport, LA, US.

[14]OHSU Parkinson Center, Oregon Health and Science University, Portland, OR, USA.

Published on bioRxiv January 14th, 2024

In Press at *Science Advances* in April 2025

A.1 Commentary on Contribution

My development of proximity ligation assays to study MYC's association with DNA double-strand breaks also enabled the investigation of other proteins at sites of DNA damage. In collaboration with Dr. Moriah Arnold in Dr. Vivek Unni's lab, I implemented this technology to support their investigation of alpha-synuclein's localization to nucleolar DNA damage in human melanoma cells. Working alongside Moriah, I performed all DI-PLA and PLA experiments and created the analysis pipeline for image acquisition and analysis. Given that these findings are currently in press and considering that I did not contribute majorly to project design, the work does not directly involve MYC, and the techniques and analyses are already represented within my own research, I have chosen to exclude the full manuscript of this collaboration from my dissertation.

References

1. Bishop, J.M., *How to Win the Nobel Prize: An Unexpected Life in Science*. 2003: Harvard University Press. 257.
2. David, A.R. and M.R. Zimmerman, *Cancer: an old disease, a new disease or something in between?* Nat Rev Cancer, 2010. **10**(10): p. 728-33.
3. Kontomanolis, E.N., et al., *Role of Oncogenes and Tumor-suppressor Genes in Carcinogenesis: A Review*. Anticancer Res, 2020. **40**(11): p. 6009-6015.
4. Duffy, M.J., et al., *MYC as a target for cancer treatment*. Cancer Treat Rev, 2021. **94**: p. 102154.
5. Schaub, F.X., et al., *Pan-cancer Alterations of the MYC Oncogene and Its Proximal Network across the Cancer Genome Atlas*. Cell Syst, 2018. **6**(3): p. 282-300.e2.
6. Vita, M. and M. Henriksson, *The Myc oncoprotein as a therapeutic target for human cancer*. Semin Cancer Biol, 2006. **16**(4): p. 318-30.
7. Potter, M. and K.B. Marcu, *The c-myc Story: Where we've been, Where we seem to be Going*, in *C-Myc in B-Cell Neoplasia: 14th Workshop on Mechanisms in B-Cell Neoplasia*, M. Potter and F. Melchers, Editors. 1997, Springer Berlin Heidelberg: Berlin, Heidelberg. p. 1-17.
8. Ellermann, V. and O. Bang, *Experimentelle leukämie bei hühnern. [Experimental leukemia in chickens]*. Fizentralbl Bakteril, 1909. **46**(1): p. 595-609.
9. Rous, P., *A TRANSMISSIBLE AVIAN NEOPLASM. (SARCOMA OF THE COMMON FOWL.)*. J Exp Med, 1910. **12**(5): p. 696-705.
10. Rous, P., *A SARCOMA OF THE FOWL TRANSMISSIBLE BY AN AGENT SEPARABLE FROM THE TUMOR CELLS*. J Exp Med, 1911. **13**(4): p. 397-411.
11. Rous, P., *The Challenge to Man of the Neoplastic Cell*. Science, 1967. **157**(3784): p. 24-28.
12. Huebner, R.J. and G.J. Todaro, *Oncogenes of RNA tumor viruses as determinants of cancer*. Proc Natl Acad Sci U S A, 1969. **64**(3): p. 1087-94.
13. Martin, G.S., et al., *Temperature-dependent alterations in sugar transport in cells infected by a temperature-sensitive mutant of Rous sarcoma virus*. Proc Natl Acad Sci U S A, 1971. **68**(11): p. 2739-41.
14. Martin, G.S., *Rous sarcoma virus: a function required for the maintenance of the transformed state*. Nature, 1970. **227**(5262): p. 1021-3.
15. Stehelin, D., et al., *DNA related to the transforming gene(s) of avian sarcoma viruses is present in normal avian DNA*. Nature, 1976. **260**(5547): p. 170-173.
16. Spector, D.H., H.E. Varmus, and J.M. Bishop, *Nucleotide sequences related to the transforming gene of avian sarcoma virus are present in DNA of uninfected vertebrates*. Proc Natl Acad Sci U S A, 1978. **75**(9): p. 4102-6.
17. Mladenov, Z., et al., *Strain MC29 avian leukosis virus. Myelocytoma, endothelioma, and renal growths: pathomorphological and ultrastructural aspects*. J Natl Cancer Inst, 1967. **38**(3): p. 251-85.
18. Graf, T. and H. Beug, *Avian leukemia viruses: interaction with their target cells in vivo and in vitro*. Biochim Biophys Acta, 1978. **516**(3): p. 269-99.

19. Sheiness, D. and J.M. Bishop, *DNA and RNA from uninfected vertebrate cells contain nucleotide sequences related to the putative transforming gene of avian myelocytomatosis virus*. J Virol, 1979. **31**(2): p. 514-21.
20. Sheiness, D., L. Fanshier, and J.M. Bishop, *Identification of nucleotide sequences which may encode the oncogenic capacity of avian retrovirus MC29*. J Virol, 1978. **28**(2): p. 600-10.
21. Duesberg, P.H., K. Bister, and P.K. Vogt, *The RNA of avian acute leukemia virus MC29*. Proc Natl Acad Sci U S A, 1977. **74**(10): p. 4320-4.
22. Hu, S.S., M.M. Lai, and P.K. Vogt, *Genome of avian myelocytomatosis virus MC29: analysis by heteroduplex mapping*. Proc Natl Acad Sci U S A, 1979. **76**(3): p. 1265-8.
23. Ramsay, G., T. Graf, and M.J. Hayman, *Mutants of avian myelocytomatosis virus with smaller gag gene-related proteins have an altered transforming ability*. Nature, 1980. **288**(5787): p. 170-2.
24. Bister, K., G.M. Ramsay, and M.J. Hayman, *Deletions within the transformation-specific RNA sequences of acute leukemia virus MC29 give rise to partially transformation-defective mutants*. J Virol, 1982. **41**(3): p. 754-66.
25. Roussel, M., et al., *Three new types of viral oncogene of cellular origin specific for haematopoietic cell transformation*. Nature, 1979. **281**(5731): p. 452-5.
26. Bunte, T., I. Greiser-Wilke, and K. Moelling, *The transforming protein of the MC29-related virus CMII is a nuclear DNA-binding protein whereas MH2 codes for a cytoplasmic RNA-DNA binding polyprotein*. Embo j, 1983. **2**(7): p. 1087-92.
27. Mellon, P., et al., *Specific RNA sequences and gene products of MC29 avian acute leukemia virus*. Proc Natl Acad Sci U S A, 1978. **75**(12): p. 5874-8.
28. Rettenmier, C.W., et al., *gag-Related polypeptides encoded by replication-defective avian oncoviruses*. J Virol, 1979. **32**(3): p. 749-61.
29. Hayward, W.S., B.G. Neel, and S.M. Astrin, *Activation of a cellular onc gene by promoter insertion in ALV-induced lymphoid leukosis*. Nature, 1981. **290**(5806): p. 475-80.
30. Neel, B.G., et al., *Avian leukosis virus-induced tumors have common proviral integration sites and synthesize discrete new RNAs: oncogenesis by promoter insertion*. Cell, 1981. **23**(2): p. 323-34.
31. Payne, G.S., J.M. Bishop, and H.E. Varmus, *Multiple arrangements of viral DNA and an activated host oncogene in bursal lymphomas*. Nature, 1982. **295**(5846): p. 209-14.
32. Cooper, G.M., *Transforming genes of chicken bursal lymphomas*. J Cell Physiol Suppl, 1982. **1**: p. 209-12.
33. Manolov, G. and Y. Manolova, *Marker band in one chromosome 14 from Burkitt lymphomas*. Nature, 1972. **237**(5349): p. 33-4.
34. Zech, L., et al., *Characteristic chromosomal abnormalities in biopsies and lymphoid-cell lines from patients with Burkitt and non-Burkitt lymphomas*. Int J Cancer, 1976. **17**(1): p. 47-56.
35. Dalla-Favera, R., et al., *Human c-myc onc gene is located on the region of chromosome 8 that is translocated in Burkitt lymphoma cells*. Proc Natl Acad Sci U S A, 1982. **79**(24): p. 7824-7.

36. Shen-Ong, G.L., et al., *Novel myc oncogene RNA from abortive immunoglobulin-gene recombination in mouse plasmacytomas*. Cell, 1982. **31**(2 Pt 1): p. 443-52.
37. Taub, R., et al., *Translocation of the c-myc gene into the immunoglobulin heavy chain locus in human Burkitt lymphoma and murine plasmacytoma cells*. Proc Natl Acad Sci U S A, 1982. **79**(24): p. 7837-41.
38. Schwab, M., et al., *Amplified DNA with limited homology to myc cellular oncogene is shared by human neuroblastoma cell lines and a neuroblastoma tumour*. Nature, 1983. **305**(5931): p. 245-8.
39. Kohl, N.E., et al., *Transposition and amplification of oncogene-related sequences in human neuroblastomas*. Cell, 1983. **35**(2 Pt 1): p. 359-67.
40. Nau, M.M., et al., *L-myc, a new myc-related gene amplified and expressed in human small cell lung cancer*. Nature, 1985. **318**(6041): p. 69-73.
41. Brodeur, G.M., et al., *Amplification of N-myc in untreated human neuroblastomas correlates with advanced disease stage*. Science, 1984. **224**(4653): p. 1121-4.
42. Schwab, M., et al., *Enhanced expression of the human gene N-myc consequent to amplification of DNA may contribute to malignant progression of neuroblastoma*. Proc Natl Acad Sci U S A, 1984. **81**(15): p. 4940-4.
43. Dhanasekaran, R., et al., *The MYC oncogene - the grand orchestrator of cancer growth and immune evasion*. Nat Rev Clin Oncol, 2022. **19**(1): p. 23-36.
44. Dang, C.V., *MYC on the path to cancer*. Cell, 2012. **149**(1): p. 22-35.
45. Chen, H., H. Liu, and G. Qing, *Targeting oncogenic Myc as a strategy for cancer treatment*. Signal Transduct Target Ther, 2018. **3**: p. 5.
46. Copie-Bergman, C., et al., *MYC-IG rearrangements are negative predictors of survival in DLBCL patients treated with immunochemotherapy: a GELA/LYSA study*. Blood, 2015. **126**(22): p. 2466-74.
47. Rosenwald, A., et al., *Prognostic Significance of MYC Rearrangement and Translocation Partner in Diffuse Large B-Cell Lymphoma: A Study by the Lunenburg Lymphoma Biomarker Consortium*. J Clin Oncol, 2019. **37**(35): p. 3359-3368.
48. Beroukhim, R., et al., *The landscape of somatic copy-number alteration across human cancers*. Nature, 2010. **463**(7283): p. 899-905.
49. Hanahan, D. and Robert A. Weinberg, *Hallmarks of Cancer: The Next Generation*. Cell, 2011. **144**(5): p. 646-674.
50. Thompson, C.B., et al., *The effect of alterations in myc gene expression on B cell development in the bursa of Fabricius*. Cell, 1987. **51**(3): p. 371-81.
51. Davis, A.C., et al., *A null c-myc mutation causes lethality before 10.5 days of gestation in homozygotes and reduced fertility in heterozygous female mice*. Genes Dev, 1993. **7**(4): p. 671-82.
52. Dubois, N.C., et al., *Placental rescue reveals a sole requirement for c-Myc in embryonic erythroblast survival and hematopoietic stem cell function*. Development, 2008. **135**(14): p. 2455-65.
53. Asami, M., et al., *A program of successive gene expression in mouse one-cell embryos*. Cell Reports, 2023. **42**(2): p. 112023.
54. Uslu, V.V., et al., *Long-range enhancers regulating Myc expression are required for normal facial morphogenesis*. Nature Genetics, 2014. **46**(7): p. 753-758.

55. Dixon, M.J., et al., *Cleft lip and palate: understanding genetic and environmental influences*. Nat Rev Genet, 2011. **12**(3): p. 167-78.
56. Mangold, E., K.U. Ludwig, and M.M. Nöthen, *Breakthroughs in the genetics of orofacial clefting*. Trends Mol Med, 2011. **17**(12): p. 725-33.
57. Illi, B. and S. Nasi, *Myc beyond Cancer: Regulation of Mammalian Tissue Regeneration*. Pathophysiology, 2023. **30**(3): p. 346-365.
58. Dani, C., et al., *Extreme instability of myc mRNA in normal and transformed human cells*. Proceedings of the National Academy of Sciences, 1984. **81**(22): p. 7046-7050.
59. Bettess, M.D., et al., *c-Myc Is Required for the Formation of Intestinal Crypts but Dispensable for Homeostasis of the Adult Intestinal Epithelium*. Molecular and Cellular Biology, 2005. **25**(17): p. 7868-7878.
60. Ashton, G.H., et al., *Focal Adhesion Kinase Is Required for Intestinal Regeneration and Tumorigenesis Downstream of Wnt/c-Myc Signaling*. Developmental Cell, 2010. **19**(2): p. 259-269.
61. Baena, E., et al., *c-Myc regulates cell size and ploidy but is not essential for postnatal proliferation in liver*. Proceedings of the National Academy of Sciences, 2005. **102**(20): p. 7286-7291.
62. Wang, H., et al., *Coordinated Cross-Talk Between the Myc and Mlx Networks in Liver Regeneration and Neoplasia*. Cell Mol Gastroenterol Hepatol, 2022. **13**(6): p. 1785-1804.
63. Murtaugh, L.C., et al., *β-Catenin is essential for pancreatic acinar but not islet development*. Development, 2005. **132**(21): p. 4663-4674.
64. Bonal, C., et al., *Pancreatic Inactivation of c-Myc Decreases Acinar Mass and Transdifferentiates Acinar Cells Into Adipocytes in Mice*. Gastroenterology, 2009. **136**(1): p. 309-319.e9.
65. Jonas, J.-C., et al., *High Glucose Stimulates Early Response Gene c-Myc Expression in Rat Pancreatic β Cells**. Journal of Biological Chemistry, 2001. **276**(38): p. 35375-35381.
66. Puri, S., et al., *Replication confers β cell immaturity*. Nature Communications, 2018. **9**(1): p. 485.
67. Rosselot, C., et al., *Myc Is Required for Adaptive β-Cell Replication in Young Mice but Is Not Sufficient in One-Year-Old Mice Fed With a High-Fat Diet*. Diabetes, 2019. **68**(10): p. 1934-1949.
68. Bywater, M.J., et al., *Reactivation of Myc transcription in the mouse heart unlocks its proliferative capacity*. Nature Communications, 2020. **11**(1): p. 1827.
69. Belin, S., et al., *Injury-induced decline of intrinsic regenerative ability revealed by quantitative proteomics*. Neuron, 2015. **86**(4): p. 1000-1014.
70. Ma, J.-J., et al., *Telomerase Reverse Transcriptase and p53 Regulate Mammalian Peripheral Nervous System and CNS Axon Regeneration Downstream of c-Myc*. The Journal of Neuroscience, 2019. **39**(46): p. 9107.
71. Blackwood, E.M. and R.N. Eisenman, *Max: a helix-loop-helix zipper protein that forms a sequence-specific DNA-binding complex with Myc*. Science, 1991. **251**(4998): p. 1211-7.

72. Blackwood, E.M., B. Lüscher, and R.N. Eisenman, *Myc and Max associate in vivo*. Genes Dev, 1992. **6**(1): p. 71-80.
73. Li, Z., et al., *A global transcriptional regulatory role for c-Myc in Burkitt's lymphoma cells*. Proc Natl Acad Sci U S A, 2003. **100**(14): p. 8164-9.
74. Blackwell, T.K., et al., *Sequence-specific DNA binding by the c-Myc protein*. Science, 1990. **250**(4984): p. 1149-51.
75. Fernandez, P.C., et al., *Genomic targets of the human c-Myc protein*. Genes Dev, 2003. **17**(9): p. 1115-29.
76. Zeid, R., et al., *Enhancer invasion shapes MYCN-dependent transcriptional amplification in neuroblastoma*. Nat Genet, 2018. **50**(4): p. 515-523.
77. Das, S.K., B.A. Lewis, and D. Levens, *MYC: a complex problem*. Trends Cell Biol, 2023. **33**(3): p. 235-246.
78. Kalkat, M., et al., *MYC Protein Interactome Profiling Reveals Functionally Distinct Regions that Cooperate to Drive Tumorigenesis*. Mol Cell, 2018. **72**(5): p. 836-848.e7.
79. Lourenco, C., et al., *MYC protein interactors in gene transcription and cancer*. Nature Reviews Cancer, 2021. **21**(9): p. 579-591.
80. Kress, T.R., A. Sabò, and B. Amati, *MYC: connecting selective transcriptional control to global RNA production*. Nat Rev Cancer, 2015. **15**(10): p. 593-607.
81. McMahon, S.B., et al., *The novel ATM-related protein TRRAP is an essential cofactor for the c-Myc and E2F oncoproteins*. Cell, 1998. **94**(3): p. 363-74.
82. McMahon, S.B., M.A. Wood, and M.D. Cole, *The essential cofactor TRRAP recruits the histone acetyltransferase hGCN5 to c-Myc*. Mol Cell Biol, 2000. **20**(2): p. 556-62.
83. Fuchs, M., et al., *The p400 complex is an essential E1A transformation target*. Cell, 2001. **106**(3): p. 297-307.
84. Frank, S.R., et al., *MYC recruits the TIP60 histone acetyltransferase complex to chromatin*. EMBO Rep, 2003. **4**(6): p. 575-80.
85. Ciurciu, A., et al., *The Drosophila histone acetyltransferase Gcn5 and transcriptional adaptor Ada2a are involved in nucleosomal histone H4 acetylation*. Mol Cell Biol, 2006. **26**(24): p. 9413-23.
86. Kenneth, N.S., et al., *TRRAP and GCN5 are used by c-Myc to activate RNA polymerase III transcription*. Proc Natl Acad Sci U S A, 2007. **104**(38): p. 14917-22.
87. Herold, S., et al., *Negative Regulation of the Mammalian UV Response by Myc through Association with Miz-1*. Molecular Cell, 2002. **10**(3): p. 509-521.
88. Staller, P., et al., *Repression of p15INK4b expression by Myc through association with Miz-1*. Nature Cell Biology, 2001. **3**(4): p. 392-399.
89. Wanzel, M., et al., *A ribosomal protein L23-nucleophosmin circuit coordinates Mizl function with cell growth*. Nat Cell Biol, 2008. **10**(9): p. 1051-61.
90. Wu, S., et al., *Myc represses differentiation-induced p21CIP1 expression via Miz-1-dependent interaction with the p21 core promoter*. Oncogene, 2003. **22**(3): p. 351-360.
91. Walz, S., et al., *Activation and repression by oncogenic MYC shape tumour-specific gene expression profiles*. Nature, 2014. **511**(7510): p. 483-7.
92. Ayer, D.E., L. Kretzner, and R.N. Eisenman, *Mad: a heterodimeric partner for Max that antagonizes Myc transcriptional activity*. Cell, 1993. **72**(2): p. 211-22.

93. Ayer, D.E., Q.A. Lawrence, and R.N. Eisenman, *Mad-Max transcriptional repression is mediated by ternary complex formation with mammalian homologs of yeast repressor Sin3*. Cell, 1995. **80**(5): p. 767-76.
94. Larsson, L.G., et al., *Expression of mad, mxi1, max and c-myc during induced differentiation of hematopoietic cells: opposite regulation of mad and c-myc*. Oncogene, 1994. **9**(4): p. 1247-52.
95. Lu, K.P., et al., *Prolyl cis-trans isomerization as a molecular timer*. Nat Chem Biol, 2007. **3**(10): p. 619-29.
96. Chen, Y., et al., *Prolyl isomerase Pin1: a promoter of cancer and a target for therapy*. Cell Death Dis, 2018. **9**(9): p. 883.
97. Takahashi, K., et al., *Prolyl isomerase, Pin1: new findings of post-translational modifications and physiological substrates in cancer, asthma and Alzheimer's disease*. Cell Mol Life Sci, 2008. **65**(3): p. 359-75.
98. Göthel, S.F. and M.A. Marahiel, *Peptidyl-prolyl cis-trans isomerases, a superfamily of ubiquitous folding catalysts*. CMLS, 1999. **55**(3): p. 423-436.
99. Ubersax, J.A. and J.E. Ferrell, Jr., *Mechanisms of specificity in protein phosphorylation*. Nat Rev Mol Cell Biol, 2007. **8**(7): p. 530-41.
100. Pearson, G., et al., *Mitogen-activated protein (MAP) kinase pathways- regulation and physiological functions*. Endocr Rev., 2001. **22**(2): p. 153-83.
101. Cheng, C.W. and E. Tse, *PIN1 in Cell Cycle Control and Cancer*. Front Pharmacol, 2018. **9**: p. 1367.
102. Morgan, D., *Cyclin-dependent kinases- engines, clocks, and microprocessors*. Annu. Rev. Cell Dev. Biol, 1997. **13**: p. 261-91.
103. Liou, Y.C., et al., *Loss of Pin1 function in the mouse causes phenotypes resembling cyclin D1-null phenotypes*. Proc Natl Acad Sci U S A, 2002. **99**(3): p. 1335-40.
104. Ryo, A., et al., *Regulation of NF-kappaB signaling by Pin1-dependent prolyl isomerization and ubiquitin-mediated proteolysis of p65/RelA*. Mol. Cell., 2003. **12**: p. 1413-1426.
105. Ryo, A., et al., *Pin1 regulates turnover and subcellular localization of beta-catenin by inhibiting its interaction with APC*. 2001.
106. Liao, Y., et al., *Peptidyl-prolyl cis/trans isomerase Pin1 is critical for the regulation of PKB/Akt stability and activation phosphorylation*. Oncogene, 2009. **28**(26): p. 2436-45.
107. Fujimori, et al., *Mice Lacking Pin1 Develop Normally, but Are Defective in Entering Cell Cycle from G0 Arrest*. Biochem Biophys Res Comm., 1999. **265**(3).
108. Su, Y., et al., *Post-translational modification localizes MYC to the nuclear pore basket to regulate a subset of target genes involved in cellular responses to environmental signals*. Genes Dev, 2018. **32**(21-22): p. 1398-1419.
109. Wulf, et al., *Modeling breast cancer in vivo and ex vivo reveals an essential role of Pin1 in tumorigenesis*. EMBO J, 2004. **23**(16): p. 3397–3407.
110. Ryo, A., et al., *PIN1 is an E2F target gene essential for Neu/Ras-induced transformation of mammary epithelial cells*. Mol Cell Biol, 2002. **22**(15): p. 5281-95.
111. Gross, S., et al., *Targeting cancer with kinase inhibitors*. J Clin Invest, 2015. **125**(5): p. 1780-9.

112. Rustighi, A., et al., *The prolyl-isomerase Pin1 is a Notch1 target that enhances Notch1 activation in cancer*. Nat Cell Biol, 2009. **11**(2): p. 133-42.
113. Lam, P.B., et al., *Prolyl isomerase Pin1 is highly expressed in Her2-positive breast cancer and regulates erbB2 protein stability*. Mol Cancer, 2008. **7**: p. 91.
114. Dougherty, M.K., et al., *Regulation of Raf-1 by direct feedback phosphorylation*. Mol Cell, 2005. **17**(2): p. 215-24.
115. Zheng, Y., et al., *FAK phosphorylation by ERK primes ras-induced tyrosine dephosphorylation of FAK mediated by PIN1 and PTP-PEST*. Mol Cell, 2009. **35**(1): p. 11-25.
116. Farrell, A.S., et al., *Pin1 regulates the dynamics of c-Myc DNA binding to facilitate target gene regulation and oncogenesis*. Mol Cell Biol, 2013. **33**(15): p. 2930-49.
117. Zhou, X.Z. and K.P. Lu, *The isomerase PIN1 controls numerous cancer-driving pathways and is a unique drug target*. Nat Rev Cancer, 2016. **16**(7): p. 463-78.
118. Liang, C., et al., *PIN1 Maintains Redox Balance via the c-Myc/NRF2 Axis to Counteract Kras-Induced Mitochondrial Respiratory Injury in Pancreatic Cancer Cells*. Cancer Res, 2019. **79**(1): p. 133-145.
119. D'Artista, L., et al., *Pin1 is required for sustained B cell proliferation upon oncogenic activation of Myc*. Oncotarget, 2016. **7**(16): p. 21786-21798.
120. Luo, M.L., et al., *Prolyl isomerase Pin1 acts downstream of miR200c to promote cancer stem-like cell traits in breast cancer*. Cancer Res, 2014. **74**(13): p. 3603-16.
121. Rustighi, A., et al., *Prolyl-isomerase Pin1 controls normal and cancer stem cells of the breast*. EMBO Mol Med, 2014. **6**(1): p. 99-119.
122. Girardini, J.E., et al., *A Pin1/mutant p53 axis promotes aggressiveness in breast cancer*. Cancer Cell, 2011. **20**(1): p. 79-91.
123. Helander, S., et al., *Pre-Anchoring of Pin1 to Unphosphorylated c-Myc in a Fuzzy Complex Regulates c-Myc Activity*. Structure, 2015. **23**(12): p. 2267-2279.
124. Sears, R., et al., *A signalling pathway controlling c-Myc degradation that impacts oncogenic transformation of human cells*. Nat Cell Biol, 2004. **6**(4): p. 308-18.
125. Vervoorts, J., J. Lüscher-Firzlaff, and B. Lüscher, *The ins and outs of MYC regulation by posttranslational mechanisms*. J Biol Chem, 2006. **281**(46): p. 34725-9.
126. Gregory, M.A., Y. Qi, and S.R. Hann, *Phosphorylation by glycogen synthase kinase-3 controls c-myc proteolysis and subnuclear localization*. J Biol Chem, 2003. **278**(51): p. 51606-12.
127. Arnold, H.K. and R.C. Sears, *Protein phosphatase 2A regulatory subunit B56alpha associates with c-myc and negatively regulates c-myc accumulation*. Mol Cell Biol, 2006. **26**(7): p. 2832-44.
128. Arnold, H.K., et al., *The Axin1 scaffold protein promotes formation of a degradation complex for c-Myc*. The EMBO journal, 2009. **28**(5): p. 500-512.
129. Gregory, M. and S. Hann, *c-Myc Proteolysis by the Ubiquitin Proteasome Pathway: Stabilization of c-Myc in Burkitt's Lymphoma Cells*. Mol. Cell. Biol, 2000. **20**(7): p. 2423-35.
130. Welcker, M., et al., *A nucleolar isoform of the Fbw7 ubiquitin ligase regulates c-Myc and cell size*. Curr Biol, 2004. **14**(20): p. 1852-7.

131. Yeh, E., et al., *A signalling pathway controlling c-Myc degradation that impacts oncogenic transformation of human cells*. Nat Cell Biol, 2004. **6**(4): p. 308-18.
132. Andresen, C., et al., *Transient structure and dynamics in the disordered c-Myc transactivation domain affect Bin1 binding*. Nucleic acids research, 2012. **40**(13): p. 6353-6366.
133. Namanja, A.T., et al., *Stereospecific gating of functional motions in Pin1*. Proc Natl Acad Sci U S A, 2011. **108**(30): p. 12289-94.
134. Guo, J., X. Pang, and H.X. Zhou, *Two pathways mediate interdomain allosteric regulation in pin1*. Structure, 2015. **23**(1): p. 237-247.
135. Min, S.H., et al., *Negative regulation of the stability and tumor suppressor function of Fbw7 by the Pin1 prolyl isomerase*. Mol Cell, 2012. **46**(6): p. 771-83.
136. Chen, C.H., et al., *SENP1 deSUMOylates and regulates Pin1 protein activity and cellular function*. Cancer Res, 2013. **73**(13): p. 3951-62.
137. Sun, X.X., et al., *SUMO protease SENP1 deSUMOylates and stabilizes c-Myc*. Proc Natl Acad Sci U S A, 2018. **115**(43): p. 10983-10988.
138. Lee, T.H., et al., *Death-associated protein kinase 1 phosphorylates Pin1 and inhibits its prolyl isomerase activity and cellular function*. Mol Cell, 2011. **42**(2): p. 147-59.
139. Jaenicke, L.A., et al., *Ubiquitin-Dependent Turnover of MYC Antagonizes MYC/PAF1C Complex Accumulation to Drive Transcriptional Elongation*. Mol Cell, 2016. **61**(1): p. 54-67.
140. Myant, K., et al., *Serine 62-Phosphorylated MYC Associates with Nuclear Lamins and Its Regulation by CIP2A Is Essential for Regenerative Proliferation*. Cell Rep, 2015. **12**(6): p. 1019-31.
141. Eisenman, R.N., et al., *V-myc- and c-myc-encoded proteins are associated with the nuclear matrix*. Mol Cell Biol, 1985. **5**(1): p. 114-26.
142. Vriz, S., et al., *Comparative analysis of the intracellular localization of c-Myc, c-Fos, and replicative proteins during cell cycle progression*. Mol Cell Biol, 1992. **12**(8): p. 3548-55.
143. Blobel, G., *Gene gating: a hypothesis*. Proc Natl Acad Sci, 1985. **82**(24): p. 8527-8529.
144. Krull, S., et al., *Protein Tpr is required for establishing nuclear pore-associated zones of heterochromatin exclusion*. Embo j, 2010. **29**(10): p. 1659-73.
145. Beck, M. and E. Hurt, *The nuclear pore complex: understanding its function through structural insight*. Nat Rev Mol Cell Biol, 2017. **18**(2): p. 73-89.
146. Rodriguez-Bravo, V., et al., *Nuclear Pores Promote Lethal Prostate Cancer by Increasing POM121-Driven E2F1, MYC, and AR Nuclear Import*. Cell, 2018. **174**(5): p. 1200-1215.e20.
147. Simon, D.N. and M.P. Rout, *Cancer and the nuclear pore complex*. Adv Exp Med Biol, 2014. **773**: p. 285-307.
148. D'Urso, A. and J.H. Brickner, *Mechanisms of epigenetic memory*. Trends Genet, 2014. **30**(6): p. 230-6.
149. Sabò, A., et al., *Selective transcriptional regulation by Myc in cellular growth control and lymphomagenesis*. Nature, 2014. **511**(7510): p. 488-492.
150. Nie, Z., et al., *c-Myc is a universal amplifier of expressed genes in lymphocytes and embryonic stem cells*. Cell, 2012. **151**(1): p. 68-79.

151. Caforio, M., et al., *Recent advances in searching c-Myc transcriptional cofactors during tumorigenesis*. J Exp Clin Cancer Res, 2018. **37**(1): p. 239.
152. Sabo, A., et al., *Selective transcriptional regulation by Myc in cellular growth control and lymphomagenesis*. Nature, 2014. **511**(7510): p. 488-+.
153. Lovén, J., et al., *Revisiting global gene expression analysis*. Cell, 2012. **151**(3): p. 476-82.
154. Muhar, M., et al., *SLAM-seq defines direct gene-regulatory functions of the BRD4-MYC axis*. Science, 2018. **360**(6390): p. 800-805.
155. Sanchez-Arévalo Lobo, V.J., et al., *Dual regulation of Myc by Abl*. Oncogene, 2013. **32**(45): p. 5261-5271.
156. Kim, M.R., et al., *Enhancement of vascular endothelial growth factor-mediated angiogenesis in tamoxifen-resistant breast cancer cells: role of Pin1 overexpression*. Mol Cancer Ther, 2009. **8**(8): p. 2163-71.
157. Wei, S., et al., *Active Pin1 is a key target of all-trans retinoic acid in acute promyelocytic leukemia and breast cancer*. Nat Med, 2015. **21**(5): p. 457-66.
158. Campaner, E., et al., *A covalent PIN1 inhibitor selectively targets cancer cells by a dual mechanism of action*. Nat Commun, 2017. **8**: p. 15772.
159. Chen, X., et al., *Integration of external signaling pathways with the core transcriptional network in embryonic stem cells*. Cell, 2008. **133**(6): p. 1106-17.
160. Lin, C.Y., et al., *Transcriptional amplification in tumor cells with elevated c-Myc*. Cell, 2012. **151**(1): p. 56-67.
161. Jha, R.K., F. Kouzine, and D. Levens, *MYC function and regulation in physiological perspective*. Front Cell Dev Biol, 2023. **11**: p. 1268275.
162. Patange, S., et al., *MYC amplifies gene expression through global changes in transcription factor dynamics*. Cell Rep, 2022. **38**(4): p. 110292.
163. See, Y.X., K. Chen, and M.J. Fullwood, *MYC overexpression leads to increased chromatin interactions at super-enhancers and MYC binding sites*. Genome Res, 2022. **32**(4): p. 629-642.
164. Levens, D., *Cellular MYCro economics: Balancing MYC function with MYC expression*. Cold Spring Harb Perspect Med, 2013. **3**(11).
165. Wei, Y., et al., *Multiple direct interactions of TBP with the MYC oncoprotein*. Nature Structural & Molecular Biology, 2019. **26**(11): p. 1035-1043.
166. Rahl, P.B., et al., *c-Myc regulates transcriptional pause release*. Cell, 2010. **141**(3): p. 432-45.
167. Eberhardy, S.R. and P.J. Farnham, *c-Myc mediates activation of the cad promoter via a post-RNA polymerase II recruitment mechanism*. J Biol Chem, 2001. **276**(51): p. 48562-71.
168. Baluapuri, A., et al., *MYC Recruits SPT5 to RNA Polymerase II to Promote Processive Transcription Elongation*. Mol Cell, 2019. **74**(4): p. 674-687.e11.
169. Guan, Q., et al., *MYC promotes global transcription in part by controlling P-TEFb complex formation via DNA-binding independent inhibition of CDK9 SUMOylation*. Sci China Life Sci, 2023. **66**(9): p. 2167-2184.
170. Yu, F., et al., *SUMO suppresses and MYC amplifies transcription globally by regulating CDK9 sumoylation*. Cell Res, 2018. **28**(6): p. 670-685.

171. Thomas, L., *"The Wonderful Mistake," The Medusa and the Snail: More Notes of a Biology Watcher* 1979, New York: Viking Press.
172. Kelly, K., et al., *Cell-specific regulation of the c-myc gene by lymphocyte mitogens and platelet-derived growth factor.* Cell, 1983. **35**(3 Pt 2): p. 603-10.
173. Armelin, H.A., et al., *Functional role for c-myc in mitogenic response to platelet-derived growth factor.* Nature, 1984. **310**(5979): p. 655-60.
174. Wang, H., et al., *c-Myc depletion inhibits proliferation of human tumor cells at various stages of the cell cycle.* Oncogene, 2008. **27**(13): p. 1905-15.
175. Bretones, G., M.D. Delgado, and J. León, *Myc and cell cycle control.* Biochim Biophys Acta, 2015. **1849**(5): p. 506-16.
176. Mateyak, M.K., et al., *Phenotypes of c-Myc-deficient rat fibroblasts isolated by targeted homologous recombination.* Cell Growth Differ, 1997. **8**(10): p. 1039-48.
177. Evan, G., et al., *Integrated control of cell proliferation and cell death by the c-myc oncogene.* Philos Trans R Soc Lond B Biol Sci, 1994. **345**(1313): p. 269-75.
178. Clay, D.E. and D.T. Fox, *DNA Damage Responses during the Cell Cycle: Insights from Model Organisms and Beyond.* Genes (Basel), 2021. **12**(12).
179. Sheen, J.H. and R.B. Dickson, *Overexpression of c-Myc alters G(1)/S arrest following ionizing radiation.* Mol Cell Biol, 2002. **22**(6): p. 1819-33.
180. Sheen, J.H., J.K. Woo, and R.B. Dickson, *c-Myc alters the DNA damage-induced G2/M arrest in human mammary epithelial cells.* Br J Cancer, 2003. **89**(8): p. 1479-85.
181. Guerra, L., et al., *Myc is required for activation of the ATM-dependent checkpoints in response to DNA damage.* PLoS One, 2010. **5**(1): p. e8924.
182. Cui, F., et al., *The involvement of c-Myc in the DNA double-strand break repair via regulating radiation-induced phosphorylation of ATM and DNA-PKcs activity.* Mol Cell Biochem, 2015. **406**(1-2): p. 43-51.
183. Luoto, K.R., et al., *Tumor cell kill by c-MYC depletion: role of MYC-regulated genes that control DNA double-strand break repair.* Cancer Res, 2010. **70**(21): p. 8748-59.
184. Chiang, Y.-C., et al., *c-Myc Directly Regulates the Transcription of the NBS1 Gene Involved in DNA Double-strand Break Repair *.* Journal of Biological Chemistry, 2003. **278**(21): p. 19286-19291.
185. Petroni, M., et al., *The MRN complex is transcriptionally regulated by MYCN during neural cell proliferation to control replication stress.* Cell Death Differ, 2016. **23**(2): p. 197-206.
186. Lee, J.-H. and T.T. Paull, *ATM Activation by DNA Double-Strand Breaks Through the Mre11-Rad50-Nbs1 Complex.* Science, 2005. **308**(5721): p. 551-554.
187. Lee, J.H. and T.T. Paull, *Direct activation of the ATM protein kinase by the Mre11/Rad50/Nbs1 complex.* Science, 2004. **304**(5667): p. 93-6.
188. Gordan, J.D., et al., *HIF-alpha effects on c-Myc distinguish two subtypes of sporadic VHL-deficient clear cell renal carcinoma.* Cancer Cell, 2008. **14**(6): p. 435-46.
189. Robson, S.C., et al., *Deciphering c-MYC-regulated genes in two distinct tissues.* BMC Genomics, 2011. **12**(1): p. 476.
190. Carey, J.P.W., et al., *Synthetic Lethality of PARP Inhibitors in Combination with MYC Blockade Is Independent of BRCA Status in Triple-Negative Breast Cancer.* Cancer Res, 2018. **78**(3): p. 742-757.

191. Liu, Y.C., et al., *Global regulation of nucleotide biosynthetic genes by c-Myc*. PLoS One, 2008. **3**(7): p. e2722.
192. Chong, S., et al., *Mechanism of Transcriptional Bursting in Bacteria*. Cell, 2014. **158**(2): p. 314-326.
193. Kotsantis, P., E. Petermann, and S.J. Boulton, *Mechanisms of Oncogene-Induced Replication Stress: Jigsaw Falling into Place*. Cancer Discov, 2018. **8**(5): p. 537-555.
194. Endres, T., et al., *Ubiquitylation of MYC couples transcription elongation with double-strand break repair at active promoters*. Mol Cell, 2021. **81**(4): p. 830-844.e13.
195. Herold, S., et al., *Recruitment of BRCA1 limits MYCN-driven accumulation of stalled RNA polymerase*. Nature, 2019. **567**(7749): p. 545-549.
196. Papadopoulos, D., et al., *MYCN recruits the nuclear exosome complex to RNA polymerase II to prevent transcription-replication conflicts*. Mol Cell, 2022. **82**(1): p. 159-176.e12.
197. García-Muse, T. and A. Aguilera, *Transcription–replication conflicts: how they occur and how they are resolved*. Nature Reviews Molecular Cell Biology, 2016. **17**(9): p. 553-563.
198. Donley, N. and M.J. Thayer, *DNA replication timing, genome stability and cancer: late and/or delayed DNA replication timing is associated with increased genomic instability*. Semin Cancer Biol, 2013. **23**(2): p. 80-9.
199. Solvie, D., et al., *MYC multimers shield stalled replication forks from RNA polymerase*. Nature, 2022. **612**(7938): p. 148-155.
200. Zhao, L.J., P.M. Loewenstein, and M. Green, *Enhanced MYC association with the NuA4 histone acetyltransferase complex mediated by the adenovirus E1A N-terminal domain activates a subset of MYC target genes highly expressed in cancer cells*. Genes Cancer, 2017. **8**(11-12): p. 752-761.
201. Gorrini, C., et al., *Tip60 is a haplo-insufficient tumour suppressor required for an oncogene-induced DNA damage response*. Nature, 2007. **448**(7157): p. 1063-7.
202. Jha, R.K., D. Levens, and F. Kouzine, *Mechanical determinants of chromatin topology and gene expression*. Nucleus, 2022. **13**(1): p. 94-115.
203. Das, S.K., et al., *MYC assembles and stimulates topoisomerases 1 and 2 in a "topoisome"*. Mol Cell, 2022. **82**(1): p. 140-158.e12.
204. Das, S.K., et al., *Excessive MYC-topoisome activity triggers acute DNA damage, MYC degradation, and replacement by a p53-topoisome*. Mol Cell, 2024. **84**(21): p. 4059-4078.e10.
205. Peto, R., et al., *Cancer and ageing in mice and men*. Br J Cancer, 1975. **32**(4): p. 411-26.
206. Peto, R., *Epidemiology, multistage models, and short-term mutagenicity tests 1*. International Journal of Epidemiology, 2016. **45**(3): p. 621-637.
207. Abegglen, L.M., et al., *Potential Mechanisms for Cancer Resistance in Elephants and Comparative Cellular Response to DNA Damage in Humans*. JAMA, 2015. **314**(17): p. 1850-1860.
208. Sulak, M., et al., *TP53 copy number expansion is associated with the evolution of increased body size and an enhanced DNA damage response in elephants*. Elife, 2016. **5**.

209. Moberg, K.H., et al., *Analysis of the c-myc P2 promoter*. Journal of Cellular Physiology, 1991. **148**(1): p. 75-84.
210. Moberg, K.H., W.A. Tyndall, and D.J. Hall, *Wild-type murine p53 represses transcription from the murine c-myc promoter in a human glial cell line*. J Cell Biochem, 1992. **49**(2): p. 208-15.
211. Porter, J.R., et al., *Global Inhibition with Specific Activation: How p53 and MYC Redistribute the Transcriptome in the DNA Double-Strand Break Response*. Mol Cell, 2017. **67**(6): p. 1013-1025.e9.
212. Ho, J.S., et al., *p53-Dependent transcriptional repression of c-myc is required for G1 cell cycle arrest*. Mol Cell Biol, 2005. **25**(17): p. 7423-31.
213. Marhin, W.W., et al., *Myc represses the growth arrest gene gadd45*. Oncogene, 1997. **14**(23): p. 2825-34.
214. Abbas, T. and A. Dutta, *p21 in cancer: intricate networks and multiple activities*. Nature Reviews Cancer, 2009. **9**(6): p. 400-414.
215. Mitchell, K.O. and W.S. El-Deiry, *Overexpression of c-Myc inhibits p21WAF1/CIP1 expression and induces S-phase entry in 12-O-tetradecanoylphorbol-13-acetate (TPA)-sensitive human cancer cells*. Cell Growth Differ, 1999. **10**(4): p. 223-30.
216. Jung, P., et al., *AP4 encodes a c-MYC-inducible repressor of p21*. Proc Natl Acad Sci U S A, 2008. **105**(39): p. 15046-51.
217. Hermeking, H., et al., *Abrogation of p53-induced cell cycle arrest by c-Myc: evidence for an inhibitor of p21WAF1/CIP1/SDI1*. Oncogene, 1995. **11**(7): p. 1409-15.
218. Seoane, J., H.V. Le, and J. Massagué, *Myc suppression of the p21(Cip1) Cdk inhibitor influences the outcome of the p53 response to DNA damage*. Nature, 2002. **419**(6908): p. 729-34.
219. Yu, Q., et al., *Identification of Myc-mediated death response pathways by microarray analysis*. J Biol Chem, 2002. **277**(15): p. 13059-66.
220. Adachi, S., et al., *c-Myc is necessary for DNA damage-induced apoptosis in the G(2) phase of the cell cycle*. Mol Cell Biol, 2001. **21**(15): p. 4929-37.
221. Pusapati, R.V., et al., *ATM promotes apoptosis and suppresses tumorigenesis in response to Myc*. Proceedings of the National Academy of Sciences, 2006. **103**(5): p. 1446-1451.
222. Albihn, A., et al., *c-Myc-dependent etoposide-induced apoptosis involves activation of Bax and caspases, and PKCdelta signaling*. J Cell Biochem, 2006. **98**(6): p. 1597-614.
223. Albihn, A., et al., *Camptothecin-induced apoptosis is enhanced by Myc and involves PKCdelta signaling*. Int J Cancer, 2007. **121**(8): p. 1821-9.
224. Eischen, C.M., et al., *Apoptosis triggered by Myc-induced suppression of Bcl-X(L) or Bcl-2 is bypassed during lymphomagenesis*. Mol Cell Biol, 2001. **21**(15): p. 5063-70.
225. Afanasyeva, E.A., et al., *Drug-induced Myc-mediated apoptosis of cancer cells is inhibited by stress protein Hsp70*. Int J Cancer, 2007. **121**(12): p. 2615-21.
226. Phesse, T.J., et al., *Endogenous c-Myc is essential for p53-induced apoptosis in response to DNA damage in vivo*. Cell Death Differ, 2014. **21**(6): p. 956-66.
227. Felsher, D.W. and J.M. Bishop, *Transient excess of MYC activity can elicit genomic instability and tumorigenesis*. Proc Natl Acad Sci U S A, 1999. **96**(7): p. 3940-4.

228. Denis, N., et al., *Stimulation of methotrexate resistance and dihydrofolate reductase gene amplification by c-myc*. Oncogene, 1991. **6**(8): p. 1453-7.
229. Ray, S., et al., *MYC can induce DNA breaks in vivo and in vitro independent of reactive oxygen species*. Cancer Res, 2006. **66**(13): p. 6598-605.
230. Vafa, O., et al., *c-Myc can induce DNA damage, increase reactive oxygen species, and mitigate p53 function: a mechanism for oncogene-induced genetic instability*. Mol Cell, 2002. **9**(5): p. 1031-44.
231. Karlsson, A., et al., *Defective double-strand DNA break repair and chromosomal translocations by MYC overexpression*. Proc Natl Acad Sci U S A, 2003. **100**(17): p. 9974-9.
232. Ahmadi, S.E., et al., *MYC: a multipurpose oncogene with prognostic and therapeutic implications in blood malignancies*. Journal of Hematology & Oncology, 2021. **14**(1): p. 121.
233. Orr, M.S., et al., *Transcriptional down-regulation of c-myc expression in the MCF-7 breast tumor cell line by the topoisomerase 11 inhibitor, VM-26*. Biochimica et Biophysica Acta (BBA) - Gene Structure and Expression, 1995. **1262**(2): p. 139-145.
234. Lu, H.R., et al., *DNA damage, c-myc suppression and apoptosis induced by the novel topoisomerase II inhibitor, salvicine, in human breast cancer MCF-7 cells*. Cancer Chemother Pharmacol, 2005. **55**(3): p. 286-94.
235. Jain, P.T., et al., *Induction of DNA damage, inhibition of DNA synthesis, and suppression of c-myc expression by the topoisomerase I inhibitor, camptothecin, in MCF-7 human breast tumor cells*. Biochem Pharmacol, 1998. **55**(8): p. 1263-9.
236. Magnet, K.J., et al., *Suppression of c-myc expression and c-Myc function in response to sustained DNA damage in MCF-7 breast tumor cells*. Biochem Pharmacol, 2001. **62**(5): p. 593-602.
237. Li, Y., et al., *MicroRNA-130a associates with ribosomal protein L11 to suppress c-Myc expression in response to UV irradiation*. Oncotarget, 2015. **6**(2): p. 1101-14.
238. Cannell, I.G., et al., *p38 MAPK/MK2-mediated induction of miR-34c following DNA damage prevents Myc-dependent DNA replication*. Proc Natl Acad Sci U S A, 2010. **107**(12): p. 5375-80.
239. Jiang, M.R., et al., *c-Myc degradation induced by DNA damage results in apoptosis of CHO cells*. Oncogene, 2003. **22**(21): p. 3252-9.
240. Popov, N., et al., *Fbw7 and Usp28 regulate myc protein stability in response to DNA damage*. Cell Cycle, 2007. **6**(19): p. 2327-31.
241. Yada, M., et al., *Phosphorylation-dependent degradation of c-Myc is mediated by the F-box protein Fbw7*. Embo j, 2004. **23**(10): p. 2116-25.
242. Britton, S., B. Salles, and P. Calsou, *c-MYC protein is degraded in response to UV irradiation*. Cell Cycle, 2008. **7**(1): p. 63-70.
243. Prochownik, E.V., *c-Myc: linking transformation and genomic instability*. Curr Mol Med, 2008. **8**(6): p. 446-58.
244. Beckman, R.A. and L.A. Loeb, *Genetic instability in cancer: theory and experiment*. Semin Cancer Biol, 2005. **15**(6): p. 423-35.
245. Kalkat, M., et al., *MYC Deregulation in Primary Human Cancers*. Genes (Basel), 2017. **8**(6).

246. Nesbit, C.E., J.M. Tersak, and E.V. Prochownik, *MYC oncogenes and human neoplastic disease*. Oncogene, 1999. **18**(19): p. 3004-16.
247. Whitfield, J.R. and L. Soucek, *The long journey to bring a Myc inhibitor to the clinic*. J Cell Biol, 2021. **220**(8).
248. Mangel, M. and F.J. and Samaniego, *Abraham Wald's Work on Aircraft Survivability*. Journal of the American Statistical Association, 1984. **79**(386): p. 259-267.
249. Casselman, B. *The Legend of Abraham Wald*. 2016; Available from: https://www.ams.org//publicoutreach/feature-column/fc-2016-06.
250. Rohban, S., et al., *The cohesin complex prevents Myc-induced replication stress*. Cell Death & Disease, 2017. **8**(7): p. e2956-e2956.
251. Robinson, K., et al., *c-Myc accelerates S-phase and requires WRN to avoid replication stress*. PLoS One, 2009. **4**(6): p. e5951.
252. Petroni, M., et al., *MRE11 inhibition highlights a replication stress-dependent vulnerability of MYCN-driven tumors*. Cell Death & Disease, 2018. **9**(9): p. 895.
253. Murayama, T., et al., *MCM10 compensates for Myc-induced DNA replication stress in breast cancer stem-like cells*. Cancer Sci, 2021. **112**(3): p. 1209-1224.
254. Rousseau, V., et al., *Trim33 masks a non-transcriptional function of E2f4 in replication fork progression*. Nature Communications, 2023. **14**(1): p. 5143.
255. Zhou, Z., et al., *Identification of synthetic lethality of PRKDC in MYC-dependent human cancers by pooled shRNA screening*. BMC Cancer, 2014. **14**: p. 944.
256. Roeschert, I., et al., *Combined inhibition of Aurora-A and ATR kinases results in regression of MYCN-amplified neuroblastoma*. Nature Cancer, 2021. **2**(3): p. 312-326.
257. Yi, J., et al., *MYC status as a determinant of synergistic response to Olaparib and Palbociclib in ovarian cancer*. EBioMedicine, 2019. **43**: p. 225-237.
258. Hsu, W.-J., et al., *PRMT1 Confers Resistance to Olaparib via Modulating MYC Signaling in Triple-Negative Breast Cancer*. Journal of Personalized Medicine, 2021. **11**(10): p. 1009.
259. Sears, R., et al., *Multiple Ras-dependent phosphorylation pathways regulate Myc protein stability*. Genes Dev, 2000. **14**(19): p. 2501-14.
260. Blobel, G., *Gene gating: a hypothesis*. Proc Natl Acad Sci U S A, 1985. **82**(24): p. 8527-9.
261. Akhtar, A. and S.M. Gasser, *The nuclear envelope and transcriptional control*. Nat Rev Genet, 2007. **8**(7): p. 507-17.
262. Dieppois, G. and F. Stutz, *Connecting the transcription site to the nuclear pore: a multi-tether process that regulates gene expression*. Journal of Cell Science, 2010. **123**(12): p. 1989-1999.
263. Mohammed, H., et al., *Rapid immunoprecipitation mass spectrometry of endogenous proteins (RIME) for analysis of chromatin complexes*. Nature Protocols, 2016. **11**(2): p. 316-326.
264. Doncheva, N.T., et al., *Cytoscape StringApp: Network Analysis and Visualization of Proteomics Data*. J Proteome Res, 2019. **18**(2): p. 623-632.
265. Shannon, P., et al., *Cytoscape: a software environment for integrated models of biomolecular interaction networks*. Genome Res, 2003. **13**(11): p. 2498-504.

266. Szklarczyk, D., et al., *STRING v10: protein-protein interaction networks, integrated over the tree of life*. Nucleic Acids Res, 2015. **43**(Database issue): p. D447-52.
267. Ibarra, A., et al., *Nucleoporin-mediated regulation of cell identity genes*. Genes Dev, 2016. **30**(20): p. 2253-2258.
268. Kadota, S., et al., *Nucleoporin 153 links nuclear pore complex to chromatin architecture by mediating CTCF and cohesin binding*. Nat Commun, 2020. **11**(1): p. 2606.
269. Kim, D.I., et al., *Probing nuclear pore complex architecture with proximity-dependent biotinylation*. Proc Natl Acad Sci U S A, 2014. **111**(24): p. E2453-61.
270. Kim, D.I., et al., *An improved smaller biotin ligase for BioID proximity labeling*. Mol Biol Cell, 2016. **27**(8): p. 1188-96.
271. Sun, X.-X., et al., *SUMO protease SENP1 deSUMOylates and stabilizes c-Myc*. Proceedings of the National Academy of Sciences, 2018. **115**(43): p. 10983-10988.
272. Lv, T., et al., *Mechanism and role of nuclear laminin B1 in cell senescence and malignant tumors*. Cell Death Discovery, 2024. **10**(1): p. 269.
273. Brickner, D.G., et al., *H2A.Z-mediated localization of genes at the nuclear periphery confers epigenetic memory of previous transcriptional state*. PLoS Biol, 2007. **5**(4): p. e81.
274. Chachoua, I., et al., *Canonical WNT signaling-dependent gating of MYC requires a noncanonical CTCF function at a distal binding site*. Nat Commun, 2022. **13**(1): p. 204.
275. Cairo, S., et al., *PML interacts with Myc, and Myc target gene expression is altered in PML-null fibroblasts*. Oncogene, 2005. **24**(13): p. 2195-203.
276. Gialitakis, M., et al., *Gamma interferon-dependent transcriptional memory via relocalization of a gene locus to PML nuclear bodies*. Mol Cell Biol, 2010. **30**(8): p. 2046-56.
277. Chen, Y., et al., *Writing and erasing MYC ubiquitination and SUMOylation*. Genes & Diseases, 2019. **6**(4): p. 359-371.
278. Dubiella, C., et al., *Sulfopin is a covalent inhibitor of Pin1 that blocks Myc-driven tumors in vivo*. Nat Chem Biol, 2021. **17**(9): p. 954-963.
279. Queitsch, K., et al., *Accessible high-throughput single-cell whole-genome sequencing with paired chromatin accessibility*. Cell Rep Methods, 2023. **3**(11): p. 100625.
280. Ashburner, M., et al., *Gene Ontology: tool for the unification of biology*. Nature Genetics, 2000. **25**(1): p. 25-29.
281. Consortium, T.G.O., et al., *The Gene Ontology knowledgebase in 2023*. Genetics, 2023. **224**(1).
282. Kumari, A., W.P. Folk, and D. Sakamuro, *The Dual Roles of MYC in Genomic Instability and Cancer Chemoresistance*. Genes, 2017. **8**(6): p. 158.
283. Stine, Z.E., et al., *MYC, Metabolism, and Cancer*. Cancer Discov, 2015. **5**(10): p. 1024-39.
284. Gabay, M., Y. Li, and D.W. Felsher, *MYC activation is a hallmark of cancer initiation and maintenance*. Cold Spring Harb Perspect Med, 2014. **4**(6).

285. Hann, S.R. and R.N. Eisenman, *Proteins encoded by the human c-myc oncogene: differential expression in neoplastic cells*. Mol Cell Biol, 1984. **4**(11): p. 2486-97.
286. Welcker, M., et al., *The Fbw7 tumor suppressor regulates glycogen synthase kinase 3 phosphorylation-dependent c-Myc protein degradation*. Proceedings of the National Academy of Sciences, 2004. **101**(24): p. 9085-9090.
287. Sun, X.-X., et al., *Targeting the MYC Ubiquitination-Proteasome Degradation Pathway for Cancer Therapy*. Frontiers in Oncology, 2021. **11**.
288. Lutterbach, B. and S.R. Hann, *Hierarchical phosphorylation at N-terminal transformation-sensitive sites in c-Myc protein is regulated by mitogens and in mitosis*. Mol Cell Biol, 1994. **14**(8): p. 5510-22.
289. Devaiah, B.N., et al., *MYC protein stability is negatively regulated by BRD4*. Proceedings of the National Academy of Sciences, 2020. **117**(24): p. 13457-13467.
290. Kim, J., et al., *A Myc network accounts for similarities between embryonic stem and cancer cell transcription programs*. Cell, 2010. **143**(2): p. 313-24.
291. Tworkowski, K.A., et al., *Adenovirus E1A targets p400 to induce the cellular oncoprotein Myc*. Proc Natl Acad Sci U S A, 2008. **105**(16): p. 6103-8.
292. Link, J.M., et al., *Ongoing replication stress tolerance and clonal T cell responses distinguish liver and lung recurrence and outcomes in pancreatic cancer*. Nature Cancer, 2025.
293. Dreyer, S.B., et al., *Targeting DNA Damage Response and Replication Stress in Pancreatic Cancer*. Gastroenterology, 2021. **160**(1): p. 362-377.e13.
294. Vesela, E., et al., *Common Chemical Inductors of Replication Stress: Focus on Cell-Based Studies*. Biomolecules, 2017. **7**(1).
295. Alvarez, M.J., et al., *Functional characterization of somatic mutations in cancer using network-based inference of protein activity*. Nat Genet, 2016. **48**(8): p. 838-47.
296. Lachmann, A., et al., *ARACNe-AP: gene network reverse engineering through adaptive partitioning inference of mutual information*. Bioinformatics, 2016. **32**(14): p. 2233-5.
297. Hann, S.R., *Role of post-translational modifications in regulating c-Myc proteolysis, transcriptional activity and biological function*. Semin Cancer Biol, 2006. **16**(4): p. 288-302.
298. Sears, R.C., *The life cycle of C-myc: from synthesis to degradation*. Cell Cycle, 2004. **3**(9): p. 1133-7.
299. Galbiati, A. and F. d'Adda di Fagagna, *DNA Damage In Situ Ligation Followed by Proximity Ligation Assay (DI-PLA)*. Methods Mol Biol, 2019. **1896**: p. 11-20.
300. van Sluis, M. and B. McStay, *A localized nucleolar DNA damage response facilitates recruitment of the homology-directed repair machinery independent of cell cycle stage*. Genes Dev, 2015. **29**(11): p. 1151-63.
301. Wang, Q., et al., *BRCA1 binds c-Myc and inhibits its transcriptional and transforming activity in cells*. Oncogene, 1998. **17**(15): p. 1939-1948.
302. Li, H., T.H. Lee, and H. Avraham, *A novel tricomplex of BRCA1, Nmi, and c-Myc inhibits c-Myc-induced human telomerase reverse transcriptase gene (hTERT) promoter activity in breast cancer*. J Biol Chem, 2002. **277**(23): p. 20965-73.

303. Epasto, L.M., et al., *NMR-identification of the interaction between BRCA1 and the intrinsically disordered monomer of the Myc-associated factor X*. Protein Sci, 2024. **33**(1): p. e4849.
304. Maere, S., K. Heymans, and M. Kuiper, *BiNGO: a Cytoscape plugin to assess overrepresentation of gene ontology categories in biological networks*. Bioinformatics, 2005. **21**(16): p. 3448-9.
305. Cohn, G.M., et al., *PIN1 Provides Dynamic Control of MYC in Response to Extrinsic Signals*. Frontiers in Cell and Developmental Biology, 2020. **8**.
306. Yeh, E., et al., *A signalling pathway controlling c-Myc degradation that impacts oncogenic transformation of human cells*. Nature Cell Biology, 2004. **6**(4): p. 308-318.
307. Gregory, M.A. and S.R. Hann, *c-Myc proteolysis by the ubiquitin-proteasome pathway: stabilization of c-Myc in Burkitt's lymphoma cells*. Mol Cell Biol, 2000. **20**(7): p. 2423-35.
308. Kaur, M. and M.D. Cole, *MYC Acts via the PTEN Tumor Suppressor to Elicit Autoregulation and Genome-Wide Gene Repression by Activation of the Ezh2 Methyltransferase*. Cancer Research, 2013. **73**(2): p. 695-705.
309. Grushko, T.A., et al., *MYC Is Amplified in BRCA1-Associated Breast Cancers*. Clinical Cancer Research, 2004. **10**(2): p. 499-507.
310. Lourenco, C., et al., *MYC protein interactors in gene transcription and cancer*. Nat Rev Cancer, 2021. **21**(9): p. 579-591.
311. Papadopoulos, D., et al., *The MYCN oncoprotein is an RNA-binding accessory factor of the nuclear exosome targeting complex*. Mol Cell, 2024. **84**(11): p. 2070-2086.e20.
312. Guo, J., et al., *Sequence specificity incompletely defines the genome-wide occupancy of Myc*. Genome Biology, 2014. **15**(10): p. 482.
313. Tworkowski, K.A., S.E. Salghetti, and W.P. Tansey, *Stable and unstable pools of Myc protein exist in human cells*. Oncogene, 2002. **21**(55): p. 8515-8520.
314. Popov, N., et al., *The ubiquitin-specific protease USP28 is required for MYC stability*. Nat Cell Biol, 2007. **9**(7): p. 765-74.
315. Link, J.M., et al., *Ongoing Replication Stress Response and New Clonal T Cell Development Discriminate Between Liver and Lung Recurrence Sites and Patient Outcomes in Pancreatic Ductal Adenocarcinoma*. bioRxiv, 2022: p. 2022.05.04.490552.
316. Beaubier, N., et al., *Clinical validation of the tempus xT next-generation targeted oncology sequencing assay*. Oncotarget, 2019. **10**(24): p. 2384-2396.
317. Hänzelmann, S., R. Castelo, and J. Guinney, *GSVA: gene set variation analysis for microarray and RNA-Seq data*. BMC Bioinformatics, 2013. **14**(1): p. 7.
318. Liberzon, A., et al., *The Molecular Signatures Database Hallmark Gene Set Collection*. Cell Systems, 2015. **1**(6): p. 417-425.
319. Ashburner, M., et al., *Gene ontology: tool for the unification of biology. The Gene Ontology Consortium*. Nat Genet, 2000. **25**(1): p. 25-9.
320. Aleksander, S.A., et al., *The Gene Ontology knowledgebase in 2023*. Genetics, 2023. **224**(1).

321. Wu, T., et al., *clusterProfiler 4.0: A universal enrichment tool for interpreting omics data*. Innovation (Camb), 2021. **2**(3): p. 100141.
322. Eng, J., et al., *A framework for multiplex imaging optimization and reproducible analysis*. Commun Biol, 2022. **5**(1): p. 438.
323. Stringer, C., et al., *Cellpose: a generalist algorithm for cellular segmentation*. Nat Methods, 2021. **18**(1): p. 100-106.
324. Greenwald, N.F., et al., *Whole-cell segmentation of tissue images with human-level performance using large-scale data annotation and deep learning*. Nat Biotechnol, 2022. **40**(4): p. 555-565.
325. Wolf, F.A., P. Angerer, and F.J. Theis, *SCANPY: large-scale single-cell gene expression data analysis*. Genome Biol, 2018. **19**(1): p. 15.
326. Eng, J.K., T.A. Jahan, and M.R. Hoopmann, *Comet: an open-source MS/MS sequence database search tool*. Proteomics, 2013. **13**(1): p. 22-4.
327. Gyori, B.M., et al., *OpenComet: An automated tool for comet assay image analysis*. Redox Biology, 2014. **2**: p. 457-465.
328. Stirling, D.R., et al., *CellProfiler 4: improvements in speed, utility and usability*. BMC Bioinformatics, 2021. **22**(1): p. 433.
329. Campaner, S. and B. Amati, *Two sides of the Myc-induced DNA damage response: from tumor suppression to tumor maintenance*. Cell Div, 2012. **7**(1): p. 6.
330. Kuzyk, A. and S. Mai, *c-MYC-induced genomic instability*. Cold Spring Harb Perspect Med, 2014. **4**(4): p. a014373.
331. Jaenicke, L.A., et al., *Ubiquitin-Dependent Turnover of MYC Antagonizes MYC/PAF1C Complex Accumulation to Drive Transcriptional Elongation*. Molecular Cell, 2016. **61**(1): p. 54-67.
332. Zacarías-Fluck, M.F., L. Soucek, and J.R. Whitfield, *MYC: there is more to it than cancer*. Front Cell Dev Biol, 2024. **12**: p. 1342872.
333. Iacovoni, J.S., et al., *High-resolution profiling of gammaH2AX around DNA double strand breaks in the mammalian genome*. Embo j, 2010. **29**(8): p. 1446-57.
334. Papadopoulos, D., et al., *Beyond gene expression: how MYC relieves transcription stress*. Trends Cancer, 2023. **9**(10): p. 805-816.
335. Thakur, B.K., et al., *Inhibition of NAMPT pathway by FK866 activates the function of p53 in HEK293T cells*. Biochem Biophys Res Commun, 2012. **424**(3): p. 371-7.
336. Felsher, D.W., *MYC Inactivation Elicits Oncogene Addiction through Both Tumor Cell-Intrinsic and Host-Dependent Mechanisms*. Genes Cancer, 2010. **1**(6): p. 597-604.
337. Beaulieu, M.E. and L. Soucek, *Finding MYCure*. Mol Cell Oncol, 2019. **6**(5): p. e1618178.
338. Massó-Vallés, D. and L. Soucek, *Blocking Myc to Treat Cancer: Reflecting on Two Decades of Omomyc*. Cells, 2020. **9**(4).
339. Soucek, L., et al., *Design and properties of a Myc derivative that efficiently homodimerizes*. Oncogene, 1998. **17**(19): p. 2463-72.
340. Soucek, L., et al., *Omomyc, a potential Myc dominant negative, enhances Myc-induced apoptosis*. Cancer Res, 2002. **62**(12): p. 3507-10.
341. Soucek, L., et al., *Modelling Myc inhibition as a cancer therapy*. Nature, 2008. **455**(7213): p. 679-83.

342. Garralda, E., et al., *MYC targeting by OMO-103 in solid tumors: a phase 1 trial*. Nat Med, 2024. **30**(3): p. 762-771.
343. Leonard, D., et al., *Selective PP2A Enhancement through Biased Heterotrimer Stabilization*. Cell, 2020. **181**(3): p. 688-701.e16.
344. Shah, V.M., I.A. English, and R.C. Sears, *Select Stabilization of a Tumor-Suppressive PP2A Heterotrimer*. Trends Pharmacol Sci, 2020. **41**(9): p. 595-597.
345. Ramos, F., et al., *Role of protein phosphatases PP1, PP2A, PP4 and Cdc14 in the DNA damage response*. Cell Stress, 2019. **3**(3): p. 70-85.
346. Pishvaian, M.J., et al., *Molecular Profiling of Patients with Pancreatic Cancer: Initial Results from the Know Your Tumor Initiative*. Clinical Cancer Research, 2018. **24**(20): p. 5018-5027.
347. Witkiewicz, A.K., et al., *Whole-exome sequencing of pancreatic cancer defines genetic diversity and therapeutic targets*. Nature Communications, 2015. **6**(1): p. 6744.
348. Waddell, N., et al., *Whole genomes redefine the mutational landscape of pancreatic cancer*. Nature, 2015. **518**(7540): p. 495-501.
349. Cox, A.D., et al., *Drugging the undruggable RAS: Mission Possible?* Nature Reviews Drug Discovery, 2014. **13**(11): p. 828-851.
350. Ostrem, J.M., et al., *K-Ras(G12C) inhibitors allosterically control GTP affinity and effector interactions*. Nature, 2013. **503**(7477): p. 548-51.
351. Skoulidis, F., et al., *Sotorasib for Lung Cancers with KRAS p.G12C Mutation*. N Engl J Med, 2021. **384**(25): p. 2371-2381.
352. Hong, D.S., et al., *KRAS(G12C) Inhibition with Sotorasib in Advanced Solid Tumors*. N Engl J Med, 2020. **383**(13): p. 1207-1217.
353. Hallin, J., et al., *The KRASG12C Inhibitor MRTX849 Provides Insight toward Therapeutic Susceptibility of KRAS-Mutant Cancers in Mouse Models and Patients*. Cancer Discovery, 2020. **10**(1): p. 54-71.
354. Buscail, L., B. Bournet, and P. Cordelier, *Role of oncogenic KRAS in the diagnosis, prognosis and treatment of pancreatic cancer*. Nat Rev Gastroenterol Hepatol, 2020. **17**(3): p. 153-168.
355. Lanman, B.A., et al., *Discovery of a Covalent Inhibitor of KRAS(G12C) (AMG 510) for the Treatment of Solid Tumors*. J Med Chem, 2020. **63**(1): p. 52-65.
356. Fell, J.B., et al., *Identification of the Clinical Development Candidate MRTX849, a Covalent KRAS(G12C) Inhibitor for the Treatment of Cancer*. J Med Chem, 2020. **63**(13): p. 6679-6693.
357. McGregor, L.M., et al., *Expanding the Scope of Electrophiles Capable of Targeting K-Ras Oncogenes*. Biochemistry, 2017. **56**(25): p. 3178-3183.
358. Hallin, J., et al., *Anti-tumor efficacy of a potent and selective non-covalent KRAS(G12D) inhibitor*. Nat Med, 2022. **28**(10): p. 2171-2182.
359. Wang, X., et al., *Identification of MRTX1133, a Noncovalent, Potent, and Selective KRAS(G12D) Inhibitor*. J Med Chem, 2022. **65**(4): p. 3123-3133.
360. Tang, D. and R. Kang, *Glimmers of hope for targeting oncogenic KRAS-G12D*. Cancer Gene Therapy, 2023. **30**(3): p. 391-393.

361. Varmus, H. *Harold E. Varmus – Banquet speech*. 1989 [cited 2025; Available from: <https://www.nobelprize.org/prizes/medicine/1989/varmus/speech/>.
362. Saebøe-Larssen, S., et al., *Ribosomal protein insufficiency and the minute syndrome in Drosophila: a dose-response relationship*. Genetics, 1998. **148**(3): p. 1215-24.
363. Morata, G. and P. Ripoll, *Minutes: Mutants of Drosophila autonomously affecting cell division rate*. Developmental Biology, 1975. **42**(2): p. 211-221.
364. Di Gregorio, A., S. Bowling, and Tristan A. Rodriguez, *Cell Competition and Its Role in the Regulation of Cell Fitness from Development to Cancer*. Developmental Cell, 2016. **38**(6): p. 621-634.
365. Levayer, R. and E. Moreno, *Mechanisms of cell competition: Themes and variations*. Journal of Cell Biology, 2013. **200**(6): p. 689-698.
366. Nagata, R. and T. Igaki, *Cell competition: Emerging mechanisms to eliminate neighbors*. Dev Growth Differ, 2018. **60**(9): p. 522-530.
367. Marques-Reis, M. and E. Moreno, *Role of cell competition in ageing*. Developmental Biology, 2021. **476**: p. 79-87.
368. Johnston, L.A., et al., *Drosophila myc regulates cellular growth during development*. Cell, 1999. **98**(6): p. 779-90.
369. de la Cova, C., et al., *Drosophila myc regulates organ size by inducing cell competition*. Cell, 2004. **117**(1): p. 107-16.
370. Moreno, E. and K. Basler, *dMyc Transforms Cells into Super-Competitors*. Cell, 2004. **117**(1): p. 117-129.
371. Vidal, M., D.E. Larson, and R.L. Cagan, *Csk-Deficient Boundary Cells Are Eliminated from Normal Drosophila Epithelia by Exclusion, Migration, and Apoptosis*. Developmental Cell, 2006. **10**(1): p. 33-44.
372. Tanimura, N. and Y. Fujita, *Epithelial defense against cancer (EDAC)*. Seminars in Cancer Biology, 2020. **63**: p. 44-48.
373. Donaldson, T.D. and R.J. Duronio, *Cancer cell biology: Myc wins the competition*. Curr Biol, 2004. **14**(11): p. R425-7.
374. Senoo-Matsuda, N. and L.A. Johnston, *Soluble factors mediate competitive and cooperative interactions between cells expressing different levels of Drosophila Myc*. Proc Natl Acad Sci U S A, 2007. **104**(47): p. 18543-8.
375. Meyer, S.N., et al., *An ancient defense system eliminates unfit cells from developing tissues during cell competition*. Science, 2014. **346**(6214): p. 1258236.
376. Li, W. and N.E. Baker, *Engulfment is required for cell competition*. Cell, 2007. **129**(6): p. 1215-25.
377. Patel, M.S., H.S. Shah, and N. Shrivastava, *c-Myc-Dependent Cell Competition in Human Cancer Cells*. J Cell Biochem, 2017. **118**(7): p. 1782-1791.
378. Clavería, C., et al., *Myc-driven endogenous cell competition in the early mammalian embryo*. Nature, 2013. **500**(7460): p. 39-44.
379. Sancho, M., et al., *Competitive interactions eliminate unfit embryonic stem cells at the onset of differentiation*. Dev Cell, 2013. **26**(1): p. 19-30.
380. Wolfer, A. and S. Ramaswamy, *MYC and metastasis*. Cancer Res, 2011. **71**(6): p. 2034-7.

381. de la Cova, C., et al., *Supercompetitor status of Drosophila Myc cells requires p53 as a fitness sensor to reprogram metabolism and promote viability*. Cell Metab, 2014. **19**(3): p. 470-83.